

Nondestructive Test Methods for Evaluation of Concrete in Structures

Reported by ACI Committee 228

A. G. Davis^{*†}
Chairman

F. Ansari	R. D. Gaynor	K. M. Lozen ^{*†}	T. J. Rowe
H. Caratin	F. D. Heidbrink	V. M. Malhotra	B. P. Simons [*]
N. J. Carino [‡]	B. H. Hertlein [†]	L. D. Olson [*]	P. J. Sullivan
K. Choi	K. R. Hindo	S. P. Pessiki	B. A. Suprenant
G. G. Clemeña [*]	R. Huyke	S. Popovics	G. Teodoru
N. A. Cumming ^{*†}	R. S. Jenkins [*]	R. W. Poston [*]	W. L. Vogt
R. L. Dilly	M. E. Leeman	P. H. Read [*]	A. B. Zoob
D. E. Dixon	A. Leshchinsky	W. M. K. Roddis [*]	
B. Dragunsky	H. S. Lew	M. J. Sansalone [*]	

* Task group members who contributed to preparation of report. Associate and Consulting Members who contributed to the report include K. Maser, U. Halabe, J. Bungey. Former member R. W. Ross also contributed to the early draft.

† Editorial task group.

‡ Chairman of report task group.

A review is presented of nondestructive test methods for evaluating the condition of concrete and steel reinforcement in structures. The methods discussed include visual inspection, stress-wave methods, nuclear methods, penetrability methods, magnetic and electrical methods, infrared thermography and ground-penetrating radar. The principle of each method is discussed and the typical instrumentation is described. The testing procedures are summarized and the data analysis methods are explained. The advantages and limitations of the methods are highlighted. The report concludes with a discussion of the planning of a nondestructive testing program. The report provides general information to individuals who are faced with the task of evaluating the condition of a concrete structure and are considering the applicability of nondestructive test methods to aid in that evaluation.

ACI Committee Reports, Guides, Standard Practices, and Commentaries are intended for guidance in planning, designing, executing, and inspecting construction. This document is intended for the use of individuals who are competent to evaluate the significance and limitations of its content and recommendations and who will accept responsibility for the application of the material it contains. The American Concrete Institute disclaims any and all responsibility for the stated principles. The Institute shall not be liable for any loss or damage arising therefrom.

Reference to this document shall not be made in contract documents. If items found in this document are desired by the Architect/Engineer to be a part of the contract documents, they shall be restated in mandatory language for incorporation by the Architect/Engineer.

Keywords: concrete; covermeter; deep foundations; half-cell potential; infrared thermography; nondestructive testing; polarization resistance; radar; radiography; radiometry; stress-wave methods; visual inspection.

CONTENTS

Chapter 1—Introduction, p. 2

- 1.1—Scope
- 1.2—Needs and applications
- 1.3—Objective of report

Chapter 2—Summary of methods, p. 2

- 2.1—Visual inspection
- 2.2—Stress-wave methods for structures
- 2.3—Stress-wave methods for deep foundations
- 2.4—Nuclear methods
- 2.5—Magnetic and electrical methods
- 2.6—Penetrability methods
- 2.7—Infrared thermography
- 2.8—Radar

Chapter 3—Planning and performing nondestructive testing investigations, p. 45

- 3.1—Selection of methods
- 3.2—Defining scope of investigation

ACI 228.2R-98 became effective June 24, 1998.
Copyright © 1998, American Concrete Institute.

All rights reserved including rights of reproduction and use in any form or by any means, including the making of copies by any photo process, or by electronic or mechanical device, printed, written, or oral, or recording for sound or visual reproduction or for use in any knowledge or retrieval system or device, unless permission in writing is obtained from the copyright proprietors.

- 3.3—Numerical and experimental simulations
- 3.4—Correlation with intrusive testing
- 3.5—Reporting results

Chapter 4—References, p. 56

- 4.1—Specified references
- 4.2—Cited references

Appendix A—Theoretical aspects of mobility plot of pile, p. 61

CHAPTER 1—INTRODUCTION

1.1—Scope

Nondestructive test (NDT) methods are used to determine hardened concrete properties and to evaluate the condition of concrete in deep foundations, bridges, buildings, pavements, dams and other concrete construction. For this report, nondestructive testing is defined as testing that causes no structurally significant damage to concrete. While some people regard coring and load testing as nondestructive, these are not considered in this report, and appropriate information is given in ACI 437R.

Nondestructive test methods are applied to concrete construction for four primary reasons:

- quality control of new construction;
- troubleshooting of problems with new construction;
- condition evaluation of older concrete for rehabilitation purposes; and
- quality assurance of concrete repairs.

Nondestructive testing technologies are evolving and research continues to enhance existing methods and develop new methods. The report is intended to provide an overview of the principles of various NDT methods being used in practice, and to summarize their applications and limitations. The emphasis is placed on methods that have been applied to measure physical properties other than the strength of concrete in structures, to detect flaws or discontinuities, and to provide data for condition evaluation. Methods to estimate in-place compressive strength are presented in ACI 228.1R.

1.2—Needs and applications

Nondestructive test methods are increasingly applied for the investigation of concrete structures. This increase in the application of NDT methods is due to a number of factors:

- technological improvements in hardware and software for data collection and analysis;
- the economic advantages in assessing large volumes of concrete compared with coring;
- ability to perform rapid, comprehensive assessments of existing construction; and
- specification of NDT methods for quality assurance of deep foundations and concrete repairs.

This increased use of NDT methods is occurring despite the lack of testing standards for many of the methods. The development of testing standards is critical for proper application and expanded use of NDT methods for evaluation of concrete constructions.

Traditionally, quality assurance of concrete construction has been performed largely by visual inspection of the construction process and by sampling the concrete for performing standard tests on fresh and hardened specimens. This approach does not provide data on the in-place properties of concrete. NDT methods offer the advantage of providing information on the in-place properties of hardened concrete, such as the elastic constants, density, resistivity, moisture content, and penetrability characteristics.

Condition assessment of concrete for structural evaluation purposes has been performed mostly by visual examination, surface sounding,* and coring to examine internal concrete conditions and obtain specimens for testing. This approach limits what can be detected. Also, cores only provide information at the core location and coreholes must be repaired. Condition assessments can be made with NDT methods to provide important information for the structural performance of the concrete, such as:

- Member dimensions;
- Location of cracking, delamination, and debonding;
- Degree of consolidation, and presence of voids and honeycomb;
- Steel reinforcement location and size;
- Corrosion activity of reinforcement; and
- Extent of damage from freezing and thawing, fire, or chemical exposure.

1.3—Objective of report

This report reviews the state of the practice for nondestructively determining non-strength physical properties and conditions of hardened concrete. The overall objective is to provide the potential user with a guide to assist in planning, conducting, and interpreting the results of nondestructive tests of concrete construction.

Chapter 2 discusses the principles, equipment, testing procedures, and data analysis of the various NDT methods. Typical applications and inherent limitations of the methods are discussed to assist the potential user in selecting the most appropriate method for a particular situation. Chapter 3 discusses the planning and performance of NDT investigations. Included in Chapter 3 are references to in-place tests covered in ACI 228.1R and other applicable methods for evaluating the in-place characteristics of concrete.

CHAPTER 2—SUMMARY OF METHODS

This chapter reviews the various NDT methods for evaluating concrete for characteristics other than strength. The underlying principles are discussed, the instrumentation is described, and the inherent advantages and limitations of each method are summarized. Where it is appropriate, examples of test data are provided. Table 2.1 summarizes the methods to be discussed. The first column lists the report section where the method is described; the second column provides a brief explanation of the underlying principles; and the third column gives typical applications.

* Sounding refers to striking the surface of the object and listening to the characteristics of the resulting sound.

Table 2.1—Summary of nondestructive testing methods

Section No.	Method and Principle	Applications
2.1	Visual inspection —observe, classify and document the appearance of distress on exposed surfaces of the structure.	Map patterns of distress such as cracking, spalling, scaling, erosion, or construction defects
2.2.1	Ultrasonic pulse velocity —measure the travel time of a pulse of ultrasonic waves over a known path length.	Determine the relative <i>condition</i> of concrete based on measured pulse velocity.
2.2.2	Ultrasonic-echo —Transducer emits short pulse of ultrasonic waves which is reflected by opposite side of member or an internal defect; arrival of reflected pulse is recorded by an adjacent receiver, and round-trip travel time is determined.	Locate delaminations and voids in relatively thin elements. Primarily a research tool.
2.2.3	Impact-echo —Receiver adjacent to impact point monitors arrival of stress waves as they undergo multiple reflections between surface and opposite side of plate-like member or from internal defects. Frequency analysis permits determination of distance to reflector if wave speed is known.	Locate a variety of defects within concrete elements such as delaminations, voids, honeycombing, or measure element thickness.
2.2.4	Spectral analysis of surface waves —Impact is used to generate a surface wave and two receivers monitor the surface motion; signal analysis allows determination of wave speed as a function of wavelength; inversion process determines elastic constants of layers.	Determine the stiffness profile of a pavement system. Also used to determine depth of deteriorated concrete. †
2.3.1	Sonic-echo —Hammer impact on surface and a receiver monitors reflected stress wave. Time-domain analysis used to determine travel time.	Determine the length of deep foundations (piles and piers); determine the location of cracks or constrictions (neck-in)
2.3.2	Impulse-response —Test is similar to sonic-echo method except that signal processing involves frequency-domain analysis of the received signal and the impact force history.	Determine the length of deep foundations (piles and piers), location of cracks or constrictions (neck in). Provides information on the low-strain dynamic stiffness of the shaft/soil system.
2.3.3	Impedance logging —Test is similar to sonic-echo or impulse-response, but the use of more complex signal analyses (time and frequency domains) allows reconstructing the approximate shape of the deep foundation.	Determine the approximate 2-dimensional shape of the deep foundation.
2.3.4	Crosshole sonic logging —Analogous to the ultrasonic pulse velocity test, but transducers are positioned within tubes cast into the deep foundation or holes drilled after construction.	Determine the location of low-quality concrete along the length of the shaft and between transducers. With drilled holes permits direct determination of shaft length.
2.3.5	Parallel seismic —Receiver is placed in hole adjacent to the foundation. Foundation is struck with a hammer and signal from receiver is recorded. Test is repeated with receiver at increasing depth.	Determine the foundation depth and determine whether it is of uniform quality.

Most NDT methods are indirect tests because the condition of the concrete is inferred from the measured response to some stimulus, such as impact or electromagnetic radiation. For favorable combinations of test method and site conditions, test results may be unambiguous and supplemental testing may be unnecessary. In other cases, the NDT results may be inconclusive and additional testing may be needed. Supplemental testing can be another NDT method or, often, it may be invasive methods to allow direct observation of the internal condition. Invasive inspection can range from drilling small holes to removing test samples by coring or sawing. The combination of nondestructive and invasive inspection allows the reliability of the NDT method to be assessed for the specific project. Once the reliability of the NDT method is established, a thorough inspection of the structure can be done economically.

2.1—Visual inspection

2.1.1 General—Normally, a visual inspection is one of the first steps in the evaluation of a concrete structure (Perenchio, 1989). Visual inspection can provide a qualified investigator with a wealth of information that may lead to positive identification of the cause of observed distress. Broad knowledge in structural engineering, concrete materials, and construction methods is needed to extract the most information from the visual inspection. Useful guides are available to help less-experienced individuals (ACI 201.1R, ACI 207.3R, ACI 224.1R, ACI 362R). These documents provide information for recognizing and classifying different types of damage, and can help to identify the probable cause of the distress.

Before doing a detailed visual inspection, the investigator should develop and follow a definite plan to maximize the

Table 2.1—Continued

2.4.2	Direct transmission radiometry — Measure the intensity of high energy electromagnetic radiation after passing through concrete.	Determine in-place density of fresh or hardened concrete. Locate reinforcing steel or voids.
2.4.3	Backscatter radiometry — Measure the intensity of high-energy electromagnetic radiation that is backscattered (reflected) by the near surface region of a concrete member.	Determine in-place density of fresh or hardened concrete.
2.4.4	Radiography — The intensity of high-energy electromagnetic radiation which passes through a member is recorded on photographic film.	Locate reinforcing and prestressing steel, conduits, pipes, voids, and honeycombing.
2.4.5	Gamma-gamma logging — see direct transmission and backscatter radiometry.	Locate regions of low density along length of foundation.
2.5.1	Covermeter — A low frequency alternating magnetic field is applied on the surface of the structure; the presence of embedded reinforcement alters this field, and measurement of this change provides information on the reinforcement.	Locate embedded steel reinforcement, measure depth of cover, and estimate diameter of reinforcement.
2.5.2	Half-cell potential — Measure the potential difference (voltage) between the steel reinforcement and a standard reference electrode; the measured voltage provides an indication of the likelihood that corrosion is occurring in the reinforcement.	Identify region or regions in a reinforced concrete structure where there is a high probability that corrosion is occurring at the time of the measurement.
2.5.3	Polarization methods — Measure the current required to change by a fixed amount the potential difference between the reinforcement and a standard reference electrode; the measured current and voltage allow determination of the polarization resistance, which is related to the rate of corrosion.	Determine the instantaneous corrosion rate of the reinforcement located below the test point.
2.6	Penetrability methods — Measure the flow of a fluid (air or water) into concrete under prescribed test conditions; the flow rate depends on the penetrability characteristics of the concrete.	Compare alternative concrete mixtures. Primarily research tools, but have the potential to be used for assessing adequacy of curing process.
2.7	Infrared thermography — The presence of flaws within the concrete affects the heat conduction properties of the concrete and the presence of defects are indicated by differences in surface temperatures when the test object is exposed to correct ambient conditions.	Locate delaminations in pavements and bridge decks. Also widely used for detecting moist insulation in buildings.
2.8	Radar — Analogous to the ultrasonic-echo methods except that electromagnetic waves are used instead of stress waves. Interface between materials with different dielectric properties results in reflection of a portion of incident electromagnetic pulse.	Locate metal embedments, voids beneath pavements, and regions of high moisture contents; determine thickness of members.

quality of the recorded data. A suitable approach typically involves the following activities:

- Cursory “walk-through” inspection to become familiar with the structure;
- Gathering background documents and information on the design, construction, ambient conditions, and operation of the structure;
- Planning the complete investigation;
- Laying out a control grid on the structure to serve as a basis for recording observations;
- Doing the visual inspection; and
- Performing necessary supplemental tests.

Various ACI documents should be consulted for additional guidance on planning and carrying out the complete investigation (ACI 207.3R, ACI 224.1R, ACI 362R, ACI 437R).

2.1.2 Supplemental tools—Visual inspection is one of the most versatile and powerful NDT methods. However, as mentioned above, its effectiveness depends on the knowl-

edge and experience of the investigator. Visual inspection has the obvious limitation that only visible surfaces can be inspected. Internal defects go unnoticed and no quantitative information is obtained about the properties of the concrete. For these reasons, a visual inspection is usually supplemented by one or more of the other NDT methods discussed in this chapter. The inspector should consider other useful tools that can enhance the power of a visual inspection.

Optical magnification allows a more detailed view of local areas of distress. Available instruments range from simple magnifying glasses to more expensive hand-held microscopes. Some fundamental principles of optical magnification can help in selecting the correct tool. The focal length decreases with increasing magnifying power, which means that the primary lens must be placed closer to the surface being inspected. The field of view also decreases with increasing magnification, making it tedious to inspect a large area at high magnification. The depth of field is the maximum difference in elevation of points on a rough textured surface that

are simultaneously in focus; this also decreases with increasing magnification of the instrument. To assure that the “hills” and “valleys” are in focus simultaneously, the depth of field has to be greater than the elevation differences in the texture of the surface that is being viewed. Finally, the illumination required to see clearly increases with the magnification level, and artificial lighting may be needed at high magnification.

A very useful tool for crack inspection is a small hand-held magnifier with a built-in measuring scale on the lens closest to the surface being viewed (ACI 224.1R). With such a crack comparator, the width of surface cracks can be measured accurately.

A stereo microscope includes two viewing lenses that allow a three-dimensional view of the surface. By calibrating the focus adjustment screw, the investigator can estimate the elevation differences in surface features.

Fiberscopes and borescopes allow inspection of regions that are otherwise inaccessible to the naked eye. A fiberscope is composed of a bundle of optical fibers and a lens system; it allows viewing into cavities within a structure by means of small access holes. The fiberscope is designed so that some fibers transmit light to illuminate the cavity. The operator can rotate the viewing head to allow a wide viewing angle from a single access hole. A borescope is composed of a rigid tube with mirrors and lenses and is designed to view straight ahead or at right angles to the tube. The image is clearer using a borescope, while the fiberscope offers more flexibility in the field of view. Use of these scopes requires drilling small holes if other access channels are absent, and the holes must intercept the cavity to be inspected. Some methods to be discussed in the remainder of the chapter may be used to locate these cavities. Therefore, the fiberscope or borescope may be used to verify the results of other NDT methods without having to take cores.

A recent development that expands the flexibility of visual inspection is the small digital video camera. These are used in a similar manner to borescopes, but they offer the advantage of a video output that can be displayed on a monitor or stored on appropriate recording media. These cameras have optical systems with a charge-coupled device (CCD), and come in a variety of sizes, resolutions, and focal lengths. Miniature versions as small as 12 mm in diameter, with a resolution of 460 scan lines, are available. They can be inserted into holes drilled into the structure for views of internal cavities, or they can be mounted on robotic devices for inspections in pipes or within areas exposed to biological hazards.

In summary, visual inspection is a very powerful NDT method. Its effectiveness, however, is to a large extent governed by the investigator’s experience and knowledge. A broad knowledge of structural behavior, materials, and construction methods is desirable. Visual inspection is typically one aspect of the total evaluation plan, which will often be supplemented by a series of other NDT methods or invasive procedures.

2.2—Stress-wave methods for structures

Several test methods based on stress-wave propagation can be used for nondestructive testing of concrete structures. The ultrasonic* through-transmission method can be used for locating abnormal regions in a member. The echo methods can be used for thickness measurements and flaw detection. The spectral analysis of surface waves (SASW) method can be used to determine the thickness of pavements and elastic moduli of layered pavement systems. The following sub-sections describe the principles and instrumentation for each method. Section 2.3 discusses stress-wave methods for integrity testing of deep foundations. Additional information is given in Sansalone and Carino (1991).

Stress waves occur when pressure or deformation is applied suddenly, such as by impact, to the surface of a solid. The disturbance propagates through the solid in a manner analogous to how sound travels through air. The speed of stress-wave propagation in an elastic solid is a function of the modulus of elasticity, Poisson’s ratio, the density, and the geometry of the solid. This dependence between the properties of a solid and the resultant stress-wave propagation behavior permits inferences about the characteristics of the solid by monitoring the propagation of stress waves.

When pressure is applied suddenly at a point on the surface of a solid half-space, the disturbance propagates through the solid as three different waves. The P-wave and S-wave propagate into the solid along hemispherical wavefronts. The P-wave, also called the dilatational or compression wave, is associated with the propagation of normal stress and particle motion is parallel to the propagation direction. The S-wave, also called the shear or transverse wave, is associated with shear stress and particle motion is perpendicular to the propagation direction. In addition, an R-wave travels away from the disturbance along the surface. In an isotropic, elastic solid, the P-wave speed C_p is related to Young’s modulus of elasticity E ; Poisson’s ratio ν ; and the density ρ as follows (Krautkrämer and Krautkrämer, 1990)

$$C_p = \sqrt{\frac{E(1-\nu)}{\rho(1+\nu)(1-2\nu)}} \quad (2.1)$$

The S-wave propagates at a slower speed C_s given by (Krautkrämer and Krautkrämer, 1990)

$$C_s = \sqrt{\frac{G}{\rho}} \quad (2.2)$$

where G = the shear modulus of elasticity.

A useful parameter is the ratio of S-wave speed to P-wave speed

* “Ultrasonic” refers to stress waves above the audible range, which is usually assumed to be above a frequency of 20 kHz.

$$\frac{C_s}{C_p} = \sqrt{\frac{1-2\nu}{2(1-\nu)}} \quad (2.3)$$

For a Poisson's ratio of 0.2, which is typical of concrete, this ratio equals 0.61. The ratio of the R-wave speed C_r to the S-wave speed may be approximated by the following formula (Krautkrämer and Krautkrämer, 1990)

$$\frac{C_r}{C_s} = \frac{0.87 + 1.12\nu}{1 + \nu} \quad (2.4)$$

For a Poisson's ratio between 0.15 and 0.25, the R-wave travels from 90 to 92 percent of the S-wave speed.

Eq. (2.1) represents the P-wave speed in an infinite solid. In the case of bounded solids, the wave speed is also affected by the geometry of the solid. For wave propagation along the axis of slender bar, the wave speed is independent of Poisson's ratio and is given by the following

$$C_b = \sqrt{\frac{E}{\rho}} \quad (2.5)$$

where C_b is the bar wave speed. For a Poisson's ratio between 0.15 and 0.25, the wave speed in a slender bar is from 3 to 9 percent slower than the P-wave speed in a large solid.

When a stress wave traveling through Material 1 is incident on the interface between a dissimilar Material 2, a portion of the incident wave is reflected. The amplitude of the reflected wave is a function of the angle of incidence and is a maximum when this angle is 90 deg (normal incidence). For normal incidence, the reflection coefficient R is given by the following

$$R = \frac{Z_2 - Z_1}{Z_2 + Z_1} \quad (2.6)$$

where

R = ratio of sound pressure of the reflected wave to the sound pressure of the incident wave,

Z_2 = specific acoustic impedance of Material 2, and

Z_1 = specific acoustic impedance of Material 1.

The specific acoustic impedance is the product of the wave speed and density of the material. The following are approximate Z -values for some materials (Sansalone and Carino, 1991)

Material	Specific acoustic impedance, kg/(m ² s)
Air	0.4
Water	1.5×10^6
Soil	$0.3 \text{ to } 4 \times 10^6$
Concrete	$7 \text{ to } 10 \times 10^6$
Limestone	$7 \text{ to } 19 \times 10^6$
Granite	$15 \text{ to } 17 \times 10^6$
Steel	47×10^6

Thus, for a stress wave that encounters an air interface as it travels through concrete, the absolute value of the reflection coefficient is nearly 1.0 and there is almost total reflection at the interface. This is why NDT methods based on stress-wave propagation have proven to be successful for locating defects within concrete.

2.2.1 Ultrasonic through transmission method—One of the oldest NDT methods for concrete is based on measuring the travel time over a known path length of a pulse of ultrasonic compressional waves. The technique is known as ultrasonic through transmission, or, more commonly, the ultrasonic pulse velocity method. Naik and Malhotra (1991) provide a summary of this test method, and Tomsett (1980) reviewed the various applications of the technique.

The development of field instruments to measure the pulse velocity occurred nearly simultaneously in the late 1940s in Canada and England (Whitehurst, 1967). In Canada, there was a desire for an instrument to measure the extent of cracking in dams (Leslie and Cheesman, 1949). In England, the emphasis was on the development of an instrument to assess the quality of concrete pavements (Jones, 1949).

Principle—As mentioned above, the speed of propagation of stress waves depends on the density and the elastic constants of the solid. In a concrete member, variations in density can arise from nonuniform consolidation, and variations in elastic properties can occur due to variations in materials, mix proportions, or curing. Thus, by determining the wave speed at different locations in a structure, it is possible to make inferences about the uniformity of the concrete. The compressional wave speed is determined by measuring the travel time of the stress pulse over a known distance.

The testing principle is illustrated in Fig. 2.2.1(a),* which depicts the paths of ultrasonic pulses as they travel from one side of a concrete member to the other side. The top case represents the shortest direct path through sound concrete, and it would result in the shortest travel time, or the fastest apparent wave speed. The second case from the top represents a path that passes through a portion of inferior concrete, and the third case shows a diffracted path around the edge of a large void (or crack). In these latter cases, the travel time would be greater than the first case. The last case indicates a travel path that is interrupted by a void. This air interface results in total reflection of the stress waves and there would be no arrival at the opposite side. The apparent wave speeds would be determined by dividing the member thickness by the measured travel time. A comparison of the wave speeds at the different test points would indicate the areas of anomalies within the member. It may also be possible to use signal attenuation as an indicator of relative quality of concrete, but this requires special care to ensure consistent coupling of the transducers at all test points (Teodoru, 1994).

Apparatus for through-transmission measurements has also been used on the same surface as shown in Fig. 2.2.2(a).

* The first two numbers of a figure or table represent the chapter and section in which the figure or table is first mentioned.

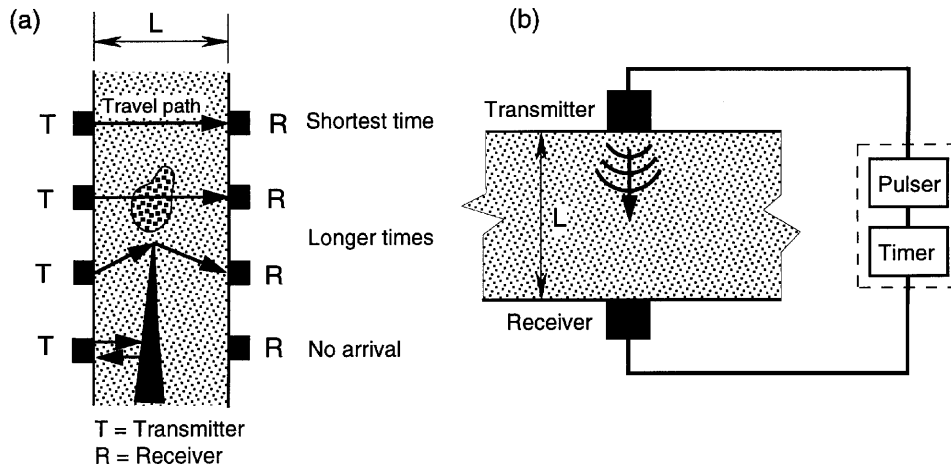


Fig. 2.2.1—(a) Effects of defects on travel time of ultrasonic pulse; and (b) schematic of through-transmission test system.

This approach has been suggested for measuring the depth of a fire-damaged surface layer having a lower wave speed than the underlying sound concrete (Chung and Law, 1985) and for measuring the depth of concrete damaged by freezing (Teodoru and Herf, 1996). The test is carried out by measuring the travel time as a function of the separation X between transmitter and receiver. The method assumes that stress-wave arrival at the receiver occurs along two paths: Path 1, which is directly through the damaged concrete, and Path 2, which is through the damaged and the sound concrete. For small separation, the travel time is shorter for Path 1, and for large separation the travel time is shorter for Path 2. By plotting the travel time as a function of the distance X , the presence of a damaged surface layer is indicated by a change in the slope of the data. The distance X_o , at which the travel times for the two paths are equal, is found from the intersection of the straight lines as shown in Fig. 2.2.2(b). The slopes of the two lines are reciprocals of the wave speeds in the damaged and sound concrete. The depth of the damaged layer is found from the following (Chung and Law, 1985)

$$d = \frac{X_o}{2} \sqrt{\frac{V_s - V_d}{V_s + V_d}} \quad (2.7)$$

The surface method relies on measuring the arrival time of low amplitude waves, and the user should understand the capabilities of the instrument to measure the correct arrival times. The user should also be familiar with the underlying theory of seismic refraction (Richart et al., 1970) that forms the basis of Eq. (2.7). The method is only applicable if the upper layer has a slower wave speed than the lower layer.

Instrumentation—The main components of modern devices for measuring the ultrasonic pulse velocity are shown schematically in Fig. 2.2.1(b). A transmitting transducer is positioned on one face of the member and a receiving transducer is positioned on the opposite face. The transducers contain piezoelectric ceramic elements. Piezoelectric materials change dimension when a voltage is applied to them, or they produce a voltage change when they are deformed. A

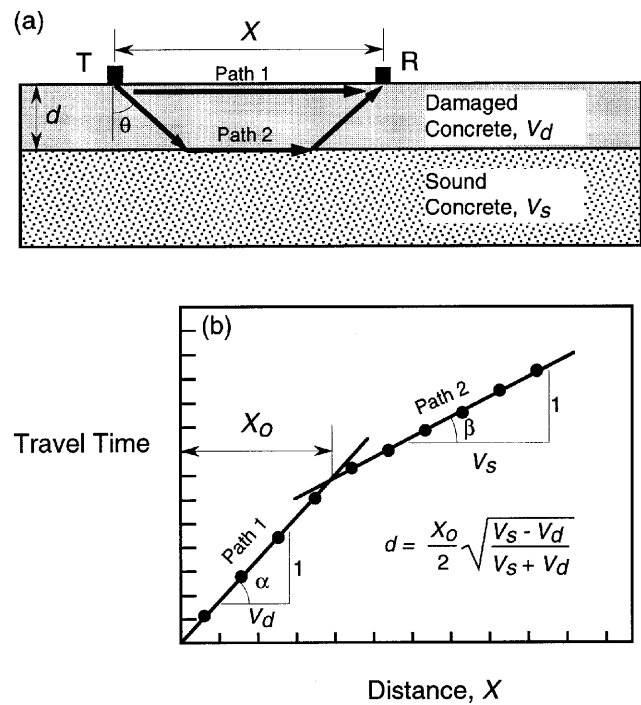


Fig. 2.2.2—(a) Wave paths for ultrasonic testing on surface of concrete having damaged surface layer; and (b) travel time as a function of distance between transmitter and receiver.

pulser is used to apply a high voltage to the transmitting transducer (source), and the suddenly applied voltage causes the transducer to vibrate at its natural frequency. The vibration of the transmitter produces the stress pulse that propagates into the member. At the same time that the voltage pulse is generated, a very accurate electronic timer is turned on. When the pulse arrives at the receiver, the vibration is changed to a voltage signal that turns off the timer, and a display of the travel time is presented. The requirements for a suitable pulse-velocity device are given in ASTM C 597.

The transducers are coupled to the test surfaces using a viscous material, such as grease, or a non-staining ultrasonic

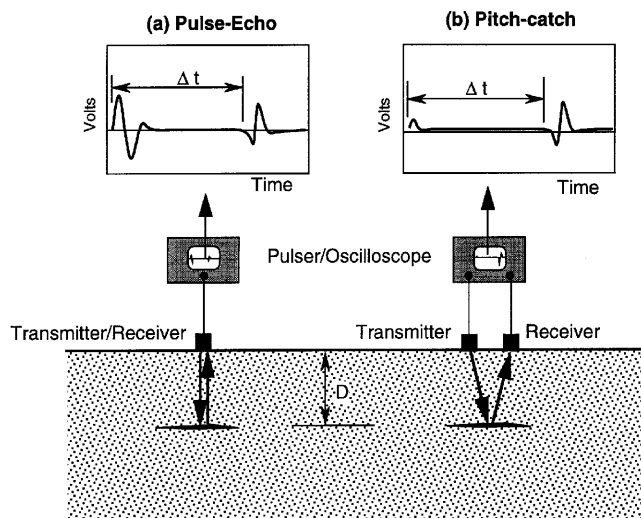


Fig. 2.2.3—Schematic of ultrasonic pulse-echo and pitch-catch methods.

gel couplant if staining of the concrete is a problem. Transducers of various resonant frequencies have been used, with 50-kHz transducers being the most common. Generally, lower-frequency transducers are used for mass concrete (20 kHz) and higher-frequency transducers (> 100 kHz) are used for thinner members where accurate travel times have to be measured. In most applications, 50-kHz transducers are suitable.

2.2.2 Ultrasonic-echo method—Some of the drawbacks of the through-transmission method are the need for access to both sides of the member and the lack of information on the location (depth) of a detected anomaly. These limitations can be overcome by using the *echo methods*, in which the testing is performed on one face of the member and the arrival time of a stress wave *reflected* from a defect is determined. This approach has been developed for testing metals, and it is known as the *pulse-echo method*. Since the 1960s, a number of different experimental ultrasonic-echo systems have been developed for concrete (Bradfield and Gatfield, 1964; Howkins, 1968). Successful applications have been limited mainly to measuring the thickness of and detecting flaws in thin slabs, pavements, and walls (Mailer, 1972; Alexander and Thornton, 1989).

Principle—In the pulse-echo method, a stress pulse is introduced into an object at an accessible surface by a transmitter. The pulse propagates into the test object and is reflected by flaws or interfaces. The surface response caused by the arrival of reflected waves, or echoes, is monitored by the same transducer acting as a receiver. This technique is illustrated in Fig. 2.2.3(a). Due to technical problems in developing a suitable pulse-echo transducer for testing concrete, successful ultrasonic-echo methods have, in the past, used a separate receiving transducer located close to the transmitting transducer. Such a system is known as *pitch-catch*, and is illustrated in Fig. 2.2.3(b). The receiver output is displayed on an oscilloscope as a time-domain waveform. The round-trip travel time of the pulse can be obtained from the waveform by determining the time from the start of the transmitted

pulse to the reception of the echo. If the wave speed in the material is known, this travel time can be used to determine the depth of the reflecting interface.

Instrumentation—The key components of an ultrasonic-echo test system are the transmitting and receiving transducer(s), a pulser, and an oscilloscope. Transducers that transmit and receive short-duration, low-frequency* (≈ 200 kHz), focused waves are needed for testing concrete. However, it is difficult to construct such transducers, and often their dimensions become very large, making the transducers cumbersome and difficult to couple to the surface of the concrete (Mailer, 1972). Recent advances have resulted in improved transducers (Alexander and Thornton, 1989), but their penetration depths are limited to about 250 mm.

A true pulse-echo system (source and receiver are one transducer) has been developed and applied to concrete with small-sized aggregate (Hillger, 1993). This system uses a heavily damped 500-kHz transducer as both the source and receiver. A micro-computer is used to process the data and display the results using conventional techniques, as in ultrasonic testing of metals. One of these display methods is the B-scan, in which successive time-domain traces, obtained as the transducer is scanned over the test object, are oriented vertically and placed next to each other. The resulting plot is a cross-sectional view of the object showing the location of reflecting interfaces along the scan line. Fig. 2.2.4(a) shows a concrete specimen made with 8-mm aggregate and containing an artificial defect at a depth of 65 mm. Fig. 2.2.4(b) shows the B-scan produced as the transducer was moved across the surface of the specimen (Hillger, 1993). The use of very high frequencies with the pulse-echo method may be beneficial in terms of improved defect resolution. However, the penetration depth is limited, and the performance in concrete with larger aggregates is not known. At this time, not much field experience has been accumulated with the ultrasonic pulse-echo method for concrete.

2.2.3 Impact-echo method—Using an impact to generate a stress pulse is an old idea that has the advantage of eliminating the need for a bulky transmitting transducer and providing a stress pulse with greater penetration ability. However, the stress pulse generated by impact at a point is not focused like a pulse from an ultrasonic transducer. Instead, waves propagate into a test object in all directions, and reflections may arrive from many directions. Since the early 1970s, impact methods, usually referred to as seismic-echo (or sonic-echo) methods, have been widely used for evaluation of concrete piles and drilled shaft foundations (Steinbach and Vey, 1975). These foundation NDT methods are discussed in Section 2.3.1. Beginning in the mid-1980s, the impact-echo technique was developed for testing of concrete structural members (Sansalone and Carino, 1986; Sansalone, 1997). Applications of the impact-echo technique include: determining the thickness of and detecting flaws in plate-like structural members, such as slabs and bridge decks with or

* A frequency of 200 kHz is considered low compared to higher frequencies used in pulse-echo systems for testing metals, where frequencies in excess of 1 MHz are common.

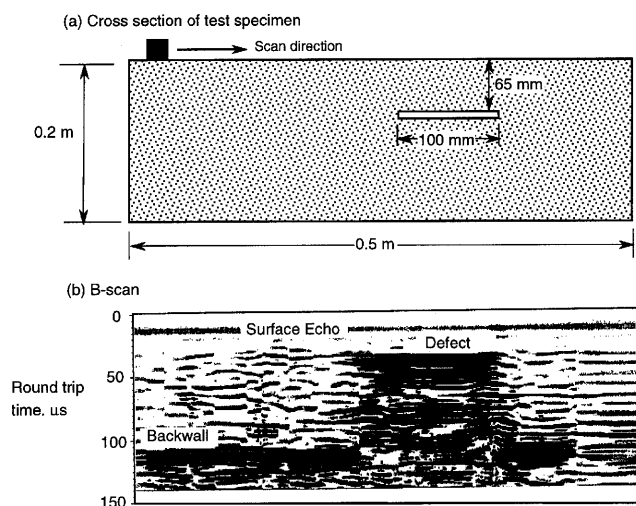


Fig. 2.2.4—Example of ultrasonic pulse-echo test on concrete: (a) test specimen with artificial defect; and (b) B-scan showing location of defect (adapted from Hillger, 1993).

without overlays; detecting flaws in beams, columns and hollow cylindrical structural members; assessing the quality of bond in overlays; and crack-depth measurement (Sansalone and Streett, 1997; Sansalone and Carino, 1988, 1989a, 1989b; Lin [Y.] and Sansalone, 1992a, 1992b, 1992c; Cheng and Sansalone, 1993; Lin [J. M.] and Sansalone, 1993, 1994a, 1994b, 1996; Lin and Su, 1996).

Principle—The principle of the impact-echo technique is illustrated in Fig. 2.2.5(a). A transient stress pulse is introduced into a test object by mechanical impact on the surface. The P- and S-waves produced by the stress pulse propagate into the object along hemispherical wavefronts. In addition, a surface wave travels along the surface away from the impact point. The waves are reflected by internal interfaces or external boundaries. The arrival of these reflected waves, or echoes, at the surface where the impact was generated produces displacements that are measured by a receiving transducer and recorded using a data-acquisition system. Interpretation of waveforms in the time domain has been successful in seismic-echo applications involving long slender structural members, such as piles and drilled shafts (Steinbach and Vey, 1975; Olson and Wright, 1990). In such cases, there is sufficient time between the generation of the stress pulse and the reception of the wave reflected from the bottom surface, or from an inclusion or other flaw, so that the arrival time of the reflected wave is generally easy to determine even if long-duration impacts produced by hammers are used.

For relatively thin structural members such as slabs and walls, time-domain analysis is feasible if short-duration impacts are used, but it is time-consuming and can be difficult depending on the geometry of the structure (Sansalone and Carino, 1986). The preferred approach, which is much quicker and simpler, is frequency analysis of displacement waveforms (Carino et al., 1986). The underlying principle of frequency analysis is that the stress pulse generated by the impact undergoes multiple reflections between the test sur-

face and the reflecting interface (flaw or boundaries). The frequency of arrival of the reflected pulse at the receiver depends on the wave speed and the distance between the test surface and the reflecting interface. For the case of reflections in a plate-like structure, this frequency is called the thickness frequency, and it varies as the inverse of the member thickness.

In frequency analysis, the time-domain signal is transformed into the frequency domain using the fast Fourier transform technique. The result is an *amplitude spectrum* that indicates the amplitude of the various frequency components in the waveforms. The frequency corresponding to the arrival of the multiple reflections of the initial stress pulse, that is, the thickness frequency, is indicated by a peak in the amplitude spectrum. For a plate-like structure, the approximate* relationship between the distance D to the reflecting interface, the P-wave speed C_p and the thickness frequency f is as follows

$$D = \frac{C_p}{2f} \quad (2.8)$$

As an example, Fig. 2.2.5(b) shows the amplitude spectrum obtained from an impact-echo test of a 0.5-m-thick concrete slab. The peak at 3.42 kHz corresponds to the thickness frequency of the solid slab, and a velocity of 3,420 m/s is calculated. Fig. 2.2.5(c) shows the amplitude spectrum for a test over a void within the same slab. The peak has shifted to a frequency of 7.32 kHz, indicating that the reflections are occurring from an interface within the slab. The ratio 3.42 kHz/7.32 kHz = 0.46 indicates that the interface is at approximately the middle of the slab with a calculated depth of 0.23 m.

In using the impact-echo method to determine the locations of flaws within a slab or other plate-like structure, tests can be performed at regularly spaced points along lines marked on the surface. Spectra obtained from such a series of tests can be analyzed with the aid of computer software that can identify those test points corresponding to the presence of flaws and can plot a cross-sectional view along the test line (Pratt and Sansalone, 1992).

Frequency analysis of signals obtained from impact-echo tests on bar-like structural elements, such as reinforced concrete beams and columns, bridge piers, and similar members, is more complicated than the case of slab-like structural members. The presence of the side boundaries gives rise to transverse modes of vibration of the cross section. Thus, prior to attempting to interpret test results, the characteristic frequencies associated with the transverse modes of vibration of a solid structural member have to be determined. These frequencies depend upon the shape and dimensions of the cross section. It has been shown that the presence of a flaw disrupts these modes, making it possible to determine that a flaw exists (Lin and Sansalone, 1992a, 1992b, 1992c).

* For accurate assessment of plate thickness, the P-wave speed in Eq. (2.8) should be multiplied by 0.96 (Sansalone and Streett 1997).

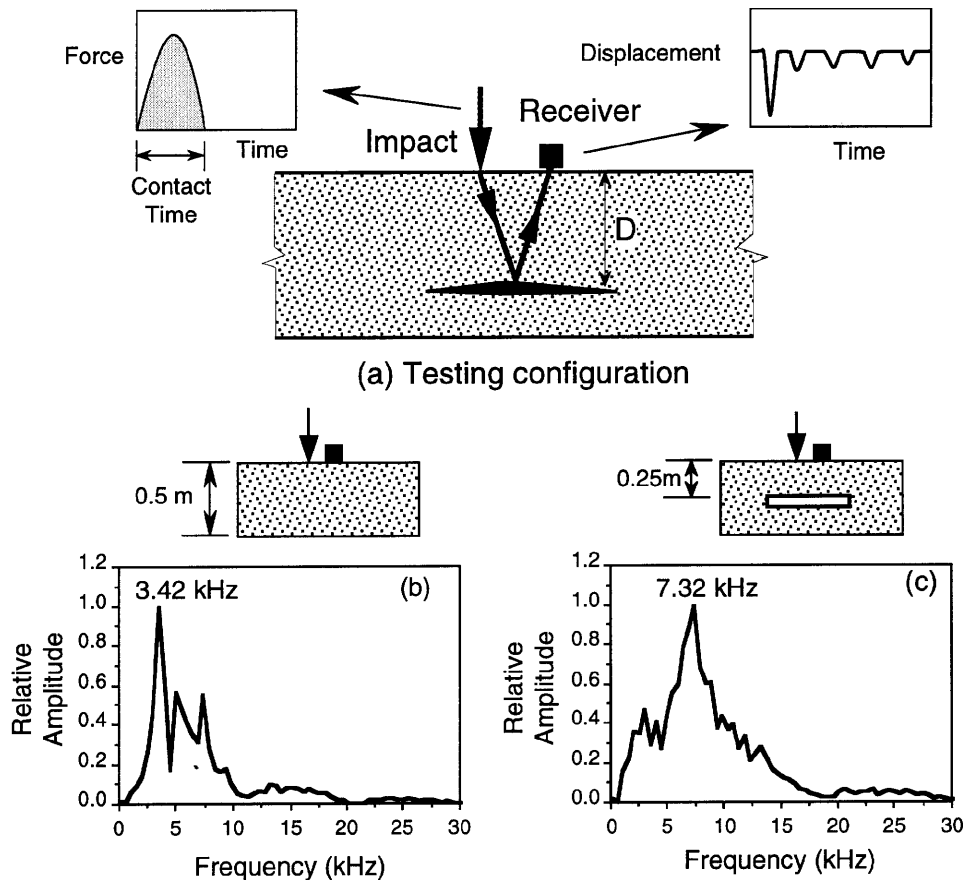


Fig. 2.2.5—(a) Schematic of impact-echo method; (b) amplitude spectrum for test of solid slab; and (c) amplitude spectrum for test over void in slab.

Instrumentation—An impact-echo test system is composed of three components: an impact source; a receiving transducer; and a data-acquisition system that is used to capture the output of the transducer, store the digitized waveforms, and perform signal analysis. A suitable impact-echo test system can be assembled from off-the-shelf components. In 1991, a complete field system (hardware and analysis software) became commercially available.

The selection of the impact source is a critical aspect of a successful impact-echo test system. The impact duration determines the frequency content of the stress pulse generated by the impact, and determines the minimum flaw depth that can be determined. As the impact duration is shortened, higher-frequency components are generated. In evaluation of piles, hammers are used that produce energetic impacts with long contact times (greater than 1 ms) suitable for testing long, slender structural members. Impact sources with shorter-duration impacts (20 to 80 μ s), such as spring-loaded spherically-tipped impactors, have been used for detecting flaws within structural members less than 1 m thick.

In evaluation of piles, geophones (velocity transducers) or accelerometers have been used as the receiving transducer. For impact-echo testing of slabs, walls, beams, and columns, a broad-band, conically-tipped, piezoelectric transducer (Proctor, 1982) that responds to surface displacement has

been used as the receiver (Sansalone and Carino, 1986). Small accelerometers have also been used as the receiver. In this case, additional signal processing is carried out in the frequency domain to obtain the appropriate amplitude spectrum (Olson and Wright, 1990). Such accelerometers must have resonant frequencies well above the anticipated thickness frequencies to be measured.

2.2.4 Spectral analysis of surface waves (SASW) method—In the late 1950s and early 1960s, Jones reported on the use of surface waves to determine the thickness and elastic stiffness of pavement slabs and of the underlying layers (Jones, 1955; Jones, 1962). The method involved determining the relationship between the wavelength and velocity of surface vibrations as the vibration frequency was varied. Apart from the studies reported by Jones and work in France during the 1960s and 1970s, there seems to have been little additional use of this technique for testing concrete pavements. In the early 1980s, however, researchers at the University of Texas at Austin began studies of a surface wave technique that involved an impactor or vibrator that excited a range of frequencies. Digital signal processing was used to develop the relationship between wavelength and velocity. The technique was called spectral analysis of surface waves (SASW) (Heisey et al., 1982; Nazarian et al., 1983). The SASW method has been used successfully to determine the stiffness

profiles of soil sites, asphalt and concrete pavement systems, and concrete structural members. The method has been extended to the measurement of changes in the elastic properties of concrete slabs during curing, the detection of voids, and assessment of damage (Bay and Stokoe, 1990; Kalinski et al., 1994).

Principle—The general test configuration is illustrated in Fig. 2.2.6 (Nazarian and Stokoe, 1986a). An impact is used to generate a surface or R-wave. Two receivers are used to monitor the motion as the R-wave propagates along the surface. The received signals are processed and a subsequent calculation scheme is used to infer the stiffnesses of the underlying layers.

Just as the stress pulse from impact contains a range of frequency components, the R-wave also contains a range of components of different frequencies or wavelengths. (The product of frequency and wavelength equals wave speed.) This range depends on the contact time of the impact; a shorter contact time results in a broader range. The longer-wavelength (lower-frequency) components penetrate more deeply, and this is the key to using the R-wave to gain information about the properties of the underlying layers (Rix and Stokoe, 1989). In a layered system, the propagation speed of these different components is affected by the wave speed in those layers through which the components propagate. A layered system is a dispersive medium for R-waves, which means that different frequency components of the R-wave propagate with different speeds, which are called phase velocities.

Phase velocities are calculated by determining the time it takes for each frequency (or wavelength) component to travel between the two receivers. These travel times are determined from the phase difference of the frequency components arriving at the receivers (Nazarian and Stokoe, 1986b). The phase differences are obtained by computing the cross-power spectrum of the signals recorded by the two receivers. The phase portion of the cross-power spectrum gives phase differences (in degrees) as a function of frequency. The phase velocities are determined as follows

$$C_{R(f)} = X \frac{360}{\phi_f} f \quad (2.9)$$

where

$C_{R(f)}$ = surface wave speed of component with frequency f ,

X = distance between receivers (see Fig. 2.2.6), and

ϕ_f = phase angle of component with frequency f .

The wavelength λ_f , corresponding to a component frequency, is calculated using the following equation

$$\lambda_f = X \frac{360}{\phi_f} \quad (2.10)$$

By repeating the calculations in Eq. (2.9) and (2.10) for each component frequency, a plot of phase velocity versus

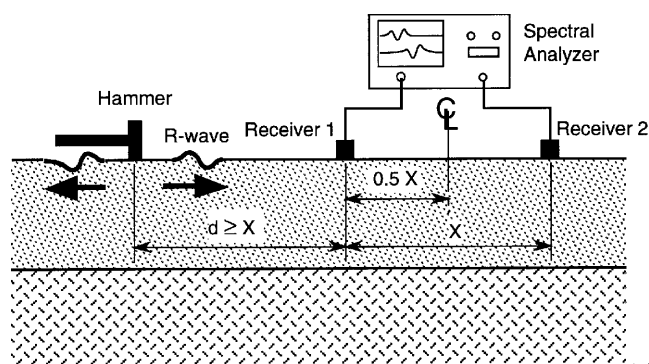


Fig. 2.2.6—Schematic of spectral analysis of surface wave (SASW) method.

wavelength is obtained. Such a plot is called a dispersion curve. Fig. 2.2.7(a) shows an example of a dispersion curve obtained by Nazarian and Stokoe (1986a) from tests on a concrete pavement. The short-wavelength components have higher speeds because they correspond to components traveling through the concrete slab.

A process called inversion* is used to obtain the approximate stiffness profile at the test site from the experimental dispersion curve (Nazarian and Stokoe, 1986b; Nazarian and Desai, 1993; Yuan and Nazarian, 1993). The test site is modeled as layers of varying thickness. Each layer is assigned a density and elastic constants. Using this information, the solution for surface wave propagation in a layered system is obtained and a theoretical dispersion curve is calculated for the assumed layered system. The theoretical curve is compared with the experimental dispersion curve. If the curves match, the problem is solved and the assumed stiffness profile is correct. If there are significant discrepancies, the assumed layered system is changed or refined and a new theoretical curve is calculated. This process continues until there is good agreement between the theoretical and experimental curves.

Instrumentation—There are three components to a SASW test system: the energy source is usually a hammer but may be a vibrator with variable frequency excitation; two receivers that are geophones (velocity transducers) or accelerometers; and a two-channel spectral analyzer for recording and processing the waveforms.

The required characteristics of the impact source depend on the stiffnesses of the layers, the distances between the two receivers, and the depth to be investigated (Nazarian et al., 1983). When investigating concrete pavements and structural members, the receivers are located relatively close together. In this case, a small hammer (or even smaller impactor/vibrator) is required so that a short-duration pulse is produced with sufficient energy at frequencies up to about 50 to 100 kHz. As the depth to be investigated increases, the distance between receivers is increased, and an impact that

* Although it is called "inversion," the technique actually uses forward modeling, with trial and error, until there is agreement between the measured and computed dispersion curves.

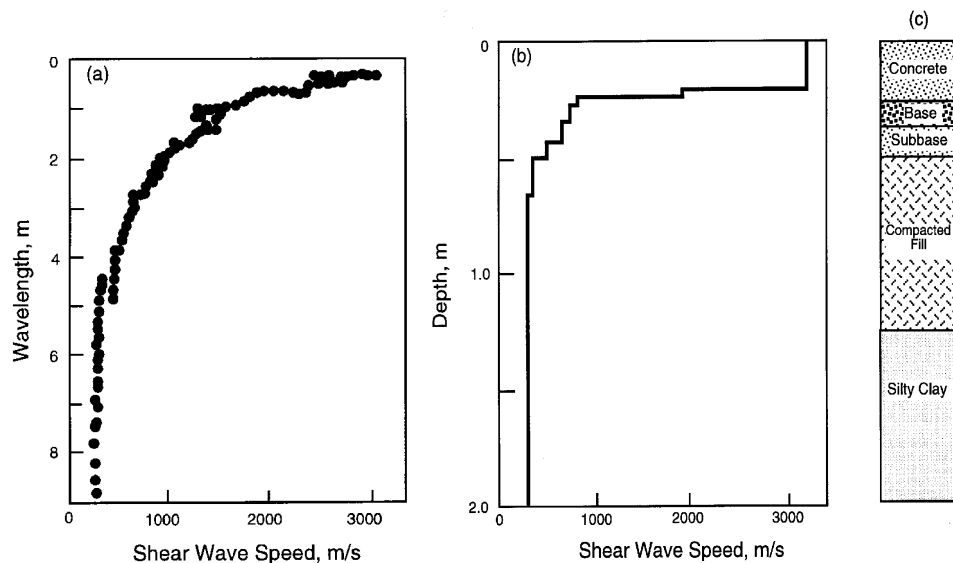


Fig. 2.2.7—(a) Dispersion curve obtained from SASW testing of concrete pavement; (b) *S*-wave speed obtained from inversion of experimental dispersion curve; and (c) soil profile based on boring (adapted from Nazarian and Stokoe, 1986a).

generates a pulse with greater energy at lower frequencies is required. Thus, heavier hammers, such as a sledge hammer, are used.

The two receiving transducers measure vertical surface velocity or acceleration. The selection of transducer type depends, in part, on the test site (Nazarian and Stokoe, 1986a). For tests where deep layers are to be investigated and larger receiver spacings are required, geophones are generally used because of their superior low-frequency sensitivity. For tests of concrete pavements, the receivers must provide accurate measurements at higher frequencies. Thus, for pavements, a combination of geophones and accelerometers is often used. For concrete structural members, small accelerometers and small impactors or high-frequency vibrators are typically used (Bay and Stokoe, 1990).

The receivers are first located close together, and the spacing is increased by a factor of two for subsequent tests. As a check on the measured phase information for each receiver spacing, a second series of tests is carried out by reversing the position of the source. Typically, five receiver spacings are used at each test site. For tests of concrete pavements, the closest spacing is usually about 0.15 m (Nazarian and Stokoe 1986b).

2.2.5 Advantages and limitations—Each of the stress-wave propagation methods have distinct advantages and limitations, as summarized in Table 2.2. The ultrasonic pulse velocity method is the only technique that has been standardized by ASTM,^{*} and a variety of commercial devices are available. The various echo-methods are not standardized, have relatively little research and field experiences, and commercial test systems are just beginning to be available. The SASW method suffers from the complexity of the signal processing, but efforts were begun to automate this signal processing (Nazarian and Desai, 1993).

2.3—Stress-wave methods for deep foundations

Since the 1960s, test methods based on stress-wave propagation have been commercially available for the nondestructive testing of concrete deep foundations and mass concrete. First developed in France and Holland, they are now routinely specified as quality control tools for new pile construction in western Europe, northern Africa, and parts of eastern Asia. Their present use on the North American continent is less widespread. Recent improvements in electronic hardware and portable computers have resulted in more reliable and faster testing systems that are less subject to operator influence both in testing procedure and in the analysis of test results.

Two distinct groupings of stress-wave methods for deep foundations are apparent:

- Reflection techniques, and
- Direct transmission through the concrete.

2.3.1 Sonic-echo method—This method is the earliest of all NDT methods to become commercially available (Paquet, 1968; Steinbach and Vey, 1975; Van Koten and Middendorp, 1981) for deep-foundation integrity or length evaluation. This method is known variously as the seismic-echo, sonic-echo, or PIT (Pile Integrity Test) (Rausche and Seitz, 1983).

Principle—The sonic-echo method uses a small impact delivered at the head of the deep foundation (pile or shaft), and measures the time taken for the stress wave generated by the impact to travel down the pile and to be reflected back to a transducer (usually an accelerometer) coupled to the pile head. The impact is typically from a small sledgehammer (hand sledge) with an electronic trigger. The time of impact

* In 1998, a standard on using the impact-echo method to measure thickness of concrete members was approved by ASTM with the designation C 1383.

Table 2.2—Advantages and limitations of stress-wave methods for structures

Method	Advantages	Limitations
Ultrasonic through or direct transmission (pulse velocity)	Portable equipment is available; relatively easy to use.	Requires access to two sides of members; does not provide information on depth of defect.
Ultrasonic-echo	Access to only one face is needed; provides information on depth of defect.	Applicable to limited member thickness; not commercially available; experienced operator is required.
Impact-echo	Access to only one face is needed; equipment is commercially available; capable of locating a variety of defects; does not require coupling materials.	Experienced operator is required; current instrumentation limited to testing members less than 2 m thick.
Spectral analysis of surface waves	Capable of determining the elastic properties of layered systems, such as pavements, interlayered good and poor-quality concrete.	Experienced operator is required; involves complex signal processing.

and the pile head vertical movement after impact are recorded either by an oscilloscope or by a digital data acquisition device that records the data on a time base. Fig. 2.3.1 illustrates the results of a sonic-echo test on a concrete shaft.

If the length of the pile shaft is known and the transmission time for the stress wave to return to the transducer is measured, then its velocity can be calculated. Conversely, if the velocity is known, then the length can be deduced. Since the velocity of the stress wave is primarily a function of the dynamic elastic modulus and density of the concrete, the calculated velocity can provide information on concrete quality. Where the stress wave has traveled the full length of the shaft, these calculations are based on the formula

$$C_b = \frac{2L}{\Delta t} \quad (2.11)$$

where

C_b = bar wave speed in concrete

L = shaft length

Δt = transit time of stress wave

Empirical data have shown that a typical range of values for C_b can be assumed, where 3800 to 4000 m/s would indicate good-quality concrete, with a compressive strength on the order of 30 to 35 MPa (Stain, 1982). The actual strength will vary according to aggregate type and mixture proportions, and these figures should be used only as a broad guide to concrete quality.

Where the length of the shaft is known, an early arrival of the reflected wave means that it has encountered a reflector (change in stiffness or density) other than the toe of the shaft. This may be a break or defect in the shaft, a significant change in shaft cross section, or the point at which the shaft is restrained by a stiffer soil layer. In certain cases, the polarity of the reflected wave (whether positive or negative with respect to the initial impact) can indicate whether the apparent defect is from an increase or decrease of stiffness at the reflective point.

The energy imparted to the shaft by the impact is small, and the damping effect of the soils around the shaft will

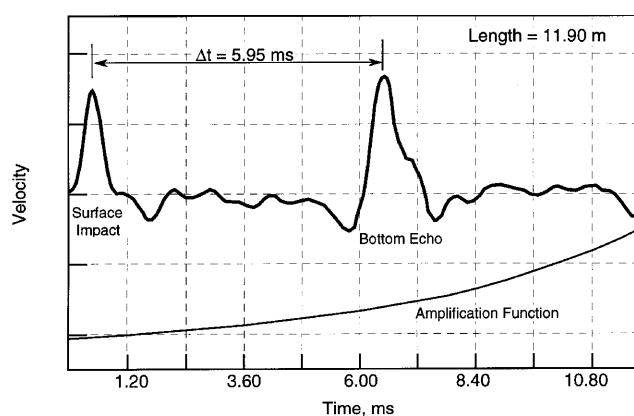


Fig. 2.3.1—Example of sonic-echo test result (signal is amplified by function at bottom of graph).

progressively dissipate that energy as the stress wave travels down and up the shaft. To increase information from the test, the signal response can be progressively amplified with time.

Depending on the stiffness of the lateral soils, a limiting length-to-diameter ratio (L/d) exists beyond which all the wave energy is dissipated and no response is detected at the shaft head. In this situation, the only information that can be derived is that there are no significant defects in the upper portion of the shaft, since any defect closer to the head than the critical L/d ratio would reflect part of the wave. This limiting L/d ratio will vary according to the adjacent soils, with a typical value of 30 for medium stiff clays.

2.3.2 Impulse-response (mobility) method—This method was originally developed as a steady state vibration test in France (Davis and Dunn, 1974), where a controlled force was applied to the pile shaft head by a swept-frequency generator. The vertical shaft response was recorded by geophone velocity transducers, and the input force from the vibrator was continuously monitored. The resulting response curve plotted the shaft *mobility* (geophone particle velocity/vibrator force v/F) against frequency, usually in the useful frequency range of 0 to 2000 Hz.

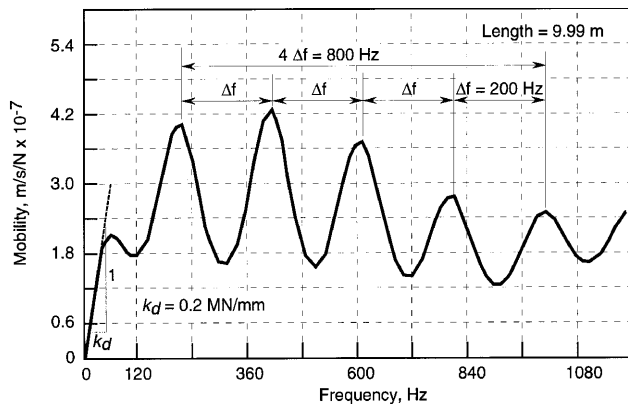


Fig. 2.3.2—Example of impulse-response (mobility) plot for test of pile.

The evolution of data-processing equipment during the 1980s and 1990s allowed the use of computers on site to transform the shaft response due to a hammer impact (similar to that used in the sonic-echo method) into the frequency domain (Stain, 1982; Olson et al., 1990). This reduced the effort to obtain the mobility as a function of frequency. Other studies demonstrated that the impulse-response method could be applied to integrity testing of other structures besides deep foundations (Davis and Hertlein, 1990).

Principle—A blow on the shaft head by a small sledgehammer equipped with a load cell generates a stress wave with a wide frequency content, which can vary from 0 to 1000 Hz for soft rubber-tipped hammers to 0 to 3000 Hz for metal-tipped hammers. The load cell measures the force input, and the vertical response of the shaft head is monitored by a geophone.

The force and velocity time-base signals are recorded by a digital acquisition device, and then processed by computer using the fast Fourier transform (FFT) algorithm to convert the data to the frequency domain. Velocity is then divided by force to provide the unit response, or transfer function, which is displayed as a graph of shaft mobility versus frequency.

An example of a mobility plot for a pile shaft is given in Fig. 2.3.2. This response curve consists of two major portions, which contain the following information:

- At low frequencies (< 100 Hz), lack of inertial effects cause the pile/soil composite to behave as a spring, and this is shown as a linear increase in amplitude from zero with increasing frequency. The slope of this portion of the graph is known as the compliance or flexibility, and the inverse of flexibility is the dynamic stiffness. The dynamic stiffness is a property of the shaft/soil composite, and can therefore be used to assess shafts on a comparative basis, either to establish uniformity, or as an aid to selecting a representative shaft for full-scale load testing by either static or dynamic means.
- The higher-frequency portion of the mobility curve represents longitudinal resonance of the shaft. The fre-

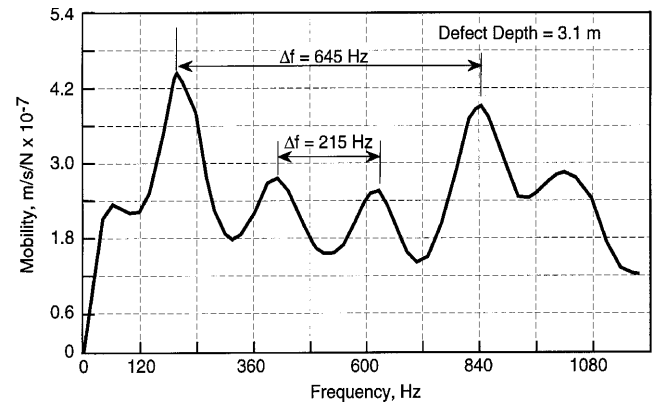


Fig. 2.3.3—Impulse-response (mobility) plot of pile with necked section at distance of 2.4 m from top.

quencies of these resonances are a function of the shaft length and the degree of shaft toe anchorage, and their relative amplitude is a function of the lateral soil damping. The frequency difference between adjacent peaks is constant and is related to the length of the shaft and the wave speed of the concrete according to Eq. (A.1) in Appendix A. The mean amplitude of this resonating portion of the curve is a function of the impedance of the pile shaft, which depends, in turn, upon the shaft cross-sectional area, the concrete density, and the bar wave propagation velocity C_b (see Appendix A).

As with the sonic-echo test, when the shaft length is known, a shorter apparent length measurement will indicate the presence of an anomaly. Appendix A describes how additional information can be derived from the mobility-frequency plot, such as the pile cross section and dynamic stiffness, which can help in differentiating between an increase or a reduction in cross section.

Fig. 2.3.3 shows a mobility plot of a 9.1-m-long pile with similar soil conditions to the pile in Fig. 2.3.2, but with a necked section at 3.1 m. The pile tip reflection from 9.1 m is clearly visible on the plot, as indicated by the constant frequency spacing between resonant peaks of 215 Hz. The frequency spacing of 645 Hz between the two most prominent peaks corresponds to the reflection from the necked section at a depth of 3.1 m.

In common with the sonic-echo test, a relatively small amount of energy is generated by the hammer impact, and soil damping effects limit the depth from which useful information may be obtained. However, even where no measurable shaft base response is present, the dynamic stiffness is still a useful parameter for comparative shaft assessment.

2.3.3 Impedance logging—A recent approach to interpreting the responses from a combination of both sonic-echo and mobility surface reflection methods is impedance logging (Paquet, 1991), where the information from the amplified time-domain response of the sonic echo is combined with the characteristic impedance of the shaft measured with the mobility test.

Principle—Even though the force applied to the head of the shaft by the surface reflection methods is transient, the

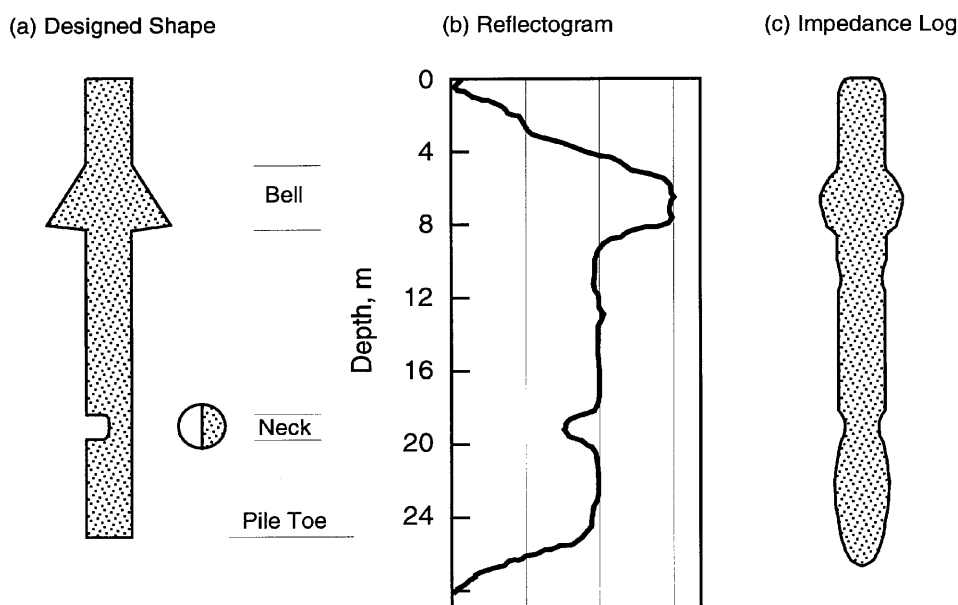


Fig. 2.3.4—(a) Planned defects in experimental pile; (b) reflectogram obtained by signal processing of sonic-echo data; and (c) impedance log obtained by combining information from reflectogram and characteristic impedance obtained from impulse-response analysis.

wave generated by the blow is not. This wave contains information about changes in shaft impedance as it proceeds downward, and this information is reflected back to the shaft head. The reflectogram so obtained in the sonic-echo test can not be quantified. However, it is possible with modern recording equipment to sample both wave reflection and impedance properties of tested shafts. Measurements of force and velocity response are stored as time-base data, with a very wide band-pass filter and rapid sampling. Resolution of both weak and strong response levels are thus favored. In the reflectogram, a complete shaft defect (zero impedance) is equivalent to 100 percent reflection, while an infinitely long shaft with no defects would give zero reflection.

If either a defect or the shaft tip is at a considerable distance from the shaft head, the reflected amplitude is reduced by damping within the shaft. With uniform lateral soil conditions, this damping function has the form $e^{-\sigma L}$, where L is the shaft length and σ is the damping factor (see Appendix A), and the reflectogram can be corrected using such an amplification function to yield a strong response over the total shaft length, as is frequently done in the treatment of sonic-echo data. Fig. 2.3.4 shows an example of a reflectogram corrected in this way.

The frequency-domain (impedance) analysis obtained from the impulse-response test confirms shaft length and gives the shaft dynamic stiffness and characteristic impedance I

$$I = \rho_c A_c C_b \quad (2.12)$$

where

- ρ_c = density of shaft concrete,
- A_c = shaft cross-sectional area, and
- C_b = concrete bar wave velocity.

In addition, simulation of the tested shaft and its surrounding soil can be carried out most efficiently in the frequency domain. The reflectogram and the characteristic impedance can then be combined to give dimensions to the reflectogram to produce a trace referred to as the impedance log [Fig. 2.3.4(c)]. The output of this analysis is in the form of a vertical section through the shaft, giving a calculated visual representation of the pile shape. The final result can be adjusted to eliminate varying soil reflections by use of the simulation technique.

Field testing equipment must have the following requirements:

- Hammer load cell and the velocity transducer or accelerometer must have been correctly calibrated (within the six months prior to testing);
- Data acquisition and storage must be digital, for future analysis; and
- Both time and frequency-domain test responses must be stored.

2.3.4 Crosshole sonic logging—The crosshole sonic logging method is designed to overcome the depth limitation of the sonic-echo and mobility methods on longer shafts, and is for use on mass concrete foundations such as slurry trench walls, dams and machinery bases (Levy, 1970; Davis and Robertson, 1975; Baker and Khan, 1971).

Principle—The method requires a number of parallel metal or plastic tubes to be placed in the structure prior to concrete placement, or core holes to be drilled after the concrete has set. A transmitter probe placed at the bottom of one tube emits an ultrasonic pulse that is detected by a receiver probe at the bottom of a second tube. A recording unit measures the time taken for the ultrasonic pulse to pass through the concrete between the tubes. The probes are sealed units, and the

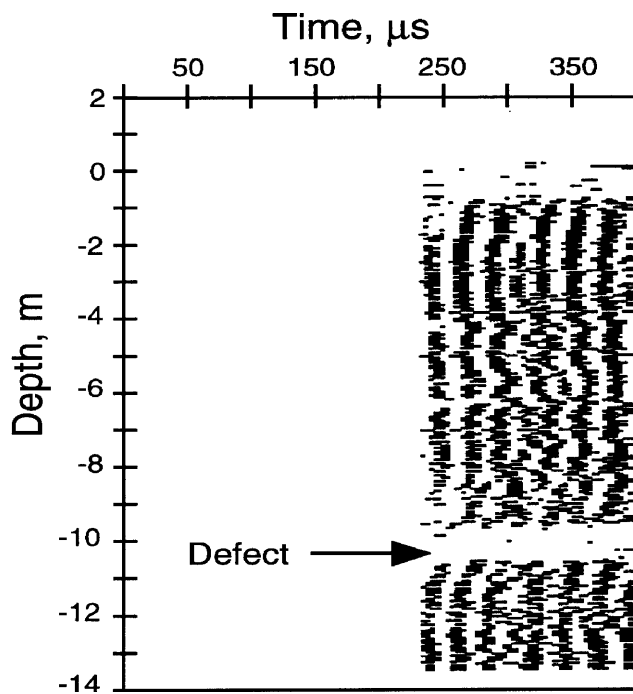


Fig. 2.3.5—Example of crosshole sonic log (absence of signal arrival at a depth of about 10 m indicates presence of defect).

tubes are filled with water to provide coupling between the probes and the concrete.

The probe cables are withdrawn over an instrumented wheel that measures the cable length and thus probe depth, or the cables can be marked along their lengths so that the probe depths are known. Continuous pulse measurements are made during withdrawal, at height increments ranging from 10 to 50 mm, providing a series of measurements that can be printed out to provide a vertical profile of the material between the tubes. A typical test result for a specific commercial system is shown in Fig. 2.3.5. The presence of a defect is indicated by the absence of a received signal.

The ultrasonic pulse velocity (UPV) is a function of the density and dynamic elastic constants of the concrete. If the signal path length is known and the transit time is recorded, the apparent UPV can be calculated to provide a guide to the quality of the concrete. A reduction in modulus or density will result in a lower UPV. If the path length is not known, but the tubes are reasonably parallel, the continuous measurement profile will clearly show any sudden changes in transit time caused by a lower pulse velocity due to low modulus or poor-quality material, such as contaminated concrete or inclusions. Voids will have a similar effect by forcing the pulse to detour around them, thus increasing the path length and the transit time. By varying the geometric arrangement of the probes, the method can resolve the vertical and horizontal extent of such defects, and locate fine cracks or discontinuities.

The method provides a direct measurement of foundation depth, and can be used to assess the quality of the interface between the shaft base and the bedrock if the access holes are

extended below the base. The major limitation of the method is the requirement for the installation of access tubes either before concrete placement or by core drilling afterwards. The major advantage is that the method has no depth limitation, unlike the surface reflection methods.

The information obtained is limited to the material immediately between pairs of tubes. Hence, in piles the access tubes should be arranged as close to the shaft periphery as possible, and in a pattern that allows the maximum coverage of the concrete between them. No information will be obtained about increases or decreases in shaft cross section outside the area covered by the access tubes.

2.3.5 Parallel-seismic method—All of the above methods depend upon clear access to the head of the pile shaft, and are therefore easiest and most practical to perform during the construction phase as foundation heads later may be inaccessible. The parallel-seismic method was developed specifically for situations arising after the foundation has been built upon, as in the evaluation of older, existing structures, where direct access to the pile head is no longer possible without some demolition (Davis, 1995).

Principle—A small-diameter access bore hole is drilled into the soil parallel and close to the foundation to be tested. The bore hole must extend beyond the known or estimated depth of the foundation, and is normally lined with a plastic tube to retain water as an acoustic couplant. An acoustic receiving probe is placed in the tube at the top, and the structure is struck as close to the head of the foundation as possible with a trigger hammer. The signals from the hammer and receiver are recorded on a data acquisition unit as the time taken for the impact stress wave to travel through the foundation and adjacent soil to the receiving probe. The probe is then lowered in uniform increments and the process repeated at each stage, with the impact at the same point each time. The recorded data are plotted as a vertical profile with each wave transit time from the point of impact to each position down the access tube (Fig. 2.3.6).

The velocity of the wave will be lower through soil than through the concrete. If the access tube is reasonably parallel to the foundation, the effect of the soil between the tube and the pile shaft will be effectively constant. However, transit time will increase, proportional to the increase in foundation depth. When the receiver has passed beyond the foundation base, the transit time of the signal will be extended by the lower velocity of the additional intervening soil, and the lines linking signal arrival points on the graph will show a distinct discontinuity at the level of the foundation base. Similarly, any significant discontinuity or inclusion in the foundation will force the signal to detour around it, increasing the path length and transit time.

2.3.6 Advantages and limitations—Table 2.3 summarizes the advantages and limitations of stress-wave methods for deep foundations.

2.4—Nuclear methods

2.4.1 Introduction—Nuclear methods for nondestructive evaluation of concrete can be subdivided into two groups:

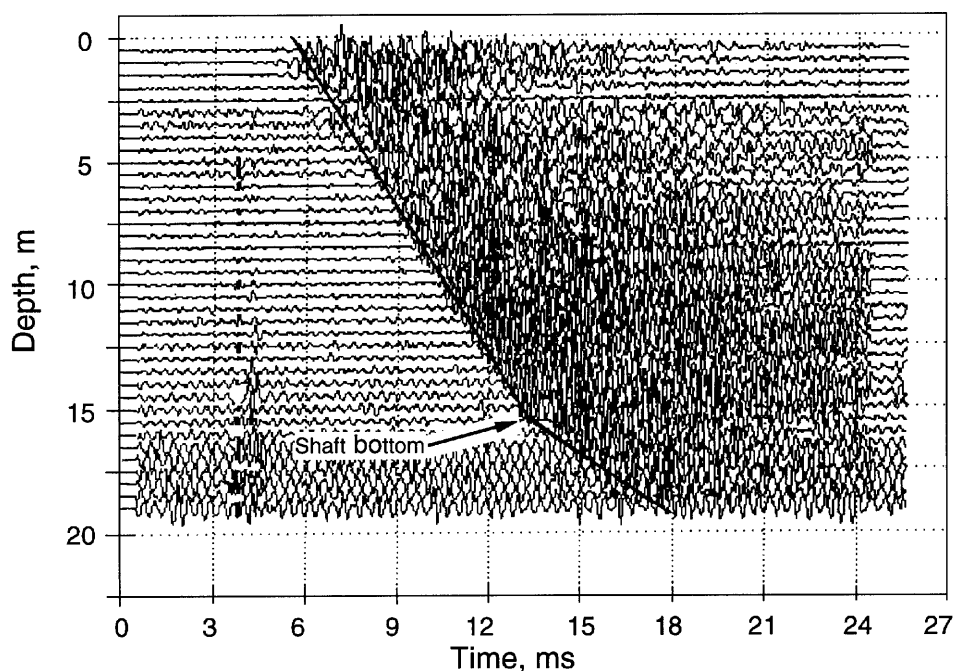


Fig. 2.3.6—Example of results from parallel-seismic test (depth of pile shaft is indicated by change in slope of line representing arrival time of stress pulse as function of depth).

radiometric methods and *radiographic methods*. Both involve gaining information about a test object due to interactions between high-energy electromagnetic radiation and the material in the test object. A review of the early developments in the use of nuclear methods (also called *radioactive method*) was presented by Malhotra (1976), and more recent developments were reviewed by Mitchell (1991). These methods use radioactive materials, and test personnel require specialized safety training and licensing.

Radiometry is used to assess the density of fresh or hardened concrete by measuring the intensity of electromagnetic radiation (gamma rays) that has passed through the concrete. The radiation is emitted by a radioactive isotope, and the radiation passing through the concrete is sensed by a detector. The detector converts the received radiation into electrical pulses, which can be counted or analyzed by other methods (Mitchell, 1991). Radiometry can be further subdivided into two procedures. One is based on measurement of gamma rays after transmission directly through the concrete, and the other is based on measurement of gamma rays reflected, or backscattered, from within the concrete. These procedures are analogous to the ultrasonic through-transmission method and the pitch-catch method using stress waves.

Radiography involves the use of the radiation passing through the test object to produce a “photograph” of the internal structure of the concrete. Typically, a radioactive source is placed on one side of the object and special photographic film is placed on the opposite side to record the intensity of radiation passing through the object. The higher the intensity of the radiation, the greater the exposure of the film. This method is identical to that used to produce medical “x-rays.”

2.4.2 Direct transmission radiometry for density—Direct transmission techniques can be used to detect reinforcement. However, the main use of the technique is to measure the in-place density, both in fresh and hardened concrete. Structures of heavyweight and roller-compacted concretes are cases where this method is of particular value.

Principle—The direct transmission radiometric method is analogous to the ultrasonic through-transmission technique. The radiation source is placed on one side of the concrete element to be tested and the detector is placed on the opposite side. As the radiation passes through the concrete, a portion is scattered by free electrons (Compton scattering) and a smaller amount is absorbed by the atoms. The amount of Compton scattering depends on the density of the concrete and the amount of absorption depends on chemical composition (Mitchell, 1991). If the source-detector spacing is held constant, a decrease (or increase) in concrete density leads to a change in the intensity of the detected radiation.

Instrumentation—Fig. 2.4.1 shows the arrangement of source and detector for direct measurement through a concrete member. This arrangement could also be used for testing fresh concrete with allowance made for the effects of the formwork material. The most widely used source is the radioactive isotope cesium-137 (^{137}Cs). The common detector is a Geiger-Müller tube, which produces electrical pulses when radiation enters the tube. Other detectors can be scintillation crystals that convert the incident radiation into light pulses.

Fig. 2.4.2 is a schematic of a commercially available nuclear transmission gauge that can be used in fresh concrete by pushing the source assembly into the concrete. It can also be used in hardened concrete by drilling a hole and inserting

Table 2.3—Advantages and limitations of stress-wave methods for deep foundations

Method	Advantages	Limitations
Surface Reflection Methods		
Sonic-echo	No pre-placed tubes. Portable equipment. Rapid.	Confuses necking and bulging. Does not measure diameter. Unable to determine defects in shafts > 30 m or with $L/d > 30$.
Impulse-response (Mobility)	No pre-placed tubes. Stiffness measurement. Portable equipment. Rapid.	Results interpretation is delicate. Limitations on geometry of pile to be tested, as for sonic-echo
Impedance logging	As for mobility test, plus effective shape of shaft derived from analysis.	Requires very good test data for accurate analysis. Full analysis can not yet be completed on site at time of test.
Direct Transmission Methods		
Sonic logging	Relatively fast. Detection of defects between tubes is more accurate than in surface reflection tests. Performance is not limited by depth.	Pre-placed tubes or coring required. May not detect defects at edge of shaft.
Paralell-seismic	Relatively fast. Foundations under existing structures can be tested. Not affected by soil damping as much as surface reflection methods.	Cost of bore hole adjacent to each foundation. Signal stops at first major anomaly. Can bypass edge defects.

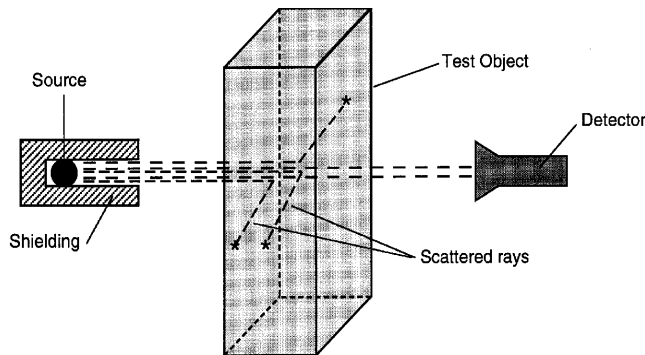


Fig. 2.4.1—Direct transmission radiometry with source and detector external to test object.

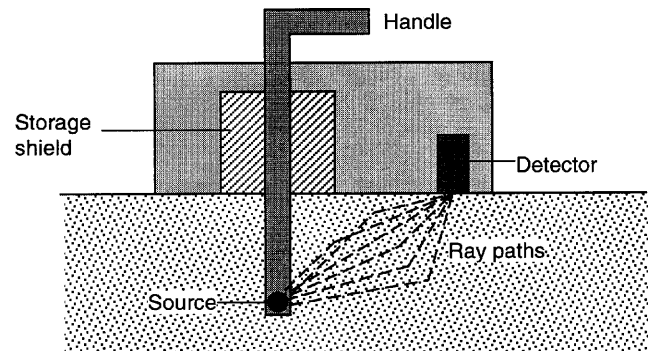


Fig. 2.4.2—Schematic of direct transmission nuclear gage.

the source assembly. The equipment is portable and provides an immediate readout of the results. Most of the available units were developed for monitoring soil compaction and measuring the in-place density of asphalt concrete.

The VUT density meter was developed (in Czechoslovakia) specifically for testing fresh concrete (Hönig, 1984). Fig. 2.4.3 is a schematic of this device. The source can be lowered up to a depth of 200 mm into a hollow steel needle that is pushed into the fresh concrete. A spherical lead shield suppresses the radiation when the source is in its retracted position. Detectors are located beneath the treads used to push the needle into the concrete. The unit is claimed to have a resolution of 10 kg/m^3 (Hönig, 1984).

The direct transmission gauges mentioned above provide a measurement of the average density between the source and detector. Fig. 2.4.4 is a schematic of a two probe source/detector system for measuring the density of fresh concrete as a function of depth (Iddings and Melancon, 1986). The source and detector are moved up and down within metal

tubes that are pushed into the fresh concrete, thus making it possible to measure density as a function of depth.

ASTM C 1040 provides procedures for using nuclear methods to measure the in-place density of fresh or hardened concrete. The key element of the procedure is development of the calibration curve for the instrument. This is accomplished by making test specimens of different densities and determining the gauge output for each specimen. The gauge output is plotted as a function of the density, and a best-fit curve is determined.

2.4.3 Backscatter radiometry for density—Backscatter techniques are particularly suitable for applications where a large number of in situ measurements are required. Since backscatter measurements are affected by the top 40 to 100 mm, the method is best suited for measurement of the surface zone of a concrete element. A good example of the use of this method is the monitoring of the density of bridge deck overlays. Non-contacting equipment has been developed that is used

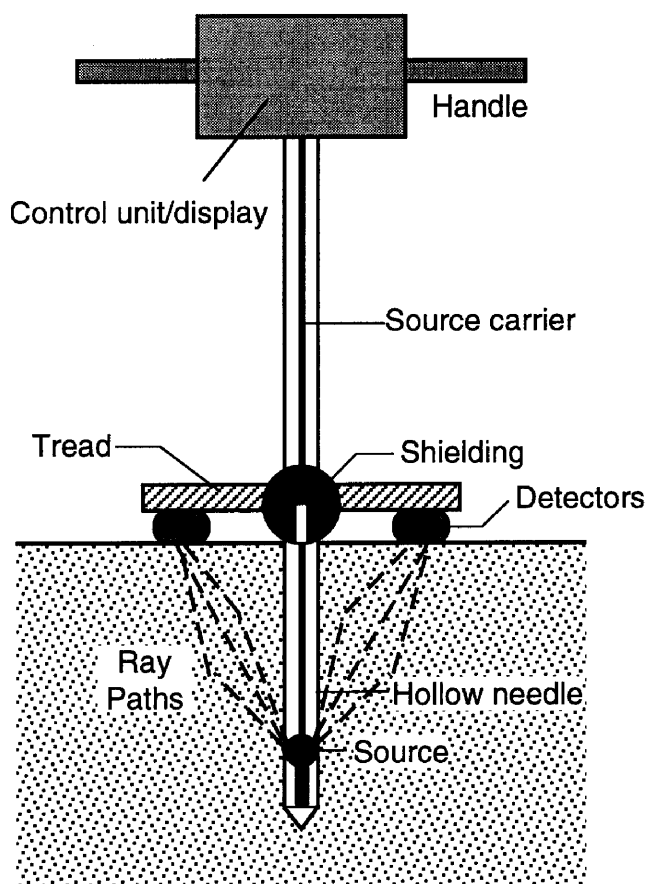


Fig. 2.4.3—Schematic of nuclear gage for measuring density of fresh concrete (based on Hönig, 1984).

for continuous monitoring of concrete pavement density during slip-form operations.

Principle—In the measurement of density by backscatter, the radiation source and the detector are placed on the same side of the sample (analogous to the pitch-catch method for stress waves). The difference between this procedure and direct transmission is that the detector receives gamma rays scattered within the concrete rather than those which pass through the concrete. The scattered rays are lower in energy than the transmitted ones and are produced when a photon collides with an electron in an atom. Part of the photon energy is imparted to the electron, and a new photon emerges, traveling in a new direction with lower energy. As mentioned, this process is known as Compton scattering (Mitchell, 1991).

Procedures for using backscatter methods to measure concrete density are given in ASTM C 1040. As is the case with direct transmission measurements, it is necessary to establish a calibration curve prior to using a nuclear backscatter gauge to measure in-place density.

Instrumentation—Fig. 2.4.5 is a schematic of a backscatter nuclear gauge for density measurement. Many commercial gauges are designed so that they can be used in either direct transmission or backscatter mode. To operate in backscatter mode, the source is positioned so that it is located above the sur-

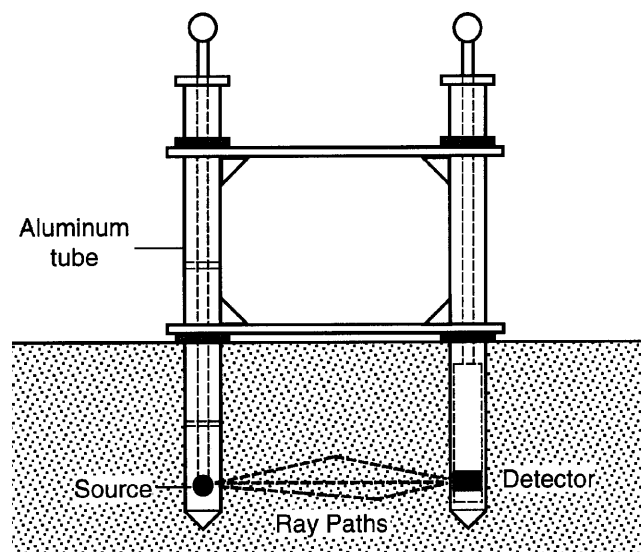


Fig. 2.4.4—Schematic of direct transmission nuclear gage for measuring density of fresh concrete at different depth (adapted from Iddings and Melancon, 1986).

face of the concrete. Shielding is provided to prevent radiation from traveling directly from the source to the detector.

Certain specialized versions of backscatter equipment have been developed. Two of particular interest are described below:

ETG probe—The ETG probe was developed in Denmark to use backscatter measurements for estimating density variation at different depths in a medium. The technique involves determination of the intensity of backscattered gamma radiation as a function of energy level. A beam of parallel (collimated) gamma rays is used and multiple measurements are made with the beam at slightly different angles of penetration. By comparing the radiation spectra for the multiple measurements, information can be obtained about the density in a specific layer of the concrete. In addition to permitting measurement of density at discrete layers, the ETG probe also permits density measurements at greater depths (up to 150 mm) than are possible by ordinary backscatter gauges.

Consolidation monitoring device—This equipment was developed for continuous monitoring of pavement consolidation during slip-form construction (Mitchell et al., 1979). The device is mounted on the rear of a highway paving machine and traverses across the finished pavement at a height of about 25 mm above the pavement surface. An air gap compensating device allows for air gap variations of ± 10 mm. The device measures the average density within the top 100 mm of the pavement.

2.4.4 Radiography—Radiography provides a means of obtaining a radiation-based photograph of the interior of concrete because denser materials block more of the radiation. From this photograph, the location of reinforcement, voids in concrete, or voids in grouting of post-tensioning ducts can be identified.

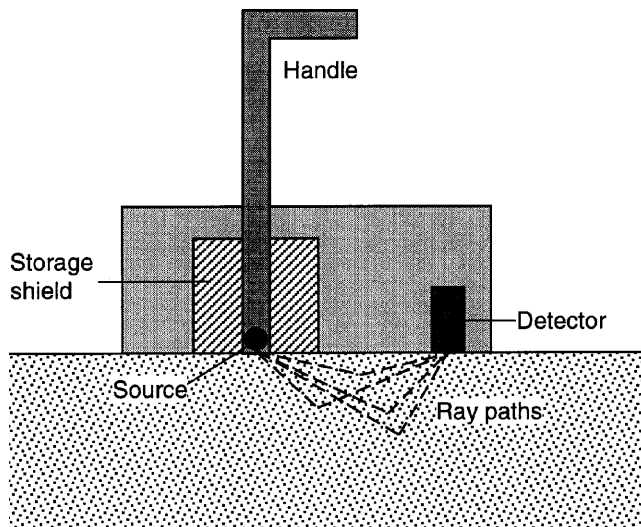


Fig. 2.4.5—Schematic of backscatter nuclear density gage.

Principle—A radiation source is placed on one side of the test object and a beam of radiation is emitted. As the radiation passes through the member, it is attenuated by differing amounts depending on the density and thickness of the material that is traversed. The radiation that emerges from the opposite side of the object strikes a special photographic film (Fig. 2.4.6). The film is exposed in proportion to the intensity of the incident radiation. When the film is developed, a two-dimensional visualization (a photograph) of the interior structure of the object is obtained. The presence of a high-density material, such as reinforcement, is shown on the developed film as a light area, and a region of low density, such as a void, is shown as a dark area.

The British Standards Institute has adopted a standard for radiographic testing of concrete (BS 1881: Part 205). The standard provides recommendations for investigators considering radiographic examinations of concrete (Mitchell, 1991).

Instrumentation—In x-radiography, the radiation is produced by an x-ray tube (Mitchell, 1991). The penetrating ability of the x-rays depends on the operating voltage of the x-ray tube. In gamma radiography, a radioactive isotope is used as the radiation source. The selection of a source depends on the density and thickness of the test object and on the exposure time that can be tolerated. The most intense source is cobalt-60 (^{60}Co), which can be used to penetrate up to 500 mm of concrete. For members with thickness of 150 mm or less, iridium-192 (^{192}Ir) or cesium-137 (^{137}Cs) can be used (Mitchell, 1991). The film type will depend on the thickness and density of the member being tested.

Most field applications have used radioactive sources because of their greater penetrating ability (higher energy radiation) compared with x-rays. A system known as “Scorpion II,” developed in France, uses a linear accelerator to produce very high energy x-rays that can penetrate up to 1 m of concrete. This system was developed for the inspection of prestressed members to establish the condition and location of

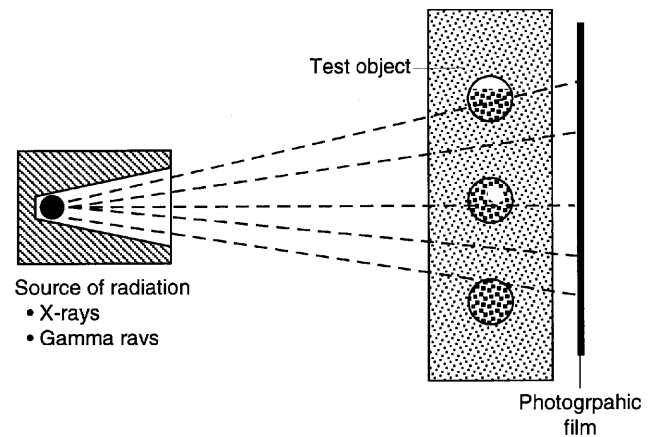


Fig. 2.4.6—Schematic of radiographic method.

prestressing strands and to determine the quality of grouting in tendon ducts (Mitchell, 1991).

2.4.5 Gamma-gamma logging of deep foundations—Used to evaluate the integrity of drilled shaft and slurry wall foundations, this method tests the density of material surrounding access tubes or holes in concrete deep foundations. Gamma-gamma logging uses a radioactive source and counter that may be either in separate probes (direct transmission) or housed in the same unit (backscatter) (Preiss and Caiserman, 1975; Davis and Hertlein, 1994).

Principle—The most common method is by backscatter, with the probe lowered down a single dry plastic access tube, and raised in steps to the surface. Low density zones, such as soil inclusions within 50 to 100 mm from the probe, will increase the radiation count, since less radiation is absorbed than in a zone of intact concrete (Fig. 2.4.7). A limitation of the method is the need for stronger radiation sources to increase the zone of influence of the probe around the tube.

The effect of different access tube materials on radiation count density is demonstrated in Fig. 2.4.7, which shows plots of radiation counts from an experimental drilled shaft with four access tubes: two of plastic and two of steel (Baker et al., 1993). The response from the shaft constriction at 11 to 12 m is attenuated by the steel tubes. The figure also shows that a small elliptical inclusion at 4 m is not detected in any of the traces, demonstrating the limitation of the method to locate small anomalies or defects.

When gamma-gamma logging is used in the direct transmission mode in parallel tubes (Preiss, 1971), the data can be analyzed in a similar manner to that from sonic logging. This technique requires a very strong source, and dedicated equipment for this purpose does not exist in North America at present.

2.4.6 Advantages and limitations—Table 2.4 summarizes the advantages and limitations of the nuclear methods. Direct transmission radiometry requires a drilled hole in hardened concrete, and it provides for rapid determination of the in-place density of concrete. The equipment is reasonably portable, making it suitable for use in the field. Minimal operator skills are needed to make the measurements. For the commercially available equipment, the source/detector

separation is limited to a maximum of about 300 mm. Furthermore, the most commonly available equipment measures an average density between the immersed source and the surface detector. It is not able to identify areas of low compaction at specific depths. All immersed-probe techniques for fresh concrete have the further drawback that the immersion of the probe may have a localized influence on the concrete being measured. Test results may be affected by the presence of reinforcing steel located near the source-detector path.

Backscatter tests can be used on finished surfaces where direct transmission measurements would be impractical or disruptive. The equipment is portable and tests can be conducted rapidly. However, the precision of backscatter gauges is less than that of direct transmission devices. ASTM C 1040 requires that a suitable backscatter gauge for density measurement should result in a standard deviation of less than 16 kg/m^3 ; for a suitable direct-transmission gauge, the standard deviation is less than 8 kg/m^3 . According to ASTM C 1040, backscatter gauges are typically influenced by the top 75 to 125 mm of material. The top 25 mm determines 50 to 70 percent of the count rate and the top 50 mm determines 80 to 95 percent of the count rate. When the material being tested is homogenous, this inherent characteristic of the method is not significant. However, when a thin overlay is placed on existing concrete, this effect has to be considered in interpreting the results. Also, the presence of reinforcing steel within the influence zone will affect the count rate.

Radiographic methods allow the possibility of seeing some of the internal structure of a concrete member where density variations exist. Although both gamma ray and x-ray sources can be used for radiography, x-ray equipment is comparatively expensive and cumbersome for field application. Because of this, less costly and more portable gamma-ray equipment is generally chosen for field use. However, x-ray equipment has the advantage that it can be turned off when its not being used. In contrast, gamma rays are emitted continuously from a radioactive source and heavy shielding is required to protect personnel. In addition, x-ray equipment can produce more energetic radiation than radioactive sources, which permits the inspection of thicker members or the use of shorter exposure times.

The main concern in the use of all nuclear methods is safety. In general, personnel who perform nuclear tests must obtain a license from the appropriate governmental agency (Mitchell, 1991). Testing across the full thickness of a concrete element is particularly hazardous and requires extensive precautions, skilled personnel, and highly specialized equipment. Radiographic procedures are costly and require evacuation of the structure by persons not involved in the actual testing. The use of x-ray equipment poses an additional danger due to the high voltages that are used. There are limits on the thicknesses of the members that can be tested by radiographic methods. For gamma-ray radiography the maximum thickness is about 500 mm, because thick members require unacceptably long exposure times. Radiography is not very useful for locating crack planes perpendicular to the radiation beam.

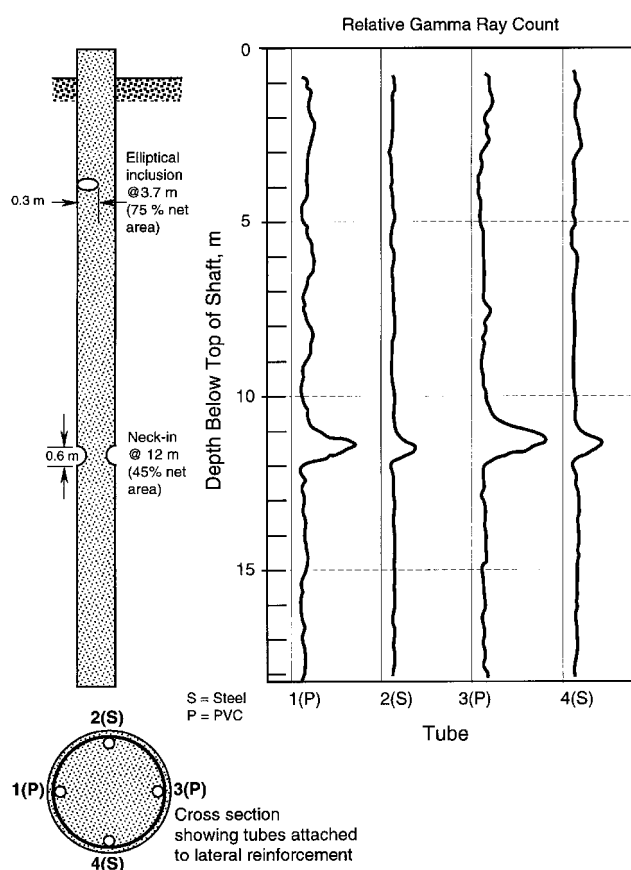


Fig. 2.4.7—Gamma-gamma backscatter log on experimental shaft with planned defects (Baker et al., 1993).

2.5—Magnetic and electrical methods

Knowledge about the quantity and location of reinforcement is needed to evaluate the strength of reinforced concrete members. Knowing whether there is active corrosion of reinforcement is necessary to assess the need for remedial actions before structural safety or serviceability is jeopardized. This section discusses some of the magnetic and electrical methods used to gain information about the layout and condition of embedded steel reinforcement (Malhotra, 1976; Bungey, 1989; Lauer, 1991). Devices to locate reinforcing bars and estimate the depth of cover are known as covermeters. Corrosion activity can be monitored using the half-cell potential technique, and information on the rate of corrosion can be obtained from linear-polarization methods.

2.5.1 Covermeters—As is common with other nondestructive test methods used to infer conditions within concrete, covermeters “measure” the depth of cover by monitoring the interaction of the reinforcing bars with some other process. For most covermeters, the interaction is between the bars and a low-frequency, electromagnetic field. The basic relationships between electricity and magnetism are the keys for understanding the operation of covermeters. One of the important principles is electromagnetic induction, which means that an alternating magnetic field intersecting an

Table 2.4—Advantages and limitations of nuclear methods

Method	Advantages	Limitations
Direct transmission radiometry	Portable equipment available for determination of in-place density. Minimal operator skill is required.	Operators must be licensed. Available equipment limited to path lengths less than 300 mm. Requires access to inside of member or opposite faces.
Backscatter radiometry	Requires access only to surface of test object and is suitable for fresh or hardened concrete. Equipment is portable and testing is rapid.	Operators must be licensed. Precision of density measurements is lower than direct transmission. Measurement is affected by near surface material and sensitive to chemical composition.
Radiography	Provides view of the internal structure of the test object.	Operators must be licensed and highly skilled. X-ray equipment is bulky and expensive. Difficult to identify cracks perpendicular to radiation beam. Gamma-ray penetration limited to 500 mm of concrete.

electrical circuit induces an electrical potential in that circuit. According to Faraday's law, the induced electrical potential is proportional to the rate of change of the magnetic flux through the area bounded by the circuit (Serway, 1983).

Commercial covermeters can be divided into two classes: those based on the principle of magnetic reluctance, and those based on eddy currents. These differences are summarized below (Carino, 1992).

Magnetic reluctance meters—When current flows through an electrical coil, a magnetic field is created and there is a flow of magnetic flux lines between the magnetic poles. This leads to a magnetic circuit, in which the flow of magnetic flux between poles is analogous to the flow of current in an electrical circuit (Fitzgerald et al., 1967). The resistance to flow of magnetic flux is called reluctance, which is analogous to the resistance to flow of current in an electrical circuit.

Fig. 2.5.1 is a schematic of a covermeter based upon changes in the reluctance of a magnetic circuit caused by the presence or absence of a bar within the vicinity of the search head. The search head is composed of a ferromagnetic U-shaped core (yoke), an excitation coil, and a sensing coil. When alternating current (less than 100 Hz) is applied to the excitation coil, an alternating magnetic field is created, and magnetic flux flows between the poles of the yoke. In the absence of a bar [Fig. 2.5.1(a)], the magnetic circuit, composed of the yoke and the concrete between ends of the yoke, has a high reluctance and the alternating magnetic flux flowing between the poles will be small. The alternating flux induces a small, secondary current in the sensing coil. If a ferromagnetic bar is present [Fig. 2.5.1(b)], the reluctance decreases, the magnetic flux amplitude increases, and the sensing coil current increases. Thus, the presence of the bar is indicated by a change in the output from the sensing coil. For a given reinforcing bar, the reluctance of the magnetic circuit depends strongly on the distance between the bar and the poles of the yoke. An increase in concrete cover increases the reluctance and reduces the current in the sensing coil. If the meter output were plotted as a function of the cover, a calibration relationship would be established that could be used to

measure the cover. Since the size of the bar affects the reluctance of the magnetic circuit, there would be a separate relationship for each bar size. These aspects are discussed further later in this section.

Eddy-current meters—If a coil carrying an alternating current is brought near an electrical conductor, the changing magnetic field induces circulating currents, known as eddy currents, in the conductor. Because any current flow gives rise to a magnetic field, eddy currents produce a secondary magnetic field that interacts with the field of the coil. The second class of covermeters is based on monitoring the effects of the eddy currents induced in a reinforcing bar. There are two categories of eddy-current meters: one is based on the continuous excitation of the coil by an alternating current (usually at about 1 kHz) and the other is based upon pulsed excitation. The latter is not discussed here, but the interested reader is referred to additional information in Carino (1992).

Fig. 2.5.2 is a schematic of a continuous eddy-current covermeter. In the absence of a reinforcing bar, the magnitude of the alternating current in the coil depends on the coil impedance.* If the coil is brought near a reinforcing bar, alternating eddy currents are established within the surface skin of the bar. The eddy currents give rise to an alternating secondary magnetic field that induces a secondary current in the coil. In accordance with Lenz's law (Serway, 1983), the secondary current opposes the primary current. As a result, the net current flowing through the coil is reduced, and the apparent impedance of the coil increases (Hagemaijer, 1990). Thus, the presence of the bar is inferred by monitoring the change in current flowing through the coil.

In summary, magnetic reluctance covermeters are based on monitoring changes in the magnetic flux flowing through the magnetic circuit composed of the path through the yoke,

* When direct current is applied to a circuit, the amount of current equals the voltage divided by the electrical resistance of the circuit. When alternating current is applied to the coil, the amount of current is governed by the value of the applied voltage, the resistance, and another quantity called inductance. The vector sum of resistance and inductance defines the impedance of the coil.

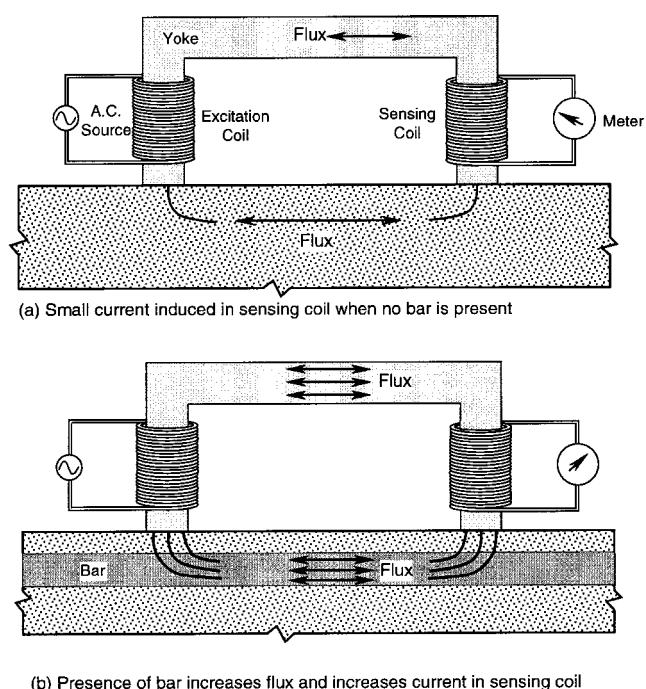


Fig. 2.5.1—Covermeter based on principle of magnetic reluctance (adapted from Carino, 1992): (a) small current induced in sensing coil when no bar is present, and (b) presence of bar increases flux and increases current in sensing coil.

concrete, and the reinforcing bar. For a given cover, the meter output depends on the area of the reinforcing bar and its magnetic properties (affected by alloy composition and type of mechanical processing). On the other hand, eddy-current covermeters depend on the electrical conductivity of the bar, and they will detect magnetic as well non-magnetic, metallic objects. However, a ferromagnetic material produces a stronger signal because of the enhanced strength of the secondary magnetic field created by the eddy currents. The response of magnetic reluctance covermeters is affected by the presence of iron-bearing aggregates in the concrete, while eddy-current meters are not.

Limitations—A reinforcing bar is detected by a covermeter when the bar lies within the zone of influence of the search head (yoke or coil). Fig. 2.5.3(a) illustrates that influence zone of the search head. The response is maximum when the search head lies directly above the reinforcing bar. An important characteristic of a covermeter is the relationship between meter amplitude and the horizontal distance from the center of the bar to the center of the search head, that is, the horizontal offset. Fig. 2.5.3(b) shows the variation in amplitude with horizontal offset for a magnetic reluctance covermeter when the search head is moved away from a No. 6 bar (19 mm) with a cover depth of 21 mm. The variation is approximately a bell-shaped curve. The width of the curve in Fig. 2.5.3(b) defines the zone of influence of the search head. Fig. 2.5.3(c) shows the relationships between amplitude and horizontal offset for two different search

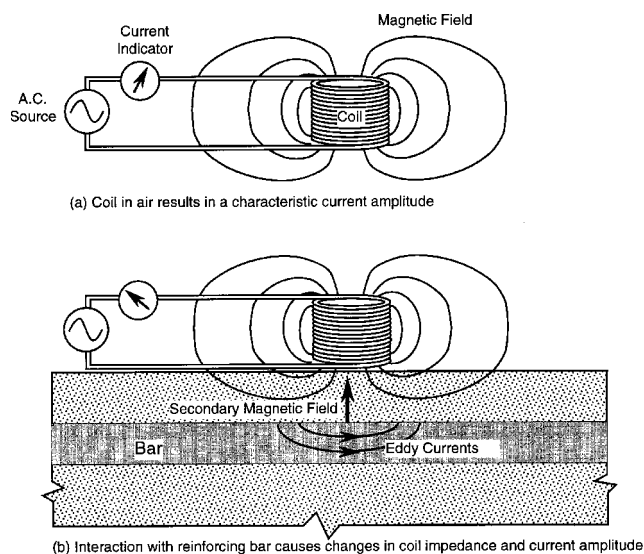


Fig. 2.5.2—Covermeter based on eddy current principle (adapted from Carino, 1992): (a) coil in air results in characteristic current amplitude, and (b) interaction with reinforcing bar causes changes in coil impedance and current amplitude.

heads (probes) of an eddy-current meter. One search head has a smaller zone of influence than the other, which means that it is a more focused search head. A covermeter with a focused search head can discern individual bars when they are closely spaced. However, focused search heads generally have less penetrating ability and are not able to locate bars with deep cover. The influence zone of the search head also affects the accuracy with which the end of a reinforcing bar can be detected (Carino, 1992).

An important distinction between covermeters is the directionality characteristics of the search heads. Due to the shape of the yoke, a magnetic reluctance meter is directional compared with a continuous eddy-current meter with a symmetrical coil. Maximum response occurs when the yoke is aligned with the axis of the bar. This directionality can be used to advantage when testing a structure with an orthogonal gridwork of reinforcing bars (Tam et al., 1977).

As mentioned previously, each covermeter has a unique relationship between meter amplitude and depth of cover. Fig. 2.5.4(a) shows a technique that can be used to develop these relationships for different bar diameters. A single bar is placed on a nonmagnetic and nonconducting surface and the meter amplitude is determined as a function of the distance between the search head and the top of the bar. Fig. 2.5.4(b) and 2.5.4(c) show these relationships for a magnetic reluctance and for an eddy-current meter, respectively. These relationships illustrate a basic limitation of covermeters. Since the amplitude is a function of bar diameter and depth of cover, one cannot determine both parameters from a single measurement. As a result, a dual measurement is needed to be able to estimate both depth of cover and diameter (BS 1881: Part 204; Das Gupta and Tam, 1983). This is done by recording the meter amplitude first with the search head in contact with the concrete, and then when the search head is located a

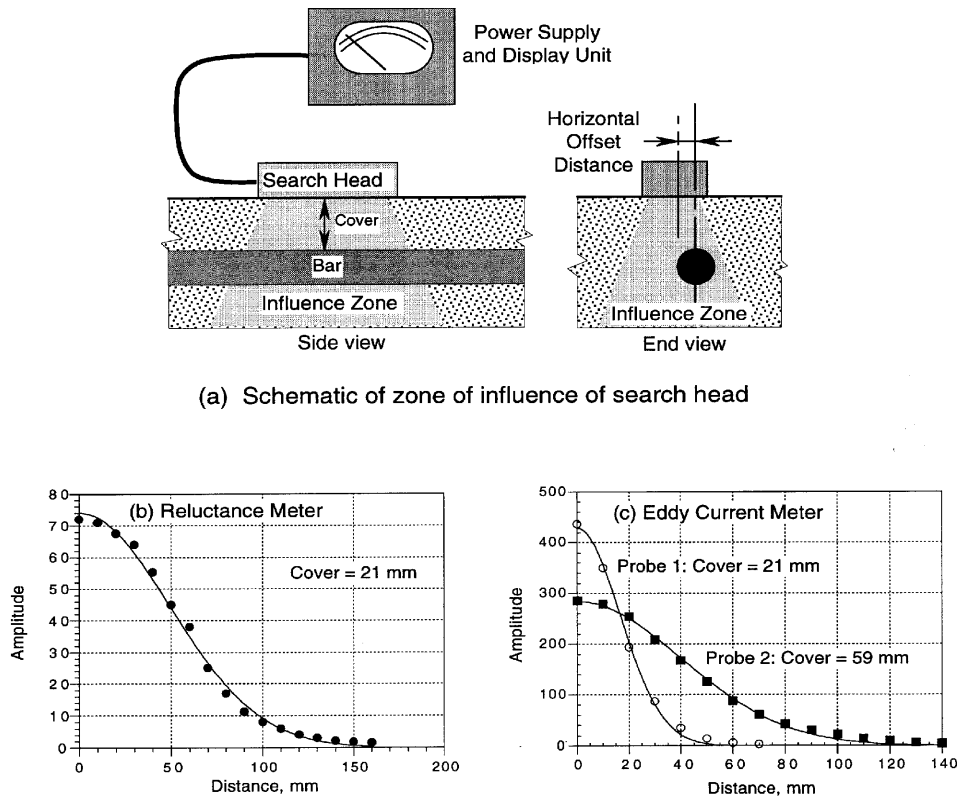


Fig. 2.5.3—(a) Zone of influence of covermeter search head; variation of amplitude with horizontal offset for: (b) magnetic reluctance covermeter, and (c) eddy current covermeter (adapted from Carino, 1992).

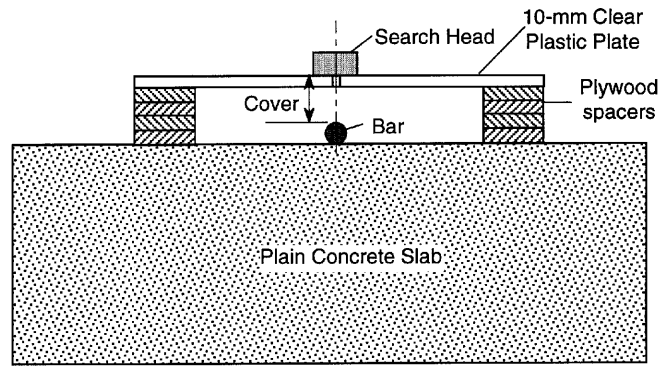
known distance above the concrete. The differences in amplitudes and the amplitude-cover relationships are used to estimate the cover and bar diameter. The accuracy of this spacer technique depends on how distinct the amplitude-cover relationships are for the different bar sizes. Because these relationships are generally similar for adjacent bar sizes, it is generally only possible to estimate bar diameter within two sizes (Bungey, 1989).

The single-bar, amplitude-cover relationships are only valid when the bars are sufficiently far apart so that there is little interference by adjacent bars. Fig. 2.5.5(a) shows a technique used to investigate the effect of bar spacing on covermeter response (Carino, 1992). For multiple, closely-spaced bars, the amplitude may exceed the amplitude for a single bar at the same cover depth. If they are closer than a critical amount, the individual bars cannot be discerned. The critical spacing depends on the type of covermeter and the cover depth. In general, as cover increases, the critical spacing also increases. Fig. 2.5.5(b) and 2.5.5(c) show the response for multiple bars at different spacing using a magnetic reluctance meter. The horizontal line is the single-bar amplitude for the same bar size and cover depth. For the 75-mm center-to-center spacing, the meter is just barely able to discern the locations of the individual bars, and the amplitude is not too much higher than the single-response. Fig. 2.5.5(d) and 2.5.5(e) show the responses for an eddy-current meter. The locations of the individual bars are easily identified for the 70-mm spacing, but

the amplitude is greater than the single-bar amplitude. Thus, the cover would be underestimated if the single-bar, amplitude-cover relationship were used. The response of a covermeter to the presence of multiple, closely-spaced bars depends on its design. Teodoru (1996) reports that problems may be encountered when bar spacings are less than approximately the lateral dimensions of the search head.

The presence of two layers of reinforcement within the zone of influence cannot generally be identified with ordinary covermeters (Bungey, 1989; Carino, 1992). The upper layer produces a much stronger signal than the deeper second layer, so that the presence of the second layer cannot be discerned. However, it has been shown that it may be possible to determine lap length when bars are in contact (Carino, 1992).

Table 2.5 summarizes the advantages and limitations of covermeters. These devices are effective in locating individual bars provided that the spacing exceeds a critical value that depends on the meter design and the cover depth. By using multiple measurement methods, bar diameter can generally be estimated within two adjacent bar sizes if the spacing exceeds certain limits that are also dependent on the particular meter. Meters are available that can estimate bar diameter without using spacers to make multiple measurements. Again, the accuracy of these estimates decreases as bar spacing decreases. To obtain reliable measurements, it is advisable to prepare mock-ups of the expected reinforcement



(a) Testing configuration

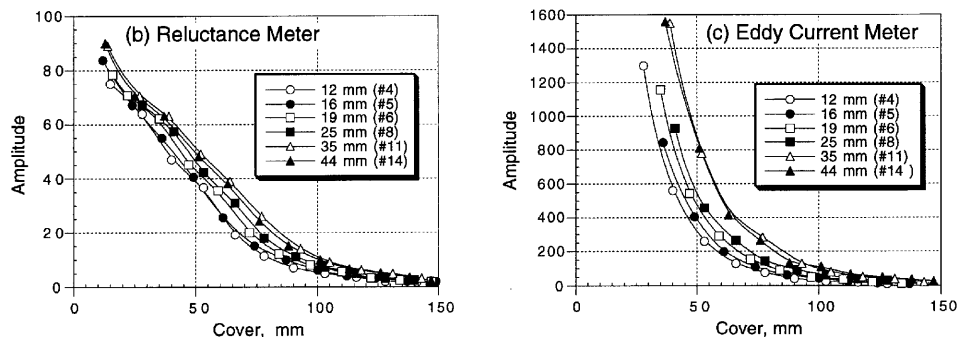


Fig. 2.5.4—Covermeter amplitude versus cover: (a) testing configuration; (b) results for magnetic reluctance meter; and (c) results for eddy current meter (adapted from Carino, 1992).

configuration to establish whether the desired accuracy is feasible. The mock-ups can be made without using concrete, provided the in-place concrete does not contain significant amounts of iron-bearing aggregates.

2.5.2 Half-cell potential method—Electrical methods are used to evaluate corrosion activity of steel reinforcement. As is the case with other NDT methods, an understanding of the underlying principles of these electrical methods is needed to obtain meaningful results. In addition, an understanding of the factors involved in the corrosion mechanism is essential for reliable interpretation of data from this type of testing. This section and the one to follow provide basic information about these methods. However, actual testing and interpretation of test results should be done by experienced personnel.

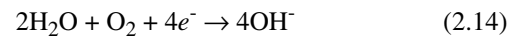
The half-cell potential method is used to delineate those portions of the structure where there is a high likelihood of corrosion activity. Before describing the test procedure, a brief discussion of the basic principles of corrosion testing is provided. Readers should consult ACI 222R for additional information on the factors affecting corrosion of steel in concrete.

Principle—Corrosion is an electrochemical process involving the flow of charges (electrons and ions). Fig. 2.5.6 shows a corroding steel bar embedded in concrete. At active sites on the bar, called anodes, iron atoms lose electrons and move into the surrounding concrete as ferrous ions. This

process is called a half-cell oxidation reaction, or the anodic reaction, and is represented as follows



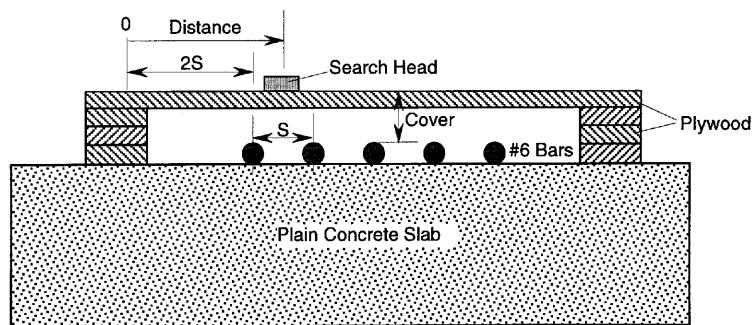
The electrons remain in the bar and flow to sites called *cathodes*, where they combine with water and oxygen present in the concrete. The reaction at the cathode is called a reduction reaction and is represented as follows



To maintain electrical neutrality, the ferrous ions migrate through the concrete to these cathodic sites where they combine to form hydrated iron oxide, or rust. Thus, when the bar is corroding, electrons flow through the bar and ions flow through the concrete. When the bar is not corroding, there is no flow of electrons and ions.

As the ferrous ions move into the surrounding concrete, the electrons left behind in the bar give the bar a negative charge. The half-cell potential method is used to detect this negative charge and thereby provide an indication of corrosion activity.

Instrumentation—The standard test method is given in ASTM C 876 and is illustrated Fig. 2.5.7. The apparatus includes a copper-copper sulfate (or electrically similar) half



(a) Testing configuration

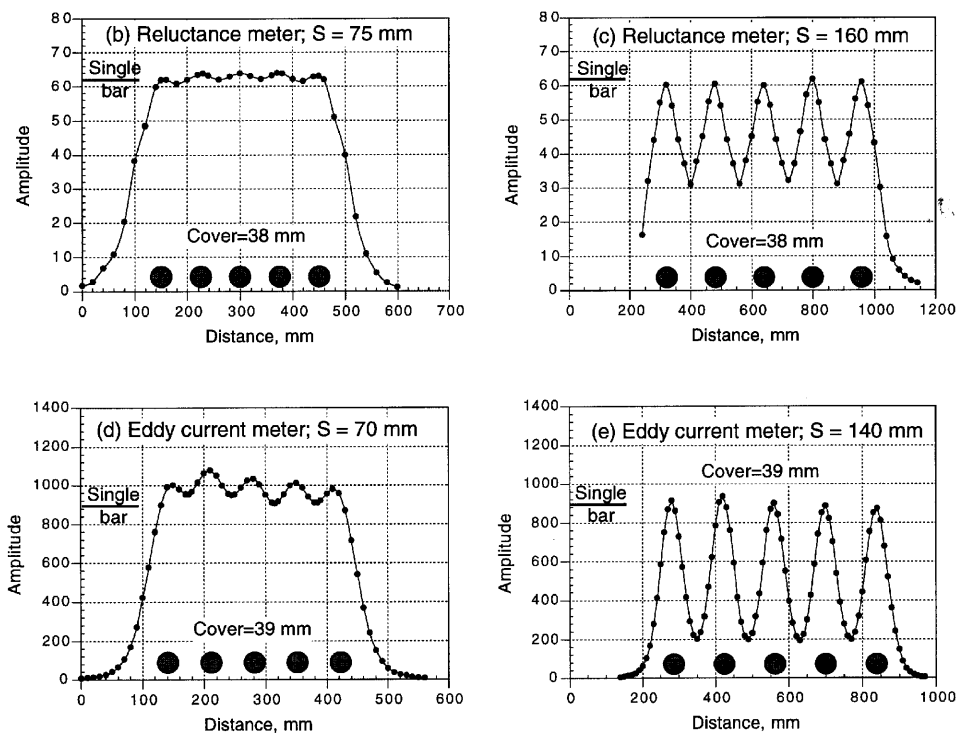


Fig. 2.5.5—Covermeter response with multiple parallel bars at different spacing: (a) testing configuration; (b) response of magnetic reluctance meter, $S = 75$ mm; (c) response of magnetic reluctance meter, $S = 160$ mm; (d) response of eddy current meter, $S = 70$ mm; and (e) response of eddy current meter, $S = 140$ mm (adapted from Carino, 1992).

cell,* connecting wires, and a high-impedance voltmeter. The positive terminal of the voltmeter is attached to the reinforcement and the negative terminal is attached to the copper-copper sulfate half cell. A high-impedance voltmeter is used so that very little current flows through the circuit. As shown in Fig. 2.5.7, the half cell makes electrical contact with the concrete by means of a porous plug and a sponge that is moistened with a wetting solution (such as liquid detergent).

* This half cell is composed of a copper bar immersed in a saturated copper sulfate solution. It is one of many half cells that can be used as a reference to measure the electrical potential of embedded bars. The measured voltage depends on the type of half cell, and conversion factors are available to convert readings obtained with other references cells to the copper-copper sulfate half cell.

If the bar is corroding, electrons would tend to flow from the bar to the half cell. At the half cell, the electrons would be consumed in a reduction reaction, transforming copper ions in the copper sulfate solution into copper atoms deposited on the rod. Because of the way the terminals of the voltmeter are connected in the electrical circuit shown in Fig. 2.5.7, the voltmeter would indicate a negative value. The more negative the voltage reading, the higher is the likelihood that the bar is corroding. If the wire connected to the bar were connected to the negative terminal of the voltmeter, the reading would be positive. The half-cell potential is also called the *corrosion potential* and it is an open-circuit potential, because it is measured under the condition of no current in the measuring circuit (ASTM G 15).

The half-cell potential readings are indicative of the probability of corrosion activity of reinforcement located beneath the reference cell. However, this is true only if all of the reinforcement is electrically connected. To assure that this condition exists, electrical resistance measurements between widely separated reinforcing bars should be carried out (ASTM C 876). Access to the reinforcement has to be provided. The method cannot be applied to concrete with epoxy-coated reinforcement.

Testing is usually performed at points arranged in a grid. The required spacing between test points depends on the particular structure. Excessive spacings can miss points of activity or provide insufficient data for proper evaluation, while closer spacings increase the cost of the survey. In surveying bridge decks, ASTM C 876 recommends a spacing of 1.2 m. If the differences in voltages between adjacent points exceed 150 mV, a closer spacing is suggested. However, others have suggested that spacing should be about one-half of this value to obtain a reliable assessment of the extent of the corrosion (Clemeña, Jackson, and Crawford, 1992a). Test apparatus is available that includes multiple cells to speed up data collection at close spacings.

A key aspect of the test is assuring that the concrete is sufficiently moist. If the measured potential at a test point does not change by more than ± 20 mV within a 5-min period (ASTM C 876), the concrete is sufficiently moist. If this condition is not satisfied, the concrete surface must be wetted, and two approaches are given in ASTM C 876. When pre-wetting is necessary, there should be no free surface water between test points. If stability can't be achieved by pre-wetting, it may be because of stray electrical currents, and the half-cell potential method should not be used. When testing is performed outside of the range of 17 to 28 C, a correction factor is applied to the measured voltages.

Data analysis—According to ASTM C 876, to formulate conclusions about corrosion activity, half-cell potential readings should be used in conjunction with other data, such as chloride content, depth of carbonation, findings of delamination surveys, and the exposure conditions. Data from a half-cell potential survey can be presented in two ways: an equipotential contour map, or a cumulative frequency diagram.

The equipotential contour map is used most often to summarize survey results. First, test locations are drawn on a scaled plan view of the test area. The half-cell voltage readings at each test point are marked on the plan, and contours of equal voltage values are sketched. Fig. 2.5.8 is an example of an equipotential contour map created from test points on a 0.76-m spacing (Clemeña et al., 1992a).

The cumulative frequency diagram is obtained by plotting the data on normal probability paper and drawing a best-fit straight line to the data, according to the procedure in ASTM C 876. The cumulative frequency diagram is used to determine the percentage of half-cell potential readings that are more negative than a certain value.

According to ASTM C 876, two techniques can be used to evaluate the results: the numeric technique, or the potential

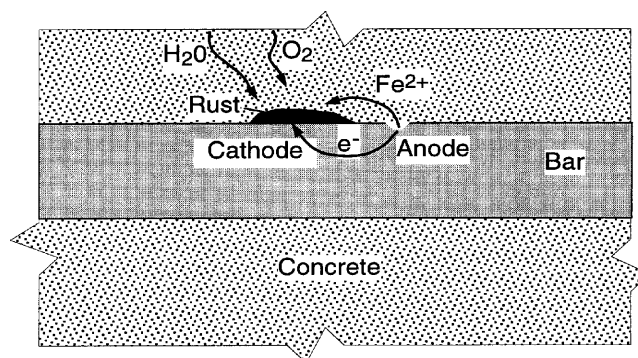


Fig. 2.5.6—Corrosion of steel bar embedded in concrete (iron is dissolved at anode and precipitates as rust at cathode).

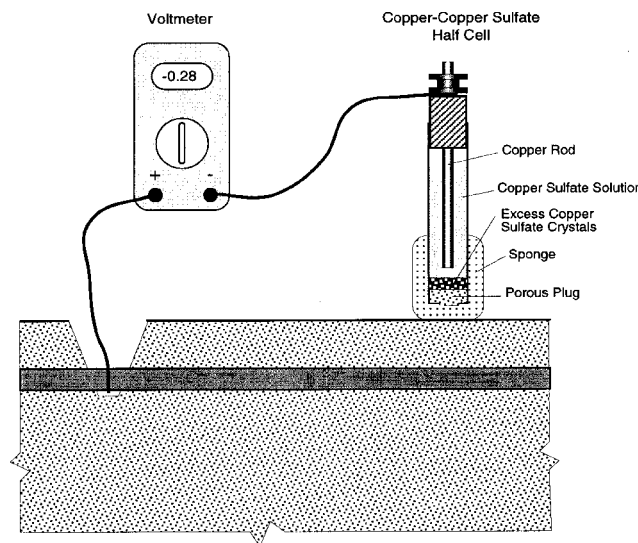


Fig. 2.5.7—Apparatus for half-cell potential method described in ASTM C 876.

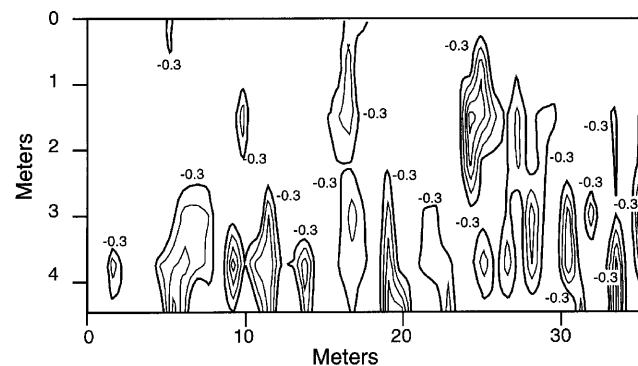


Fig. 2.5.8—Equipotential contours from survey data of bridge deck at grid spacing of 0.76 m (only contours less than -0.30 V are shown and contour interval is -0.05 V (adapted from Clemeña et al., 1992a).

difference technique. In the numeric technique, the value of the potential is used as an indicator of the likelihood of corrosion activity. If the potential is more positive than -200 mV, there is a high likelihood that no corrosion is occurring at the time of the measurement. If the potential is more negative than

Table 2.5—Advantages and limitations of magnetic and electrical methods

Method	Advantages	Limitations
Covermeter	Able to locate reinforcing bars and other embedded metal objects. Equipment is lightweight, portable, and easy to use. Cover depth can be estimated.	Accuracy of estimated cover depth affected by bar size and bar spacing. Bar diameters difficult to estimate with precision. Cannot identify presence of second layer of reinforcement. Ability to discern individual bars is affected by the meter design, cover depth, and bar spacing. Meters based on magnetic reluctance can detect only ferromagnetic objects. Maximum penetration is limited and depends on meter design.
Half-cell potential	Lightweight, portable equipment. Provides indication of likelihood of corrosion activity at time of testing.	Requires a connection to embedded reinforcement, and reinforcement must be electrically connected. Not applicable to epoxy-coated bars. Concrete has to be moist. No indication of corrosion rate. Testing and interpretation must be done by experienced personnel.
Linear polarization	Lightweight portable equipment. Provides indication of corrosion rate at time of testing.	Requires a connection to embedded reinforcement, and reinforcement must be electrically connected. Not applicable to epoxy-coated or galvanized bars. No standards for interpreting test results. Cover depth has to be less than 100 mm. Concrete surface has to be smooth, uncracked, free of impermeable coating, and free of visible moisture. Testing and interpretation must be done by experienced personnel.

-350 mV, there is a high likelihood of active corrosion. Corrosion activity is uncertain when the voltage is in the range of -200 to -350 mV. ASTM C 876 states that, unless there is positive evidence to suggest their applicability, these numeric criteria should not be used:

- If carbonation extends to the level of the reinforcement,
- To evaluate indoor concrete that has not been subjected to frequent wetting,
- To compare corrosion activity in outdoor concrete with highly variable moisture or oxygen content, or
- To formulate conclusions about changes in corrosion activity due to repairs that changed the moisture or oxygen content at the level of the steel.

In the potential difference technique, the areas of active corrosion are identified on the basis of the corrosion gradients. In the equipotential contour plot, regions of high gradients are indicated by the close spacing of the voltage contours. In Fig. 2.5.8, areas of corrosion activity are indicated by the closely spaced contours.

Limitations—The advantages and limitations of the half-cell potential method are summarized in Table 2.5. As has been stated, valid potential readings can be obtained only if the concrete is sufficiently moist, and the user must understand how to recognize when there is insufficient moisture.

Because of the factors that affect corrosion testing results, a corrosion specialist is recommended to properly interpret half-cell potential surveys under the following conditions (ASTM C 876):

- Concrete is saturated with water,
- Concrete is carbonated to the depth of the reinforcement, or
- Steel is coated (galvanized).

In addition, potential surveys should be supplemented with tests for carbonation and water soluble chloride content. A major limitation of the half-cell potential method is that it does not measure the rate of corrosion of the reinforcement. It only provides an indication of the likelihood of corrosion activity at the time the measurement is made. The corrosion rate of the reinforcement depends on the availability of oxygen needed for the cathodic reaction. It also depends on the electrical resistance of the concrete that controls the ease with which ions can move through the concrete. The electrical resistance depends on the microstructure of the paste and the moisture content of the concrete.

2.5.3 Linear-polarization method—The major drawback of the half-cell potential method has led to the development of techniques to measure the rate of corrosion. Several approaches have been investigated (Rodriguez et al., 1994).

However, the linear-polarization method appears to be used most frequently in the field (Flis et al., 1992) and is under consideration for standardization (Cady and Gannon, 1992). This section provides an overview of the method, but it is emphasized that actual testing and interpretation of test results should be done by experienced personnel.

Principle—In the field of corrosion science, the term polarization refers to the change in the open-circuit potential as a result of the passage of current (ASTM G 15). In the polarization resistance test, the current to cause a small change in the value of the half-cell potential of the corroding bar is measured. For a small perturbation about the open circuit potential, a linear relationship exists between the change in voltage ΔE , and the change in current per unit area of bar surface Δi . This ratio is called the polarization resistance R_p

$$R_p = \frac{\Delta E}{\Delta i} \quad (2.15)$$

Because the current is expressed per unit area of bar that is polarized, the units of R_p are ohms times area. The quantity R_p is not a resistance in the usual sense of the term (Stern and Roth, 1957), but the term is widely used (ASTM G 15). The underlying relationships between the corrosion rate of the bar and the polarization resistance were established by Stern and Geary (1957). No attempt is made to explain these relationships in this report. Simply stated, the corrosion rate is inversely related to the polarization resistance. The corrosion rate is expressed usually as the corrosion current per unit area of bar, and it is determined as follows

$$i_{corr} = \frac{B}{R_p} \quad (2.16)$$

where

i_{corr} = corrosion rate in ampere/cm²;

B = a constant in volts; and

R_p = polarization resistance in ohms-cm².

The constant B is a characteristic of the corrosion system and a value of 0.026 V is commonly used for corrosion of steel in concrete (Feliu et al. 1989). It is possible to convert the corrosion rate into the mass of steel that corrodes per unit of time. If the bar size is known, the corrosion rate can be converted to a loss in diameter of the bar (Clear, 1989).

Instrumentation—Basic apparatus for measuring the polarization resistance is the three-electrode system shown in Fig. 2.5.9 (Escalante, 1989; Clear, 1989). It is often called a “3LP” device. One electrode is composed of a reference half cell, and the reinforcement is a second electrode called the working electrode. The third electrode is called the counter electrode, and it supplies the polarization current to the bar. Supplementary instrumentation measures the voltages and currents during different stages of the test. Such a device can be operated in the potentiostatic mode, in which the current is varied to maintain constant potential of the working electrode; or it can be operated in the galvanostatic mode, in

which the potential is varied to maintain constant current from the counter electrode to the working electrode.

In simple terms, the procedure for using the 3LP device in the potentiostatic mode is as follows (Cady and Gannon, 1992):

- Locate the reinforcing steel grid with a covermeter and mark it on the concrete surface.
- Record the cover depth and bar diameters in area of interest.
- Make an electrical connection to the reinforcement (the working electrode).
- Locate the bar whose corrosion rate is to be measured, wet the surface, and locate the device over the center of the bar.
- Measure the corrosion potential of the reinforcement relative to the reference electrode, that is, measure the half-cell potential [Fig. 2.5.9(a)].
- Measure the current from the counter electrode to the working electrode that is necessary to produce a -4 mV change in the potential of the working electrode [Fig. 2.5.9(b)].
- Repeat the previous step for different values of potential, namely, -8 and -12 mV beyond the corrosion potential.
- Determine the area of bar affected by the measurement (perimeter of bar multiplied by the length below the counter electrode).
- Plot the potential versus the current per unit area of the bar, and determine the slope of the best-fit straight line. This is the polarization resistance.

A major uncertainty in obtaining the polarization resistance is the area of the steel bar that is affected by the current flowing from the counter electrode. In the application of the 3LP device, it is assumed that current flows in straight lines perpendicular to the bar (working electrode) and the counter electrode. Thus, the bar area affected during the tests is the bar circumference multiplied by the length of the bar below the counter electrode. However, numerical simulations show that the assumption is incorrect and that the current lines are not confined to the region directly below the counter electrode (Feliu et al., 1989; Flis et al., 1992). In an effort to better control the current path from the counter electrode to the bar, a device has been developed that includes a fourth electrode, called a guard or auxiliary electrode, that surrounds the counter electrode (Feliu et al., 1990a; Feliu et al., 1990b). Fig. 2.5.10 is a schematic of this type of corrosion meter. The guard electrode is maintained at the same potential as the counter electrode, and as a result the current flowing to the working electrode is confined to the region below the counter electrode.

A comparative study was conducted using laboratory and field tests of three commercially available corrosion-rate devices (Flis et al., 1992). Field test sites were chosen in three different environments representing the range of conditions that might be encountered in practice. Measurements were made on bridge structures at identical locations using the three devices. One of the devices was of the 3LP type (Clear,

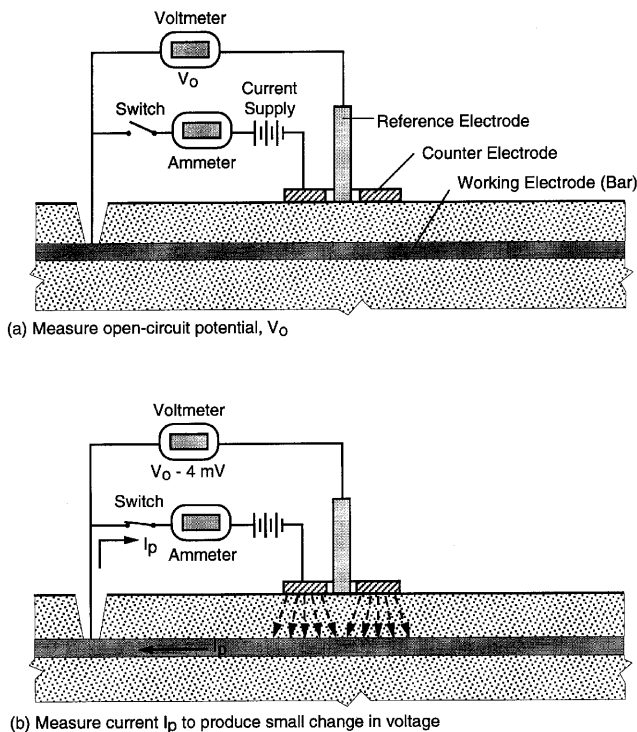


Fig. 2.5.9—Three-electrode, linear-polarization method to measure corrosion current: (a) measurement of open-circuit potential, and (b) measurement of current to produce small change in potential of working electrode (bar).

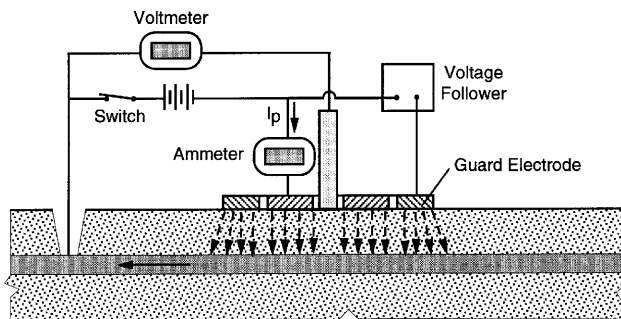


Fig. 2.5.10—Linear-polarization technique using guard electrode to confine current flow from counter electrode to reinforcement (adapted from Feliu et al., 1990a).

1989) and the other two used guard electrodes. The 3LP device gave higher values of corrosion current at the same test sites. The device developed in Spain (Feliu et al., 1990a) gave corrosion rates closest to the true corrosion currents. However, each device was capable of distinguishing between passive and active sites, and there were well-defined relationships between the corrosion currents measured by the different devices. It was concluded that all three devices could be used to locate active corrosion in a structure.

Limitations—Advantages and limitations of the linear-polarization method are summarized in Table 2.5. The corrosion rate at a particular point in a structure is expected to depend on several factors, such as the moisture content of the concrete, the availability of oxygen, and the temperature.

Thus, the corrosion rate at any point in an exposed structure would be expected to have seasonal variations. Such variations were observed during multiple measurements that extended over a period of more than one year (Clemeña et al., 1992b). To project the amount of corrosion that would occur after an extended period, it is necessary to repeat the corrosion-rate measurements at different times of the year. As suggested by Clemeña et al. (1992b), several alternatives could be used to predict the future condition of the reinforcement:

- Use the maximum measured corrosion rates to obtain a conservative estimate of remaining life,
- Use the yearly average corrosion rate at a typical or worst location in the structure, or
- Use the minimum and maximum corrosion rates to estimate the range of remaining life.

At this time, there are no standard procedures for interpreting corrosion-rate measurements obtained with different devices, and a qualified corrosion specialist should be consulted. For example, based on years of experience from laboratory and field testing, Clear (1989) developed the following guidelines for interpreting corrosion-rate measurements using a specific 3LP device:

- If i_{corr} is less than 2 mA/m^2 , no corrosion damage is expected,
- If i_{corr} is between 2 and 10 mA/m^2 , corrosion damage is possible within 10 to 15 years, and
- If i_{corr} is between 10 and 100 mA/m^2 , corrosion damage is expected within 2 to 10 years.

These guidelines assume that the corrosion rate is constant with time.

Other limitations should be considered when planning corrosion-rate testing. Some of these have been outlined in a proposed test method (Cady and Gannon, 1992) and are as follows:

- The concrete surface has to be smooth (not cracked, scarred, or uneven),
- The concrete surface has to be free of water impermeable coatings or overlays,
- The cover depth has to be less than 100 mm,
- The reinforcing steel can not be epoxy coated or galvanized,
- The steel to be monitored has to be in direct contact with the concrete,
- The reinforcement is not cathodically protected,
- The reinforced concrete is not near areas of stray electric currents or strong magnetic fields,
- The ambient temperature is between 5 and 40 C,
- The concrete surface at the test location must be free of visible moisture, and
- Test locations must not be closer than 300 mm to discontinuities, such as edges and joints.

2.5.4 Advantages and limitations—Table 2.5 summarizes the advantages and limitations of the magnetic and electrical

* Guidelines were given in mA/ft^2 . These have been converted approximately to mA/m^2 by multiplying by 10.

methods that can be used to gain information about the location and condition of steel reinforcement in concrete members. Covermeters are effective in locating bars, but there are difficulties when the steel is congested or the concrete cover is thick. Half-cell potential provides an indication of the likelihood of active corrosion, but data interpretation is not simple. The linear-polarization methods provide information about corrosion rate at the time of testing, but data interpretation is also not simple.

2.6—Penetrability methods

2.6.1 Introduction—Many of the degradation mechanisms in concrete involve the penetration of aggressive materials, such as sulfates, carbon dioxide, and chloride ions. In most cases, water is also required to sustain the degradation mechanisms. As a result, concrete that has a surface zone that is highly resistant to the ingress of water will generally be durable.

The ability of concrete to withstand environmental deterioration depends on the materials that were used to make the concrete, the mixture proportions, the degree of consolidation, and the curing conditions. The quality of the surface zone has been increasingly acknowledged as the major factor affecting the rate of degradation of a concrete structure (Kropp and Hilsdorf, 1995). To assess the potential durability of in-place concrete, it is necessary to focus on methods that assess the ability of the surface zone to restrict the passage of external agents that may lead to direct deterioration of the concrete or to depassivation and corrosion of embedded reinforcement. The tests described in this section are surface zone tests that provide useful information for evaluation of the potential durability of concrete.

2.6.2 Ingress mechanisms—There are three principal mechanisms by which external agents can penetrate into concrete.

Absorption—This term refers to the ingress of liquids due to capillary forces. Contaminants, such as chloride ions and sulfates, are transported within the liquid. The term *sorptivity* is used to describe the tendency of a material to absorb a fluid. For one-dimensional water absorption into an initially dry porous solid, the volume of absorbed fluid can be related to time by the following empirical equation (Hall, 1989)

$$V = As\sqrt{t} \quad (2.17)$$

where

V = volume of fluid absorbed (m^3);
 A = wetted area (m^2);
 s = sorptivity (m/\sqrt{s}); and
 t = time (s).

Permeation—This term refers to the flow of a fluid under the action of a pressure head. For steady-state, unidirectional flow of a liquid through a saturated porous material, the flow rate is described by Darcy's law, as follows

$$Q = kAI \quad (2.18)$$

where

Q = flow rate (m^3/s);
 k = the coefficient of permeability (m/s);
 A = cross-sectional area of flow (m^2); and
 I = hydraulic gradient (m/m).

The coefficient of permeability depends on both the structure of the material and the properties of the fluid. In the case of concrete, the coefficient of permeability depends primarily on the mixture proportions, the water-cement ratio and the maturity, that is, the extent of hydration (and pozzolanic reaction, if applicable). If the fluid is a gas, an equation analogous to Eq. (2.18) can be used to describe the unidirectional flow rate in terms of the differential pressure.

Diffusion—This term refers to the movement of molecular or ionic substances from regions of higher concentration to regions of lower concentration of the substances. The rate of movement of the substance is proportional to the concentration gradient along the direction of movement and the diffusion coefficient, and is given mathematically by Fick's first law of diffusion (Kropp and Hilsdorf, 1995)

$$F = \frac{\partial m}{\partial t} \frac{1}{A} = -D \frac{\partial C}{\partial x} \quad (2.19)$$

where

F = mass flux (kg/m^2s);
 m = mass of flowing substance (kg);
 t = time (s);
 A = area (m^2);
 D = diffusion coefficient (m^2/s);
 C = concentration (kg/m^3); and
 x = distance (m).

2.6.3 Penetrability tests—Various test methods have been devised for assessing the durability potential of a concrete surface. Most of the techniques attempt to model one of the above transport mechanisms. The term *penetrability tests* encompasses all of these test methods and is used in this report as the general term to describe this class of test methods. The penetrability tests can be grouped into the following three categories:

1. Those based on water absorption,
2. Those based on water permeability, and
3. Those based on air permeability.

The following sections describe the instrumentation and procedures for some of the commonly used or promising new test procedures.

2.6.4 Description of test methods

Absorption tests—Absorption tests measure the rate at which water is absorbed into the concrete under a relatively low pressure head. The absorption rate is a function of the capillary porosity, which is in turn dependent on the water/cement ratio and curing history. Of the tests to be described, one is a surface-absorption technique and the others measure absorption within a hole drilled into the concrete.

Initial surface-absorption test (ISAT)—In this method (Levitt, 1971), a circular cap with a minimum surface area of 5000 mm^2 is sealed to the concrete surface. A reservoir attached to the cap is filled with water so that the water level is

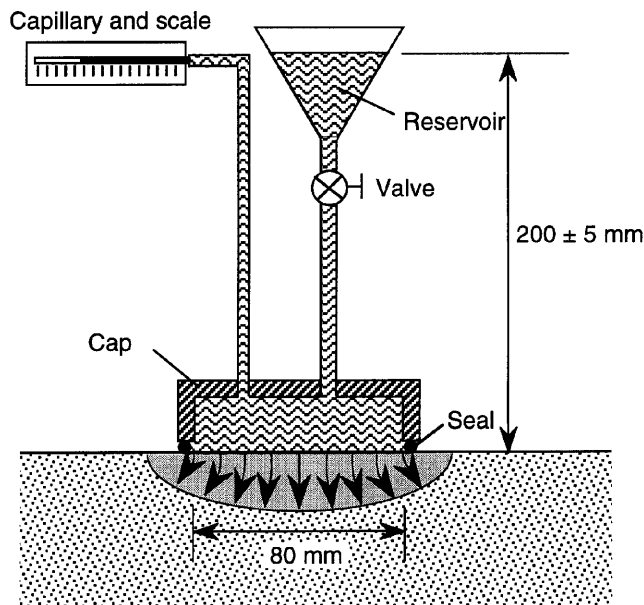


Fig. 2.6.1—Schematic of initial surface-absorption test (ISAT).

200 mm above the concrete surface. The cap is also connected to a horizontal capillary positioned at the same height as the water in the reservoir (Fig. 2.6.1). At specified intervals (10 min, 30 min, 1 hr, and 2 hr) from the start of the test, the valve below the reservoir is closed and the rate at which water is absorbed into the concrete is measured by the movement of water in the capillary attached to the cap. This test is standardized in the United Kingdom (BS 1881: Part 5).

Figg water-absorption Test—Figg's original test procedure required a 5.5-mm diameter hole to be drilled into the concrete to a depth of 30 mm. The hole was cleaned, a disk of a rigid polymeric foam was pushed into the hole to a depth of 20 mm from the surface, and the hole was sealed with silicone rubber (Figg, 1973). A hypodermic needle was inserted through the silicone rubber seal and connected to a syringe and capillary via a series of connectors (Fig. 2.6.2). A water head of 100 mm was applied and the time for the meniscus to travel 50 mm in the horizontal capillary (similar to that used in the ISAT) was recorded. The value obtained was called the absorption index and was measured in seconds. A higher absorption index corresponds to better-quality concrete. Since Figg's initial work, a number of modifications were made to the equipment and procedure to improve the accuracy and repeatability of the results (Cather et al., 1984; Figg, 1989). These modifications include a larger hole, an automated measurement of the meniscus travel, and the use of a pre-molded plug, alleviating the need to wait for the silicone rubber to cure before performing a test. Equipment for this test is commercially available.

Covercrete-absorption test—A deficiency of the ISAT is that the absorption is influenced predominantly by the surface zone. In the Figg test, the absorption is controlled by the concrete deeper than 20 mm. The covercrete-absorption test tries to overcome these two deficiencies (Dhir et al., 1987) by

making an absorption measurement that includes the surface as well as the interior concrete, the so-called "covercrete." A 13-mm diameter hole is drilled to a depth of 50 mm, and a gasketed cap is placed over the hole. A tube connected to a reservoir passes through the cap and empties into the hole. The cap contains a second tube connected to a horizontal capillary as in the ISAT and Figg test. The reservoir and capillary are positioned so that a water head of 200 mm is maintained above the center of the hole. The tube to the reservoir is shut off and the movement of the meniscus in the capillary is measured between 10 and 11 min after initial contact with water. The main advantage of this test compared with the ISAT and Figg tests is the ability to obtain an integrated absorption measurement of the surface zone to a depth of 50 mm.

Water-permeability tests—The above absorption tests involve a low water head (200 mm of water is about 2 kPa above atmospheric pressure*), and the flow is governed primarily by the sorptivity of the concrete. In-place water-permeability tests have been developed that use higher pressures to obtain indications of the coefficient of permeability of the concrete.

CLAM test—This method involves measuring the flow of water into the concrete surface under a fixed pressure (Montgomery and Adams, 1985). A specially designed cap is glued to the concrete surface (Fig. 2.6.3), and pressurized water is provided by a micrometer-screw piston. A pressure gauge in the chamber measures the water pressure. To perform the test, the chamber is filled with water, the micrometer screw is turned so as to maintain a constant water pressure of about 150 kPa above atmospheric pressure, and the movement of the piston is recorded at periodic intervals for a 20- to 30-min period. The travel of the piston multiplied by the area of the cylinder gives the volume of water that penetrates into the concrete. A plot of the volume of water versus time provides information on the permeability of the concrete. Since the flow of water into the concrete is not unidirectional and a steady-state condition is not attained, the test provides a permeability index, rather than the coefficient of permeability.

The CLAM test can also be performed at a lower water pressure so that penetration is controlled primarily by absorption, rather than by a combination of absorption and permeation. For the absorption measurement, the piston is advanced at a rate that maintains the water pressure at 1 kPa (Basheer et al., 1992). Again, because the resulting absorption is not unidirectional, a sorptivity index is obtained rather than the true sorptivity.

Steinert method—This test method, reported by Steinert (1979), uses the guard ring principle to attain a better approximation of unidirectional flow under pressure (Fig. 2.6.4). The cap, which is composed of two concentric chambers separated by a circular rubber seal, is glued to the concrete surface. The concentric chambers are filled with water and pressurized to 600 kPa with compressed air. Flow under the inner chamber is approximately unidirectional, so that the

* As a point of reference, atmospheric pressure at sea level is about 100 kPa.

record of flow as a function of time is easier to interpret than in the CLAM test.

Air-permeability tests—A wide variety of tests have been proposed that are based on measurement of the flow of air, or other gases, through concrete. There are relationships between air permeability and other durability indicators, such as water-cementitious materials ratio, strength, and curing efficiency (Whiting, 1987). Similar to the water-based tests, air-permeability tests involve either drilling a hole into the concrete surface or the application of a chamber to the surface. In most cases, a vacuum is applied and the decrease of the vacuum with time is taken as an indicator of the air permeability. In general, air-permeability tests are simpler to perform than the water-based tests.

Figg air-permeability test—The original Figg air-permeability test involves the same hole preparation procedure as for the water-absorption test described above (Figg, 1973). The tube, however, is connected to a vacuum pump instead of the syringe and manometer apparatus used for the water test. The vacuum pump is activated until the pressure inside the hole is decreased to a prescribed value below atmospheric pressure. The valve is closed, and flow of air into the hole reduces the vacuum. The time to obtain a prescribed pressure increase in the hole is measured, and the time in seconds is called the air-permeability index. A higher air-permeability index indicates a less permeable concrete. In the original Figg test, the prescribed vacuum pressure was -85 kPa and the prescribed pressure increase was 5 kPa. In a subsequent modification (Fig. 2.6.5) intended to improve repeatability, the hole size was increased to 10 mm in diameter and 40 mm in depth and the prescribed initial vacuum pressure was changed from -85 kPa to -55 kPa (Cather et al., 1984). The reduced vacuum was selected to permit the use of hand-operated vacuum pumps. In another modified form of the Figg test (Dhir et al., 1987) intended to improve the repeatability further, the hole diameter was increased to 13 mm, the depth increased to 50 mm, and the prescribed pressure change was taken from -55 kPa to -45 kPa.

Schönlin test—The Figg test gives a measure of the air permeability of the cover zone traversed by the open portion of the hole and requires drilling a hole into the concrete. To avoid having to drill a hole, surface test methods have been proposed. In Schönlin's method (Fig. 2.6.6), a 50-mm diameter chamber of known volume is placed on the surface, and a vacuum pump is used to evacuate the chamber to a pressure less than -99 kPa (Schönlin and Hilsdorf, 1987). The valve is closed, and the time when the vacuum pressure reaches -95 kPa is taken as the start of the test. The time required for the vacuum pressure to increase to -70 kPa is measured. For dense concrete, the vacuum pressure change during 120 seconds is measured instead. Based on these measurements and the known volume of the chamber, a permeability index in units of m^2/s is calculated. In an effort to attain a standard moisture condition prior to testing, the surface is dried with hot air for 5 min prior to testing.

Surface airflow test—The surface airflow test (SAF) is based on a method used within the petroleum industry for

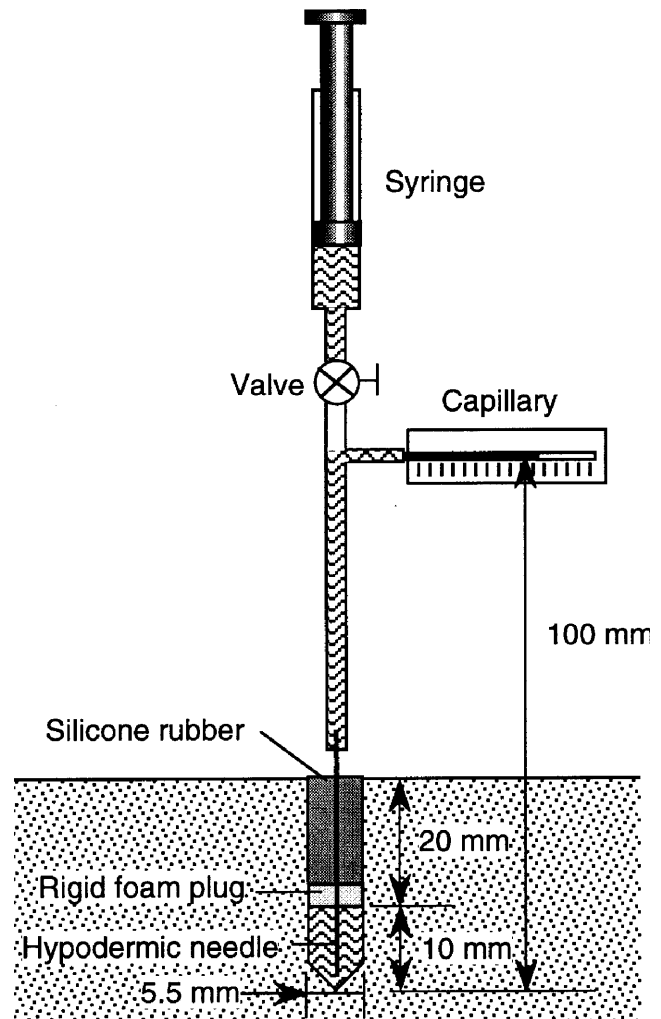


Fig. 2.6.2—Schematic of original Figg water-absorption test.

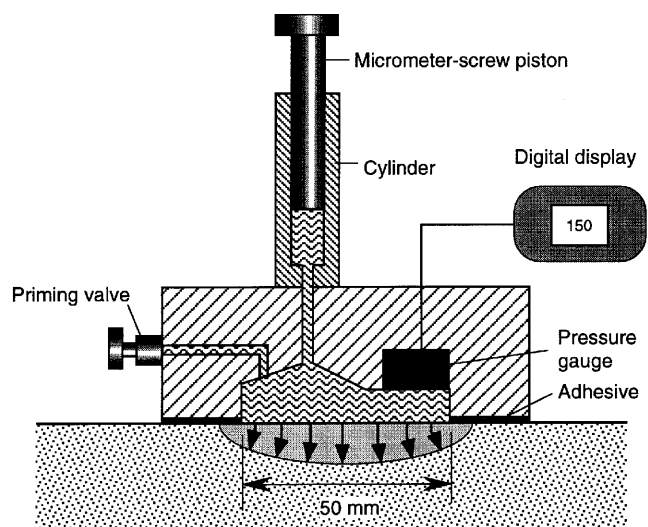


Fig. 2.6.3—Schematic of CLAM apparatus.

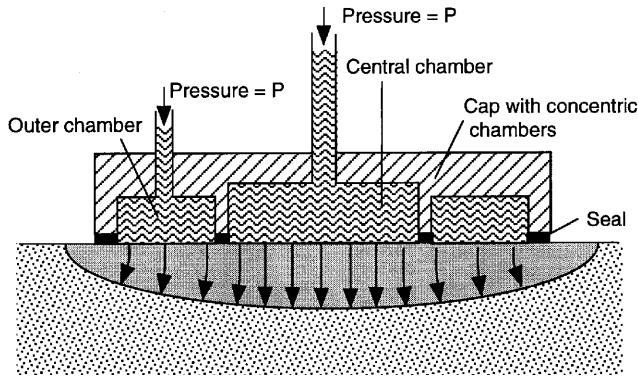


Fig. 2.6.4—Schematic of Steinert's "guard ring" method to approximate unidirectional flow.

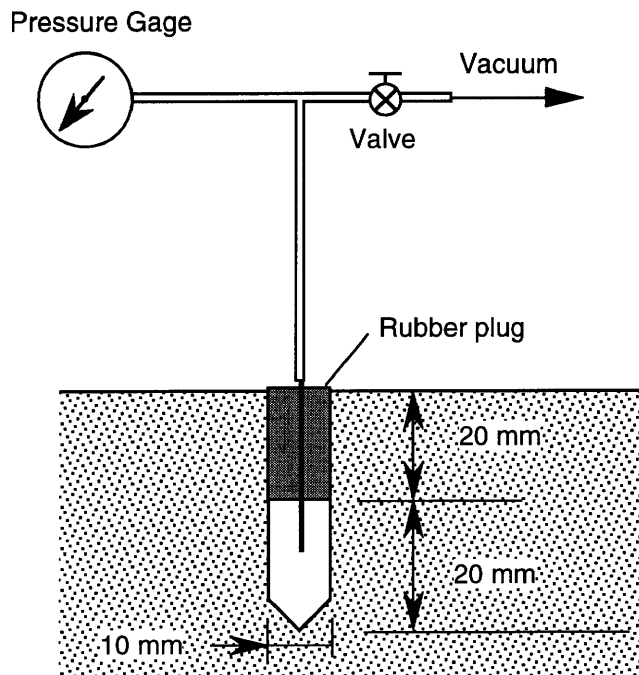


Fig. 2.6.5—Schematic of modified Figg air-permeability test.

the rapid determination of the permeabilities of rock cores (Whiting and Cady, 1992). A schematic of the apparatus is shown in Fig. 2.6.7. A vacuum plate, with a soft rubber ring to provide an airtight seal, is placed on the concrete surface. To conduct the test, valves A, B, and C are closed and the vacuum pump is activated. The pump is of such capacity that the vacuum pressure should stabilize at about -83 kPa within 15 sec. Valve A is opened and the vacuum pressure should again stabilize at -83 kPa. Valve B is opened and valve A is closed, directing airflow through the flowmeter. After 15 sec, the reading of the flowmeter is recorded. The flow rate in mL/m is used as an indicator of the surface air permeability. Experiments have demonstrated that the effective depth of the measurement is about 13 mm (Whiting and Cady, 1992). As in the Schönlin test, the surface should be dried with hot air if it is suspected that the surface layer may have a high moisture content.

Pressure Gage

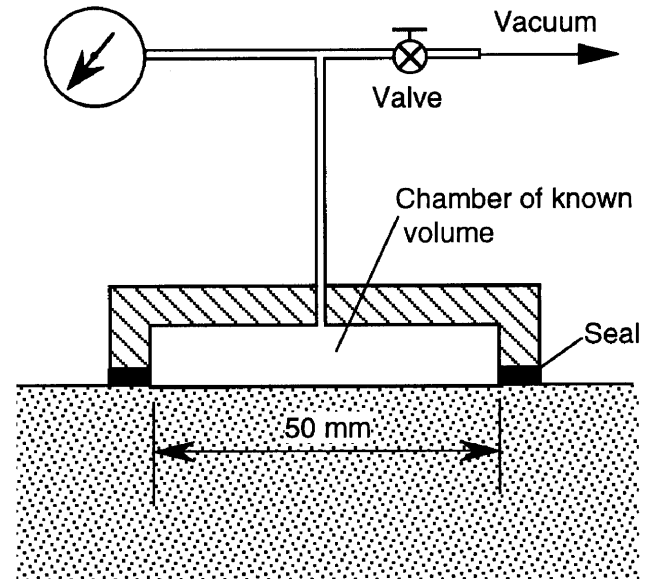


Fig. 2.6.6—Schematic of Schönlin's surface air-permeability test.

2.6.5 Advantages and limitations—The advantages and limitations of the various penetrability methods that have been discussed are summarized in Table 2.6.

Absorption tests—The initial surface-absorption test (ISAT) provides a surface measurement and models water absorption, which is the most common ingress mechanism associated with concrete deterioration. The test has been used extensively in the United Kingdom and a considerable amount of field data and experience in using the equipment has been gained. The test is totally nondestructive and can be used on both vertical and horizontal surfaces. Limitations of the ISAT are as follows:

- For concretes with a low surface sorptivity, the flow path may be considered approximately unidirectional, and the ISAT measurements are related to unidirectional sorptivity measurements (Hall, 1989). However, as the sorptivity of the surface layer increases, radial flow becomes significant and there is no reliable relationship between ISAT measurements and sorptivity measurements.
- Achievement of a watertight seal between the cap and the concrete surface can be difficult in the field. Investigation of modifications to overcome this problem have been performed with some success in the United Kingdom.
- The ISAT is capable of testing only the outer 10 to 15 mm of the concrete. When considering reinforcement corrosion, it may be desirable to assess the complete cover zone.
- Test results are affected by the presence of curing compounds or other surface coatings.

The Figg test requires holes to be drilled into the concrete and the outer 20 mm of the concrete has to be sealed off. Surface skin properties are therefore excluded from the

measurement. The test is not affected by surface coatings or curing compounds. The covercrete-absorption test also requires drilling a hole, but the measurement includes the effect of all the concrete surrounding the hole, including the surface zone.

Water-permeability tests—Both the CLAM and the Steiner water-permeability tests produce an empirical permeability index for a particular concrete. Measurement of an absolute property, rather than an empirical permeability index, is preferable because there are well-defined relationships between the coefficient of permeability and other durability related factors (Whiting, 1987). In-place methods based on water permeability, however, do not correlate with these durability factors as well as the air-permeability tests. The interference of concrete moisture content prior to testing appears to have a more serious effect on water-permeability tests than on air-permeability tests.

Other drawbacks of water-permeability tests are the long testing times and the need to glue or clamp the equipment to the concrete surface to effectively sustain the applied water pressure.

Air-permeability tests—In general, most air-permeability techniques are quick and simple to perform. In the case of vacuum-mounted devices, no permanent attachment is needed. Unlike water tests, air-permeability tests do not affect the penetrability properties of the concrete. As a result, an air-permeability test can be repeated at the same location. Air-permeability tests appear to be less affected by the moisture content of the concrete than water-permeability tests.

Surface tests, such as the SAF test and Schönlin's method, are affected primarily by the top 15 mm of concrete and do not provide an indication of the penetrability properties of the entire cover zone. Tests based on Figg's method require drilling a hole and exclude the near surface layer in the measurement.

Generally, each test method results in an air-permeability index that can be related to other factors that govern the durability of concrete. In most cases, however, the index obtained by a specific method is not related to the index obtained by another method that uses a different geometry and test pressure.

General limitations—Although the penetrability techniques are related to the mechanisms associated with concrete deterioration, certain limitations must be considered when using a particular test method in practice. These limitations include: sensitivity to moisture and temperature changes; changes in transport mechanism during the test (for example, sorption to diffusion); variance of air permeability with applied pressure; and the influence of drilling on test values. The empirical nature of the tests and the associated complex flow characteristics have prevented the conversion of test results to absolute property measurements.

The most important limitation is, by far, the effect of concrete moisture content at the time of testing. A dry concrete will absorb more water and allow more air flow than the same concrete in a saturated state. A poor-quality concrete tested in a moist condition can result in apparently better

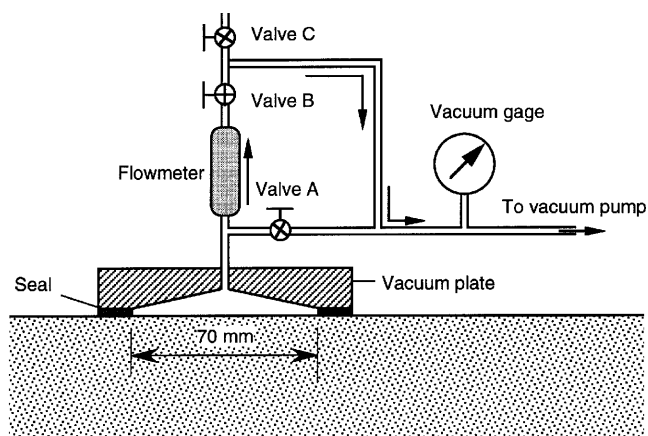


Fig. 2.6.7—Schematic of surface air flow (SAF) test.

indicators of durability than a higher-quality concrete tested in a dry condition. Some methods try to account for this problem by specifying that the test should not be conducted within a certain period after a rainfall. However, since the drying of the concrete is a function of the ambient temperature and relative humidity, specifying a natural drying time does not assure that the moisture content is at a "standard" level. Other methods specify a period of drying with hot air prior to testing (Kropp and Hilsdorf, 1995).

For methods based on drilling a test hole, the percussion action of the hammer-drill can have a detrimental and uncontrollable effect on the concrete in the vicinity of the hole. Cracks can be produced in the concrete that allow air and water to flow more readily along them. This condition can produce discrepancies between test results, especially in water-absorption tests.

2.7—Infrared thermography

Infrared thermography has been used for detecting subsurface anomalies within and below concrete elements. The method has been applied to the identification of internal voids, delaminations, and cracks in concrete structures such as bridge decks (Holt and Manning, 1978), highway pavements (Weil, 1991), parking garages, pipelines (Weil, 1989), and buildings. ASTM D 4788 describes the use of infrared thermography for detecting delaminations in concrete bridge decks, with and without asphalt overlays.

2.7.1 Principle—Infrared thermography senses the emission of thermal radiation and produces a visual image from this thermal signal. Thermography, like any system using infrared radiation, measures variation in surface radiance and does not directly measure surface temperature. However, it can be used to detect anomalies in surface radiance that may relate to subsurface conditions of the concrete member.

Infrared thermography for testing concrete is based on two principles. The first principle is that a surface emits energy in the form of electromagnetic radiation. The rate of energy emitted per unit surface area is given by the Stefan-Boltzmann law (Halliday and Resnick, 1978)

Table 2.6—Advantages and limitations of penetrability methods

Method	Advantages	Limitations
ISAT	Simple and inexpensive to perform. Portable equipment. Sensitive to changes in concrete quality. Totally nondestructive. Considerable experience has been gained in its use.	Unreliable for concrete with a high sorptivity surface layer. Measures absorption of outer surface concrete only and is affected by surface coatings. Difficult to seal circular cap at the concrete surface. Sensitive to concrete moisture condition.
Figg Water - Absorption Test	Not affected by coatings and surface concrete layer. Inexpensive and simple to use.	Intrusive because drilling is necessary. Drilling may affect concrete under test. Sensitive to aggregate characteristics. Sensitive to concrete moisture condition.
Covercrete-Absorption Test	Gives an integrated measure of the entire cover zone.	Intrusive because drilling is necessary. Drilling may affect concrete under test. Sensitive to concrete moisture condition
CLAM (Water Permeability)	Measures flow under constant pressure conditions.	Provides a permeability index, not coefficient of permeability. Sensitive to concrete moisture condition. Concrete surface is damaged. Long test time required.
Steinert Method (Water Permeability)	Measures unidirectional flow. Easier to interpret than CLAM.	Provides a permeability index, not coefficient of permeability. Sensitive to concrete moisture condition. Concrete surface is damaged. Long test time required.
Figg Air-permeability Test	Inexpensive and simple to use. Not influenced by surface layer or coatings. Less sensitive to moisture condition than water tests.	Sensitive to aggregate characteristics. Intrusive because drilling is required. Drilling may affect concrete under test . Provides a permeability index, not coefficient of permeability.
Schönlin Test (Air Permeability)	Nondestructive. Less sensitive to moisture condition than water tests. Includes concrete moisture conditioning procedure.	Provides a permeability index, not coefficient of permeability. Measures outer surface concrete only and is affected by surface coatings.
Surface Airflow Test	Nondestructive. Less sensitive to moisture condition than water tests. Includes concrete moisture conditioning procedure	Provides permeability index, not coefficient of permeability. Measures outer surface concrete only and is affected by surface coatings.

$$R = e\sigma T^4 \quad (2.20)$$

where

R = rate of energy radiation per unit area of surface, W/m²;

e = the emissivity of the surface;

σ = the Stefan-Boltzmann constant, 5.67×10^{-8} W/m²·K⁴; and

T = absolute temperature of the surface K.

The wavelength of the emitted radiation depends on the temperature. As the temperature increases, the wavelength becomes shorter. At a sufficiently high temperature, the radiation is in the visible spectrum. For example, this phenomenon is observed when a nail is heated and emits visible light at high temperatures. However, in the range of room temperature, the wavelength of the emitted radiation is on the order of 10 μ m, which is in the infrared region of the spectrum.

This radiation can be detected by special sensors that produce electrical signals in proportion to the amount of incident radiant energy. With proper calibration, the output of an infrared sensor can be converted to temperature. Thus, it is possible to measure the surface temperature of the concrete without having to make contact with a thermometer or thermocouple.

The second principle is that subsurface anomalies in the concrete affect heat flow through the concrete (Fig. 2.7.1). If the anomalies are not too deep, these changes in heat flow cause localized differences in surface temperature. By measuring surface temperature under conditions of heat flow, the subsurface anomalies can be located.

The required heat-flow condition can be created artificially by using heating lamps, or it can occur naturally by solar heating (heat flow into the structure) and night-time cooling

(heat flow out of the structure). The latter methods are obviously the economical approach.

In summary, infrared thermography for testing concrete exploits two main heat transfer mechanisms: conduction and radiation. Sound concrete is more thermally conductive than low density or cracked concrete. Radiation from the concrete surface depends upon the emissivity of the material, which is defined as the ability of the material to radiate energy compared to a perfect black body radiator. Rougher surfaces of the same material have higher emissivity values. Some values of emissivity are (Weil, 1991):

- Rough clean concrete $e = 0.95$, and
- Shiny steel $e = 0.05$.

Different surface textures and finishes (brush marks, rubber, or oil residues) will affect the surface radiation properties. Thus, care must be exercised to assure that apparent measured temperature differences are not due to differences in emissivity.

The physical parameters determining the emitted infrared radiation measured during a thermographic survey are: concrete surface emissivity, surface temperature, concrete thermal conductivity, concrete volumetric-heat capacity, thickness of the heated layer, and intensity of incident solar radiation. The environmental conditions present at the time of testing also affect surface temperature measurements. Clouds reduce solar radiation during the day and reflect infrared radiation at night, slowing heat transfer at the concrete surface. Wind and surface moisture reduce temperature gradients, and water below 0 C forms ice in voids and cracks. The optimum weather conditions are: clear skies, mild wind, dry concrete surface, and intense solar radiation. To overcome environmental influences on testing, the following guidelines are suggested (ASTM D 4788):

- Remove debris from surface.
- Do not test when standing water, ice or snow are present; allow surface to dry at least 24 hr before testing.
- Do not test if wind speeds exceed 25 kph.
- The ground temperature should be above 0 C.
- Testing at night should be done under clear skies.

Above all else, testing should be performed when the largest heating or cooling gradients are present in the concrete. When cooling conditions are present (testing at night, for example), the concrete above any anomalies will be cooler than the surrounding sound concrete. The reverse is true during heating conditions. The suggested best time for doing infrared surveys is soon after sunrise or one-half to one hour after sunset. If testing is performed too long after a thermal change, the concrete surface may become thermally saturated such that the thermal anomalies have passed. The amount of time required in direct sunlight to develop detectable anomalies differs for various applications. For example, ASTM D 4788 recommends 4 hr of direct sunshine on concrete and 6 hr on asphalt-covered concrete decks for detecting delaminations in bridge decks.

2.7.2 Equipment—Thermographic scanning and analysis systems comprise three main components: a scanner/detec-

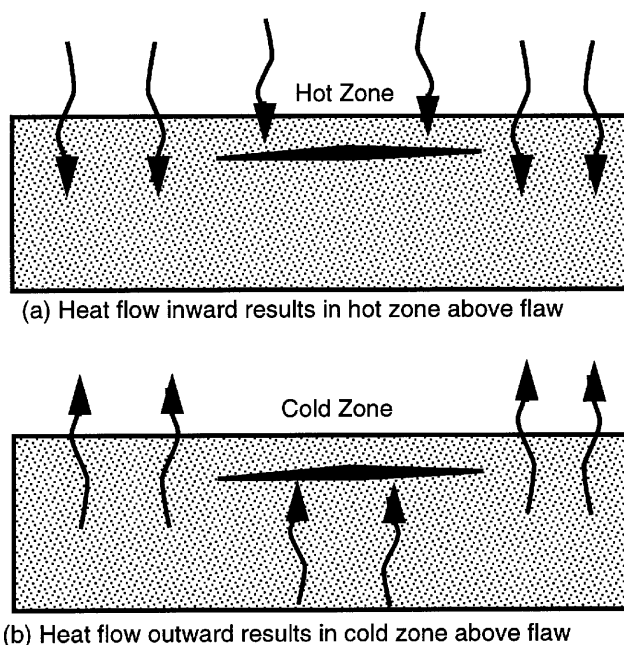


Fig. 2.7.1—Effect of internal anomaly on surface temperature during heat flow.

tor unit, a data acquisition/analysis device, and a visual image recorder. The infrared scanner head is an optical camera, with lenses that transmit only infrared radiation with wavelengths in the range of 3 to 5.6 μm (shortwave), or 8 to 12 μm (medium wave). A system of rotating mirrors is used to enable a two-dimensional scan of the test object (Fig. 2.7.2). The infrared detector is normally cooled by liquid nitrogen to a temperature of -196 C, and can detect temperature variations as small as 0.1 C. However, new sensors have been developed that do not require cooling (Kaplan, 1994; Matthews et al., 1994). These sensors are composed of a two-dimensional array of materials sensitive to incident infrared radiation. The use of a 2-D array eliminates the need for rotating mirrors as in conventional optical-mechanical, infrared cameras. The data acquisition and analysis unit includes an analog-to-digital (A/D) converter, a computer with a high resolution monitor and a data storage device, and data analysis software. For rapid coverage of large areas, such as highway or airfield pavements, the equipment can be mounted on an automotive vehicle.

Data obtained by the scanner/detector unit are digitized and displayed as shades of gray or color, depending on the data analysis software. Cooler or hotter regions are identified by a different gray shading or color compared with the surrounding concrete. A visual image recording unit, such as a videotape recorder, a film camera, or a digital video camera, is used to provide a record of the region scanned by the infrared camera. Comparison of the visual and infrared images is necessary to ensure that apparent temperature differences in the infrared image are not due to differences in surface emissivities. As an example, Fig. 2.7.3 shows an optical photograph (top) and the corresponding infrared thermogram (bottom) of a bridge deck. The locations of delamination are

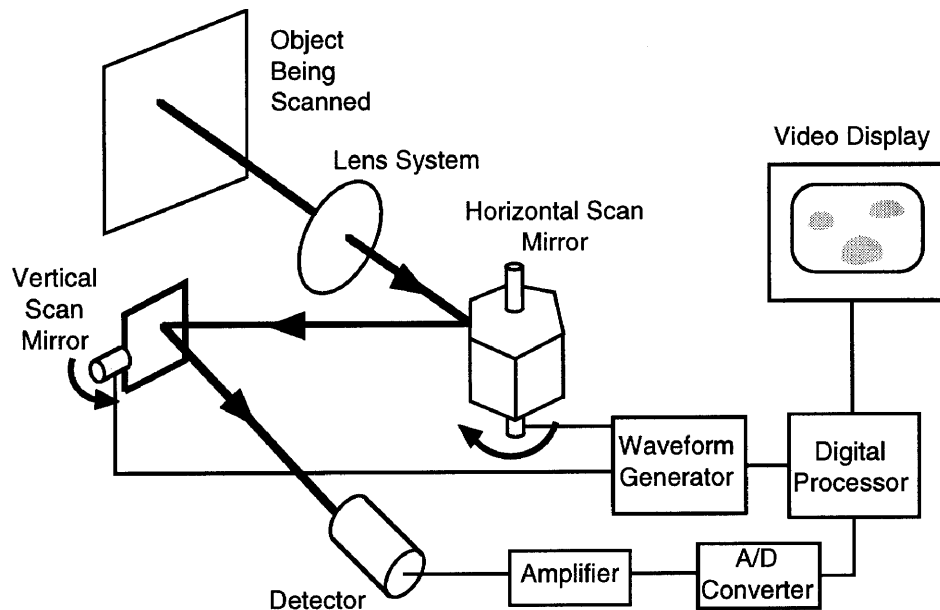


Fig. 2.7.2—Schematic of infrared scanner system used to create thermal image (adapted from Schlessinger, 1995).

identified by the brighter “hot” spots in the thermographic image. Note that the asphalt patch results in a false indication because of its different emissivity and thermal properties.

2.7.3 Advantages and limitations—The advantages and limitations of infrared thermography are summarized in Table 2.7. Infrared thermography is a global inspection method, and permits large surface areas to be surveyed in a short period of time. Its main application in civil engineering has been to detect delaminations in bridge decks and reinforced concrete pavements.

Among its disadvantages is the requirement for the appropriate environmental conditions to achieve the heat-flow conditions needed to detect the presence of subsurface anomalies. However, even with the proper heat-flow conditions, not all delaminations are detectable. Maser and Roddis (1990) performed analytical studies to gain an understanding of the factors affecting the differences in the surface temperature of a solid concrete slab and a slab with a delamination. Examples of the results of such analyses are shown in Fig. 2.7.4. Fig. 2.7.4(a) shows the analytical model that was used. In the analyses (based on the finite element method), the concrete slab was subjected to a sinusoidal variation of ambient temperature with a 24-hr cycle and a parabolic variation in incident solar radiation. The air temperature varied from 16 to 30 C. Fig. 2.7.4(b) shows the differences in surface temperature compared with a solid slab for different cover depth and a 1.27-mm-wide air-filled crack. It is seen that the maximum differential temperature decreases as the depth of the delamination increases. Fig. 2.7.4(c) shows the results for different crack widths at a cover depth of 38 mm. It is seen that the crack width has a strong effect on the maximum temperature differential. It was also found that a water-filled delamination resulted in nearly identical surface temperatures as in a solid slab. Finally, it is noted that while infrared thermography can provide information on the areal extent of

a subsurface anomaly, it is not able to provide information on its depth.

2.8—Radar

2.8.1 Introduction—Radar (acronym for Radio Detection and Ranging) is analogous to the pulse-echo technique discussed in Section 2.2.2, except that electromagnetic waves (radio waves or microwaves) are used instead of stress waves. The early uses of the technique were for military applications, but radar techniques are now used in a variety of fields. The earliest civil engineering applications were for probing into soil to detect buried pipelines and tanks. This was followed by studies to detect cavities below airfield pavements, and more recently for determining concrete thickness, locating voids and reinforcing bars, and identifying deterioration (Bungey and Millard, 1993; Cantor, 1984; Carter et al., 1986; Clemeña, 1983; Kunz and Eales, 1985; Maser, 1986, 1989, 1990; Maser and Roddis, 1990; Steinway et al., 1981; Ulriksen, 1983). The most attractive features of this technology are: its ability to penetrate into the subsurface and detect unseen conditions; its ability to scan large surface areas in a short period of time; and its high sensitivity to subsurface moisture and embedded metal.

In civil engineering applications, inspection depths are relatively shallow compared with other uses of radar. As a result, devices for these applications emit short pulses of electromagnetic waves (microwaves). For this reason, the technique is often called short-pulse radar, impulse radar,* or ground-penetrating (probing) radar (GPR). In this report, it

* Two other approaches that have been considered potentially appropriate for structural applications are frequency modulation and synthetic-pulse radar (Bungey and Millard, 1993). These approaches have been excluded from this section because pulsed systems have gained the greatest practical acceptance and are most readily available commercially.

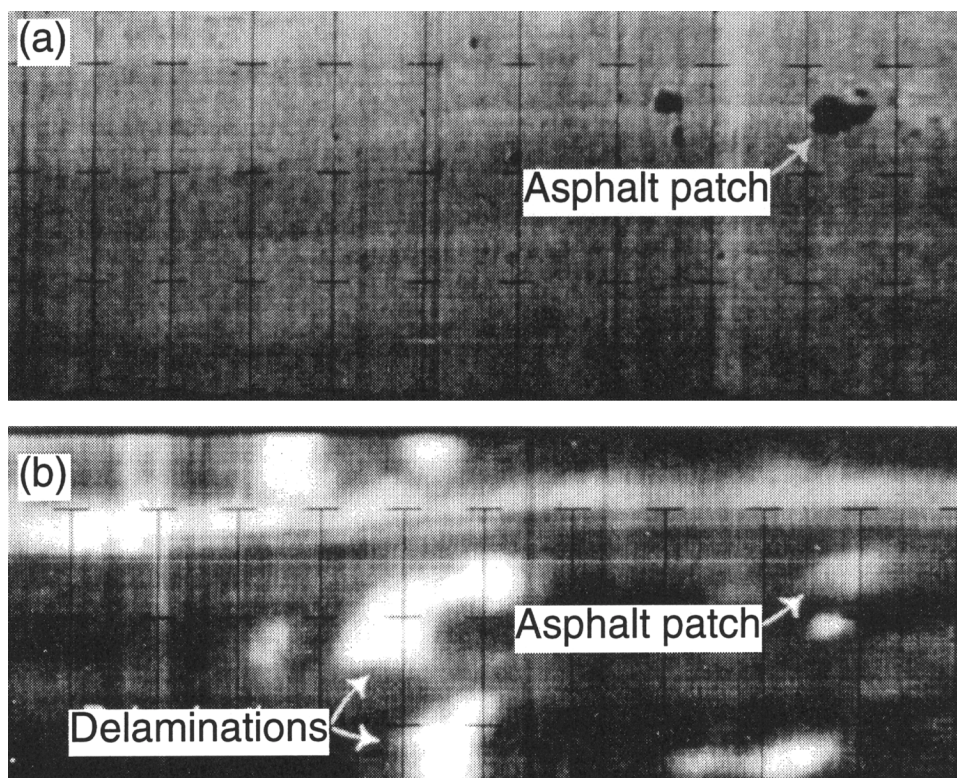


Fig. 2.7.3—Example of infrared thermography: (a) optical photograph of concrete bridge deck, and (b) infrared thermogram showing “hot spots” corresponding to locations of concrete delaminations and false indication due to asphalt patch.

Table 2.7—Advantages and limitations of infrared thermography

Advantages	Limitations
<p>A global technique that covers much greater areas than other test methods, and is therefore cost effective.</p> <p>Results provide an indication of the percentage of deteriorated area in the survey region</p>	<p>Expensive equipment.</p> <p>Requires proper environmental conditions for testing.</p> <p>The depth and thickness of a subsurface anomaly cannot be measured.</p> <p>Variations in test response occur with varying environmental conditions (temperature gradient, shaded or direct sunlight, cloud cover, and surface water).</p> <p>As the depth of the anomaly increases, it becomes more difficult to detect.</p> <p>Trained individual needed to assure that acquired data are meaningful and correctly interpreted</p>

will be called GPR. This section discusses the principles of GPR, the instrumentation that is used, data analysis techniques, and some of the inherent limitations. A detailed review of the principles and applications of GPR was published by Clemeña (1991).

2.8.2 Principle—The operating principle of GPR is illustrated in Fig. 2.8.1. An antenna, which is either dragged across the surface or attached to a survey vehicle, transmits short pulses of electromagnetic energy (within a specific broad frequency band) that penetrate into the surveyed material. The most commonly used pulses for concrete evaluation range from 1 to 3 nanoseconds (nsec) in duration and

often contain three or four peaks as shown in Fig. 2.8.1. Analysis and interpretation of the signal is based on well-defined nominal center frequency values, most commonly between 500 MHz and 1 GHz for structural surveys (Bungey and Millard, 1993). Each pulse travels through the material, and a portion of the energy is reflected back to the antenna when an interface between materials of dissimilar dielectric properties is encountered. The antenna receives the reflected energy and generates an output signal proportional to the amplitude of the reflected electromagnetic field. The received signal thus contains information on what was reflected, how quickly the signal traveled, and how much of the signal was

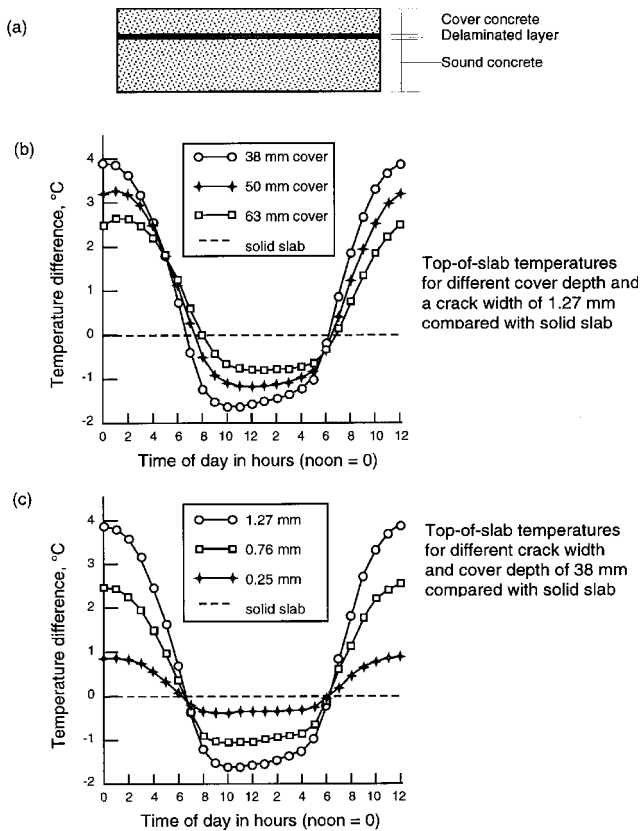


Fig. 2.7.4—Analytical study of infrared thermography: (a) model of concrete bridge deck used in numerical simulation; (b) effect of depth of cover on surface temperature compared with solid slab; and (c) effect of width of air-filled crack on surface temperature compared with solid slab (adapted from Maser and Roddis, 1990).

attenuated. These quantities depend on the spatial configuration and electrical properties of the member under investigation.

The theory of propagation of electromagnetic waves is complicated. The following presentation is simplified based on assumptions suitable for civil engineering applications. More detailed treatments are available (Daniels et al., 1988; Halabe et al., 1993, 1995). The primary material properties that affect the transmitted and reflected energy are the dielectric constant and the conductivity. Materials of interest for structural applications of GPR, with the exception of metals, are low-loss dielectrics. A material's dielectric constant, also known as dielectric permittivity, is the amount of electrostatic energy stored per unit volume for a unit potential gradient. Electrical conductivity, the reciprocal of electrical resistivity, is a measure of the ease with which an electrical current can be made to flow through a material. The ratio of a material's dielectric constant to that of free space is defined as the relative dielectric constant ϵ_r ,

$$\epsilon_r = \frac{\epsilon}{\epsilon_0} \tag{2.21}$$

where

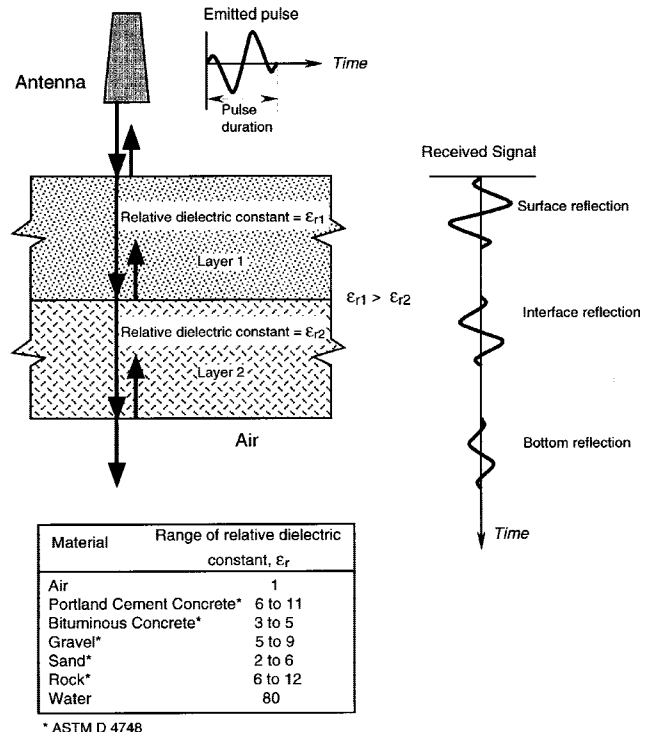


Fig. 2.8.1—Reflections of electromagnetic radiation pulse at interfaces between materials with different relative dielectric constants (adapted from Carino, 1994).

ϵ = dielectric constant (farad/meter), and
 ϵ_0 = dielectric constant of free space (air), which is 8.85×10^{-12} farad/m.

The relative dielectric constant governs the speed of the electromagnetic wave in a particular material. For low loss materials, the speed of electromagnetic waves C is given by the following

$$C = \frac{C_0}{\sqrt{\epsilon_r}} \tag{2.22}$$

where

C_0 = speed of light in air (3×10^8 m/s), and
 ϵ_r = relative dielectric constant.

Analysis of the recorded time-domain waveforms permits determination of the depth of the reflecting interface assuming the relative dielectric constant is known. The depth of the reflecting interface is obtained from the measured round trip travel time and the speed of the electromagnetic wave. If the round trip travel time for the pulse is t , the depth D would be

$$D = \frac{Ct}{2} \tag{2.23}$$

The contrast in dielectric constant determines the amount of reflected energy at the interface between two dissimilar materials. For low-loss dielectrics, the ratio of the reflected to incident amplitudes of the electromagnetic field (reflection coefficient)

reflected at an interface is given by the following equation (Clemeña, 1991; Bungey and Millard, 1993)

$$\rho_{1,2} = \frac{\sqrt{\epsilon_{r1}} - \sqrt{\epsilon_{r2}}}{\sqrt{\epsilon_{r1}} + \sqrt{\epsilon_{r2}}} \quad (2.24)$$

where

- $\rho_{1,2}$ = reflection coefficient,
 ϵ_{r1} = relative dielectric constant of Material 1 (incident wave), and
 ϵ_{r2} = relative dielectric constant of Material 2.

The dielectric constant of concrete is affected by the nature of the materials and moisture content. By definition, the relative dielectric constant of air equals 1, and typical values for other materials are given in Fig. 2.8.1. Note that the dielectric constant of water is much higher than the other listed materials. This makes water the most significant dielectric contributor to construction materials and explains why radar is highly sensitive to moisture. As the moisture content increases, the dielectric constant of the material, such as concrete, also increases.

An important difference between GPR and stress-wave methods, such as the impact-echo method, is the amplitude of the reflections at a concrete-air interface. For stress waves, the reflection is almost 100 percent because the acoustic impedance of air is negligible compared with concrete. On the other hand, the mismatch in dielectric constants at a concrete-air interface is not as drastic, and only about 50 percent of the incident energy is reflected at a concrete-air interface. This condition results in two significant differences between GPR and stress-wave methods. GPR is not as sensitive to the detection of concrete-air interfaces as are stress-wave methods. However, because the energy is not totally reflected at a concrete-air interface, GPR is able to penetrate beyond such an interface and “see” features below the interface.

Eq. (2.24) shows that when the dielectric constant of Material 2 is greater than that of Material 1, the reflection coefficient is negative. This indicates a phase reversal (change in polarity) of the reflected wave, which means that the positive part of the wave is reflected as a negative part (Fig. 2.8.1). At a metal interface, such as between concrete and steel reinforcement, there is complete reflection and the polarity of the reflected wave is reversed. This makes GPR very effective for locating metallic embedments. On the other hand, strong reflections from embedded metals can obscure weaker reflections from other reflecting interfaces that may be present, and reflections from reinforcing bars may mask signals from greater depths.

The conductivity and, to a lesser extent, the dielectric constant, determine the energy loss in a particular material. Signal attenuation may be approximated as follows (Bungey and Millard, 1993)

$$\alpha = 1.69 \times 10^3 \frac{\sigma}{\sqrt{\epsilon_r}} \quad (2.25)$$

where

- α = signal attenuation (dB/m) and
 σ = conductivity ($\Omega^{-1}\text{m}^{-1}$).

The conductivity of concrete increases with frequency (Halabe et al. 1993). For example, the conductivity at 1 GHz is about 1.5 times the direct current (0 Hz) conductivity.

Radar detects the arrival time and energy level of a reflected electromagnetic pulse. Since electromagnetic wave propagation is affected by changes in dielectric properties, variations in the condition and configuration of a structure will cause changes in the signal. Information is obtained by observing the return time, amplitude, shape, and polarity of the signal. Concrete conditions such as voids, honeycombing, and high moisture and chloride content can be inferred from changes in the dielectric constant and conductivity of the concrete. For example, theoretical studies have shown that characteristics of the radar signal are affected by variations in concrete moisture content (Shaw et al., 1993), and by variations in moisture and chloride contents under an asphalt overlay (Maser and Roddis, 1990). Other studies have considered the effects of shape and size of voids within concrete (Bungey and Millard, 1995) and of void size under concrete pavement (Steinway et al., 1981). Halabe et al. (1993) developed theoretical models for predicting the dielectric properties of concrete as a function of temperature, porosity, moisture and salt contents, and radar frequency. In addition, models were developed for radar waveform synthesis and inversion (Halabe et al., 1995). The synthesis (forward) model can be used to generate theoretical radar waveforms and conduct parametric studies for layered media, such as overlaid bridge decks and pavements, with features such as reinforcing bars and delaminations. The inversion model has been used, with moderate success, to estimate the physical properties of concrete bridge decks from radar waveforms (Halabe et al., 1995). Others have used the finite element method to simulate the propagation of electromagnetic pulses through concrete (Millard et al., 1993).

Since the radar pulse has a finite duration, the material layers being surveyed have to be sufficiently thick in order for the reflections from successive layers to be clearly separated. This minimum required thickness can be calculated by using Eq. (2.23) with t equal to the pulse duration. For example, for a pulse duration of 1.5 nsec in concrete and a relative dielectric constant of 6 (speed = 122 mm/nsec), the minimum required thickness would be about 90 mm.

2.8.3 Instrumentation—Typical instrumentation for GPR includes the following main components: an antenna unit, a control unit, a display device, and a storage device. The antenna emits the electromagnetic wave pulse and receives the reflections. For a given material, the depth of penetration and resolution of GPR are functions of the frequency content of the pulse. Lower frequencies penetrate deeper but provide less resolution, while higher frequencies provide more detail but have less depth of penetration. For an antenna with a 1-GHz nominal frequency, the penetration depth in concrete is about 400 mm (Bungey and Millard, 1993).

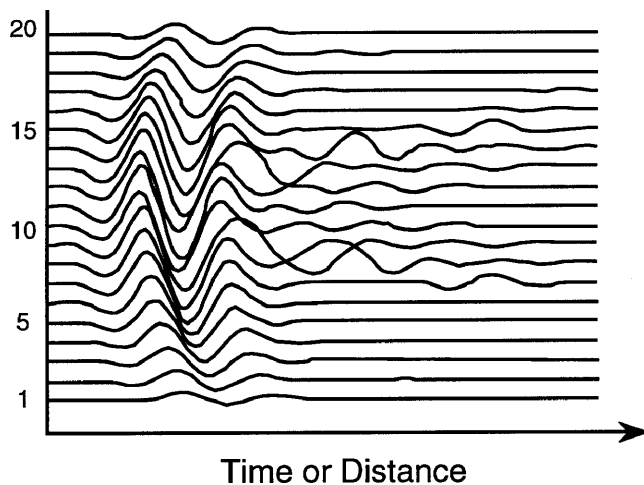


Fig. 2.8.2—Illustration of topographic plotting technique to reveal differences in radar signals (adapted from Cantor, 1984).

For a given antenna, the actual penetration depends on the moisture content of the concrete.

Much of the research into the use of GPR has centered around the evaluation of reinforced concrete bridge decks and pavements. The equipment used for this purpose is configured to mount on and within a vehicle to allow continuous acquisition of the data as the vehicle travels along the roadway. In this configuration, a non-contact horn antenna is mounted 150 to 500 mm above the pavement surface.

Another configuration is a portable arrangement, in which a small, hand-held dipole antenna is used. It is normally placed in contact with the surface to be surveyed. This equipment is used for locating items such as reinforcing bars, embedments, voids, and other anomalies within a concrete mass (Bungey and Millard, 1993). It has also been used to locate voids below slabs or behind concrete walls.

The control unit is the heart of a GPR system. It controls the repetition frequency of the pulse, provides the power to emit the pulse, acquires and amplifies the received signal, and provides output to a display device. Data are usually stored in an analog recorder or in a digital storage device for later analysis and interpretation.

Display devices include oscillographs that plot a succession of recorded waveforms (topographic or waterfall plot), from which it is possible to readily observe changes in the waveform patterns. Other common display devices are graphic facsimile recorders that provide a cross-sectional representation of the tested object, and are discussed further in the next section. Computer software is also available to permit various signal processing methods to aid in data interpretation, such as subtraction of a reference signal or color display based on signal amplitude and polarity (Bungey et al., 1991; Chen et al., 1994).

2.8.4 Data analysis—GPR systems emit pulses continuously at high repetition rates (typically 50 kHz). While this permits scanning of test objects, it also results in a large amount of data. As a result, several techniques employing

computer processing, color enhancement, or comparison methods, have been developed.

Cluster analysis is a technique for comparing signals (waveforms) with reference signals caused by known conditions. The received signals are normalized to allow direct comparison. Each signal is compared to the previous signals and is assigned to a “cluster” of similar signals (Cantor, 1984). If no other similar signals have been identified, it is assigned to a new cluster. The clusters are then correlated with known conditions as determined through visual inspection, coring or excavation. The output of the results is in the form of a strip chart that indicates the nature of the defect at the test position and a measure of the confidence of the prediction. The confidence measure indicates the closeness of fit of an individual signal to the reference signal for that cluster. See Cantor (1984) for examples of this type of analysis.

Topographic plotting is a technique that continuously displays or prints each radar trace displaced a fixed distance from the previous trace (Fig. 2.8.2). When a series of traces are viewed in this way, they take on an appearance similar to a topographic drawing (Cantor, 1984). Where the traces are parallel to one another, a uniform material is indicated. Where traces overlap or shift from one another, changes are indicated that might signify items such as deterioration, delamination, separation, patches, joints, different materials, and varying thicknesses.

Quantitative peak tracking is a technique that utilizes signal processing to quantitatively compute the amplitudes and arrival times of significant reflection peaks in the radar waveform (Maser, 1989, 1990; Ulriksen, 1983; Steinway et al., 1981; Carter et al., 1986). These quantitative computations can then be used to calculate and display concrete properties as depth profiles or area contour maps.

Peak plotting is a technique for presenting GPR data with a graphic recorder or a video display, and is commonly used in the field for real-time display of GPR data. Fig. 2.8.3(a) shows a ground-coupled, dipole antenna emitting a radar pulse into a test object containing a void. The time history of the emitted pulse is sketched above the antenna. Fig. 2.8.3(b) shows the waveform received by the antenna. The vertical axis represents time, or it can be transformed to depth by knowing ϵ_r and using Eq. (2.22) and (2.23). The received signal at the start of the waveform represents the emitted pulse that is picked up directly by the receiving side of the antenna. The second received signal is the reflection from the void, and the third is the reflection from the bottom boundary of the test object.

The peak plotting routine used by the graphic recorder is illustrated in Fig. 2.8.3(b). Although the following description assumes a graphic recorder for ease in explanation, analogous images are readily produced digitally for display on a gray-scale or color video monitor. First, the operator selects a threshold voltage range. When the amplitude of the received signal exceeds the threshold range, the pen of the graphic recorder plots a solid line on the recording paper. The line is plotted in varying shades of gray depending on the actual amplitude of the signal. Thus the waveform from

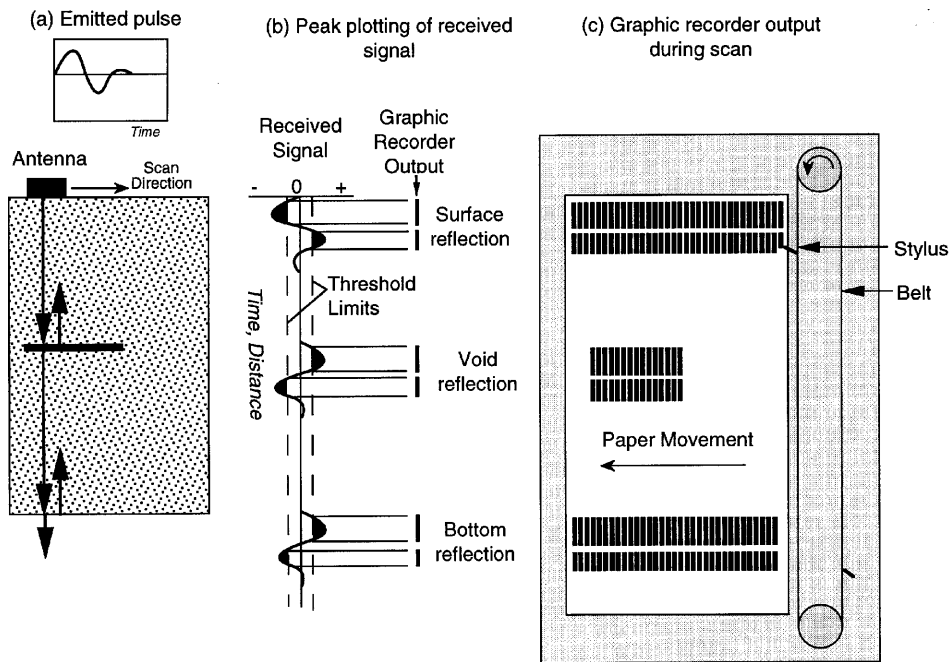


Fig. 2.8.3—(a) Reflections of electromagnetic pulse in test object with void; (b) received waveform and graphic recorder output based on threshold limits; and (c) display on graphic recorder during scan across test object (adapted from Carino, 1994).

the antenna output is represented on the graphic recorder as a series of dashes as shown in Fig. 2.8.3(b). Note that each echo is associated with two dashes. The actual number of dashes that are displayed depends on the number of cycles in the emitted pulse and the threshold level. This is an important point to understand for proper interpretation of GPR results. As the antenna is moved along the surface, changes in the received signal are displayed on the graphic recorder. The paper on the recorder moves at a constant speed that is independent of the speed of the antenna motion (hardware is available to synchronize paper feed with antennae movement). The resulting pattern on the graphic recorder represents a cross-sectional view of the test object, as illustrated in Fig. 2.8.3(c).

As previously mentioned, metals are strong reflectors of electromagnetic waves. This characteristic makes GPR very effective in locating buried metal objects, such as reinforcing bars and conduit. The presence of reinforcing bars results in characteristic patterns in the graphic recorder output that make them relatively easy to locate. For example, Fig. 2.8.4(a) and (b) show the graphic recorder output obtained in a laboratory specimen in which reinforcing bars were placed 300 mm apart with cover depths of 50, 100, and 150 mm. The bars were embedded in sand contained in a wooden box, 200 mm deep. This is a convenient way to study the effects of reinforcement on GPR signals because the relative dielectric constant of sand is similar to dry concrete. Fig. 2.8.4(a) shows the results for 10-mm (No. 3) bars, and Fig. 2.8.4(b) shows the results for 35-mm (No. 11) bars. The vertical dashed lines are reference markers placed on the output by the operator. Since bar locations were known in this study,

the reference markers were created by the operator as the center of the antenna passed directly over the centerlines of the bars. The arch-shaped patterns are typical of reflections from round metallic targets. The centerline of the bars are clearly identified and closer examination of the patterns reveals that the bar depth increases from left to right. The actual shapes of the arches (that is, whether they are flat or peaked) depend on the scanning speed of the antenna and the speed of the paper feed. It is not possible to infer the bar sizes by simply looking at the patterns in the graphic recorder output.

In field scans, the operator lays out a system of grid lines on the surface, and the grid is used to reference the graphic recorder output to positions on the structure. Fig. 2.8.5 shows the graphic recorder output from a scan across a reinforced concrete slab with bars at unknown locations. The arch-shaped patterns caused by reflection from the bars are clearly evident. Five arches are shown, corresponding to five targets. The four arches at the same depth correspond to reinforcing bars. It is seen that one of the arches is closer to the top of the display and has a different pattern than the others. The operator identified this reflection as being due to a metal conduit rather than a reinforcing bar. The vertical distance markers generated as the antenna crossed grid points can be used to locate the approximate positions of the bars within the slab. In this display, the graphic recorder settings have been configured so that the positive and negative portions of the waveforms are shown as solid or dashed bands. A comparison with Fig. 2.8.4 shows that the arches are more peaked in Fig. 2.8.5. This condition is due to differences in the relative values of antenna scan speed and paper feed speed.

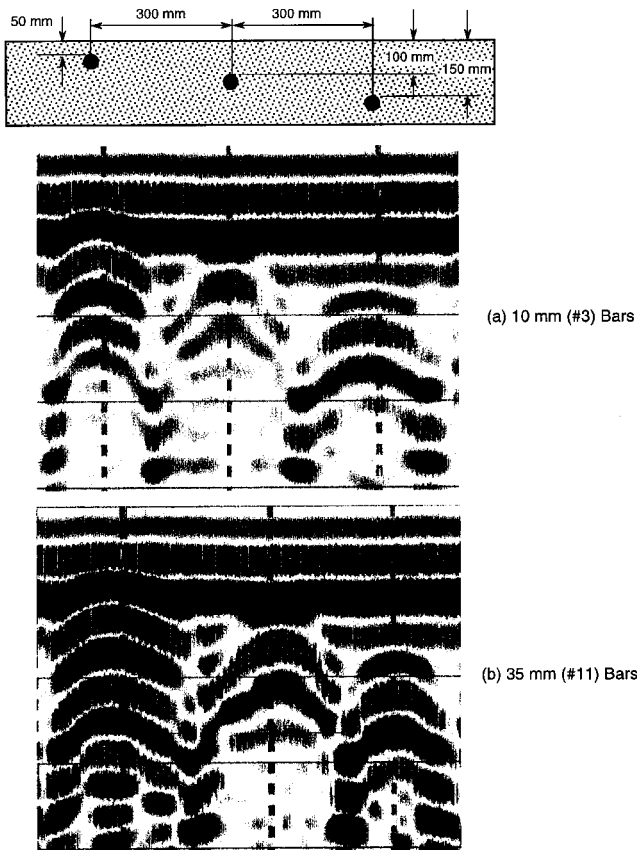


Fig. 2.8.4—Graphic recorder outputs for scans over reinforcing bars embedded at different depth in dry sand: (a) 10-mm bars, and (b) 35-mm bars.

2.8.5 Advantages and limitations—The commonly used antennas irradiate a cone-shaped volume of concrete. At a depth of 200 mm, an area of about 0.1 m² is irradiated. Hence, at that depth, multiple passes about 0.3 m apart would be required to survey a larger section of concrete.

When multiple reinforcing bars are present, there will be multiple arch patterns as shown in Fig. 2.8.4. As the bar spacing decreases, the arch patterns overlap. Below a certain spacing, the individual bars can no longer be discerned, and the reflection pattern is similar to the case of a solid embedded steel plate. The ability to discern individual bars depends on bar size, bar spacing, cover depth, and the configuration of the antenna (Bungey et al., 1994). Fig. 2.8.6 summarizes results obtained using a 1-GHz, hand-held antenna. In these experiments, the reinforcing bars were placed in a tank filled with an oil/water emulsion that was formulated to simulate the dielectric properties of concrete. It is seen that for cover depths up to about 150 mm, the minimum spacing at which individual bars can be discerned increases with greater cover depth. For cover depths greater than 150 mm, the minimum spacing is unaffected by cover depth, and depends primarily on bar size (Bungey et al., 1994).

Closely spaced bars will also prevent detection of features below the layer of reinforcement. This “masking” effect depends on the wavelength of the electromagnetic waves, the bar size, and cover depth. For the 1-GHz, hand-held antenna,

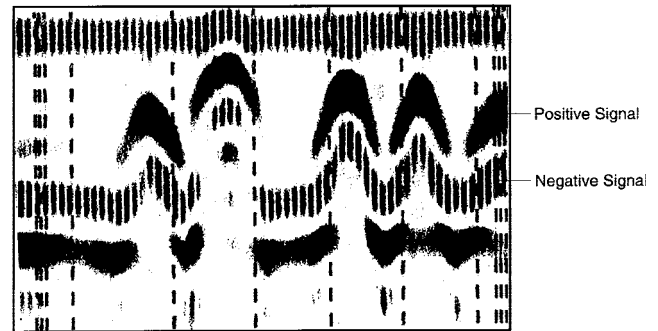


Fig. 2.8.5—Graphic recorder output for scan across reinforced concrete slab (dashed and solid bands correspond to negative and positive portions of waveforms).

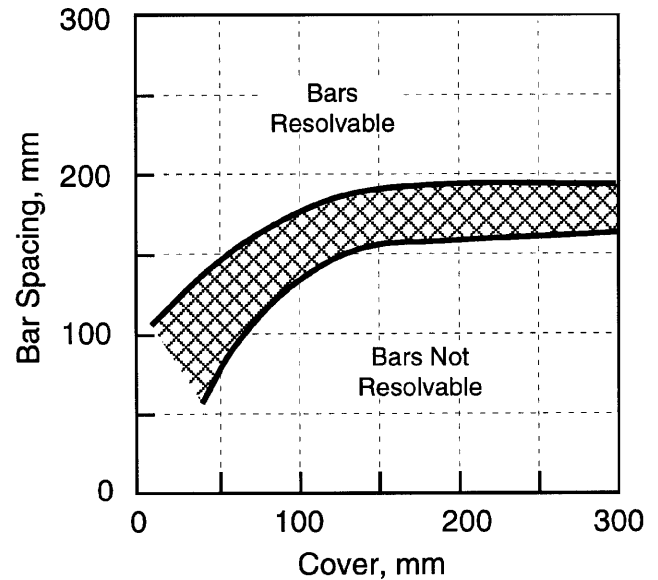


Fig. 2.8.6—Minimum spacing at which individual reinforcing bars can be resolved (adapted from Bungey et al., 1994)

32-mm bars at cover depths of 25 to 50 mm will prevent detection of underlying features when bar spacings are less than 200 mm (Bungey et al., 1994).

Simple methods do not exist to determine bar size from graphic recorder output. Researchers have attempted to better understand the interactions of GPR with cracks, voids, and reinforcing bars (Mast et al., 1990). The objective of these studies is to develop procedures to use the recorded data to construct an image of the interior of the concrete. Some advances in this direction have occurred in France, where a prototype system has been developed that uses tomographic techniques to reconstruct the two-dimensional layout of reinforcement in concrete (Pichot and Trouillet, 1990). In the U.S., there have been demonstrations of successful three-dimensional reconstruction of artificial defects and reinforcement embedded in a concrete slab (Mast and Johansson, 1994). These imaging methods rely on an antenna array to make multiple measurements and require extensive computational time to reconstruct the internal image.

Table 2.8—Advantages and limitations of ground-penetrating radar (GPR)

Advantages	Limitations
<p>Non-contact antennas permit fast speed scanning.</p> <p>Very sensitive to presence of embedded metal objects.</p> <p>Ability to penetrate across concrete-air interfaces.</p> <p>Sensitive to the presence of moisture.</p>	<p>Region irradiated by the antenna is limited to cone-shaped volume directly below antenna.</p> <p>Congested reinforcement can prevent penetration beyond the reinforcement.</p> <p>Cracks and delaminations are not easy to detect unless moisture is also present in the cracks or region of the delamination.</p> <p>Pulses from high resolution antennae have limited depth of penetration (400 to 750 mm).</p> <p>The behavior of electromagnetic pulses propagating through reinforced concrete structures is not completely known.</p> <p>Experienced operator required to operate equipment and interpret results. Large amounts of data obtained during scans.</p>

The depth of concrete that can be effectively surveyed depends to some extent on the required resolution (hence, frequency used). Generally, a thickness of 400 to 750 mm can be surveyed, depending on the nominal antenna frequency and the moisture content of the material. Other discontinuities, such as voids, that reflect a large proportion of the energy, will also limit the depth that can be surveyed.

The detection of delaminations in reinforced bridge decks using GPR is not straightforward. In studies by Maser and Roddis (1990), it was found that a 3-mm air gap in concrete produced little noticeable effect in the received waveform. However, the addition of moisture to the simulated crack resulted in stronger reflections that could be noticed in the waveform. It was also found that the presence of chlorides in moist concrete resulted in high attenuation, because of the increased conductivity due to chloride ions [Eq. (2.25)]. Thus, the ability to detect delaminations will depend on the in situ conditions at the time of testing. In addition, because the reflections from reinforcing bars are much stronger than from a delamination, it is difficult to detect the delamination in the presence of reinforcing bars.

Due to complexities in using GPR to test reinforced concrete, standardized test procedures for flaw detection do not exist. However, an ASTM standard has been developed (Method D 4748) to measure the thickness of the upper layer of a multi-layer pavement system. Basically, the technique involves measuring the transit time of the pulse through the pavement layer, and using relationships similar to Eq. (2.22) and (2.23) to calculate the layer thickness. The procedure in ASTM D 4748 is based on using a non-contact horn antenna, and some modifications are required for measurements with a contact antenna. The calculated depth depends on the value of the relative dielectric constant. Errors in the assumed value of the relative dielectric constant can lead to substantial inaccuracies in depth estimations (Bungey et al., 1994). For data obtained with a horn antenna, the relative dielectric constant of the concrete can be computed directly from the radar signals. For data obtained using a contact antenna, it is necessary to take occasional cores to determine the appropriate dielectric constant value for the pavement materials. The

user is cautioned against using this method on saturated concrete, because of the high attenuation and limited penetration of the pulse. In ASTM D 4748, it is stated that inter-operator testing of the same materials resulted in thickness measurements within ± 5 mm of the actual thickness. Finally, the ASTM standard notes that reliable interpretation of received signals can only be performed by an experienced radar data analyst.

The properties of concrete, as revealed by the radar data, are generally inferences based on the connection between dielectric properties and real conditions of interest. The dimensions of concrete, such as thickness and reinforcing bar depth, can generally be revealed with greater accuracy than properties such as moisture content, chloride content, delamination, and other forms of deterioration, which should be confirmed by exploratory drilling or excavations at key locations. Due to the large number of physical properties affecting the received signal, current application to structural concrete (other than measurements of the spatial configuration of concrete and reinforcement) is largely restricted to qualitative comparative uses.

The advantages and limitations of ground-penetrating radar are summarized in Table 2.8.

CHAPTER 3—PLANNING AND PERFORMING NONDESTRUCTIVE TESTING INVESTIGATIONS

3.1—Selection of methods

The previous chapter reviewed the principles and highlighted the advantages and limitations of well-known nondestructive test methods for evaluation of concrete and reinforcement in structures. However, the list of available methods to determine a concrete structural property or to assess structural conditions is rapidly expanding. Based on reliability, simplicity, and cost, some methods or techniques are preferable over others.

In this section, “primary” and “secondary” methods are suggested to determine particular properties or to evaluate particular conditions. A “primary” method indicates the preferred method. A “secondary” method indicates an acceptable method that typically would require a greater level of experience to implement, be less reliable, or be less rapid. The

method chosen must be tailored to the objective of the evaluation. NDT methods can be valuable tools, but a given technique may not be the most practical or yield the most applicable results in all cases. Often times, the most sensible and effective approach is to use a variety of nondestructive testing techniques to obtain mutually complementary information.

3.1.1 Concrete material properties—Table 3.1 summarizes the suggested NDT methods to determine various material properties of hardened concrete. Some of these methods require cores or other types of concrete samples for laboratory testing in order to establish correlations between the desired concrete property and the NDT results. Some of these methods may also be appropriate for testing laboratory-prepared specimens or for acceptance testing of field concrete. ASTM standard test methods, or other relevant documents, are noted where appropriate.

3.1.2 Structural properties and conditions—Table 3.2 summarizes selected nondestructive test methods for determining structural properties and conditions. Information derived from conducting these types of tests is important in evaluating the integrity of a concrete structure. Such information can be used to assess remaining service life or to develop strategies for repair and strengthening.

3.1.3 Evaluation of repairs—Table 3.3 summarizes selected NDT methods that can be used to evaluate the effectiveness of repairs. This type of testing is important to ensure consistent quality throughout a repair project. In some circumstances, the results from these tests may be used to determine payment under a contract.

3.1.4 Personnel qualifications—With most of the NDT techniques described in this report, the evaluation investigator is attempting to assess a property of concrete or changes in that property caused by the presence of a defect or discontinuity. From that information, the investigator infers the nature of the defect and its severity. Hence, to obtain reliable results often involves a high degree of judgement by the evaluation investigator, supported by a limited amount of corroboration by coring or other forms of direct examination. This judgement should come from individuals who have knowledge of the physics of the NDT method they are using, and who have sufficient experience in both the use of the method and the investigation of structures to allow them to accurately interpret NDT results.

In many cases, the investigation requires preliminary interpretation in the field as the testing is in progress. This is necessary to allow the investigator to plan and modify the program on the basis of the results that are being recorded in order to obtain sufficient data at appropriate locations. For this reason, it is usually not advisable to delegate the field investigation and data acquisition to less experienced personnel, unless the lead evaluation investigator is confident that sufficient data of the required quality will be obtained.

3.2—Defining scope of investigation

After the appropriate NDT methods are selected, the next important consideration is to decide the scope of the investigation.

This is one of the most difficult aspects of the evaluation process. Ideally, one would like to do sufficient testing to have a high degree of assurance that all important defects or anomalies that may be present are detected. In most situations, the amount of testing is limited by the available funds and time constraints, and the evaluation investigator has to design a testing scheme that will yield the most information. The experience of the investigator is critical for designing a successful testing scheme. The investigator should not only understand the inherent capabilities and limitations of the chosen methods, but should also have an understanding of concrete construction, structural behavior, and deterioration mechanisms. Knowledge of concrete construction is helpful in anticipating the most likely locations of internal anomalies. Knowledge of structural behavior is valuable in selecting those portions of the structure that are most vulnerable to the presence of defects. Knowledge of deterioration mechanisms is important in deciding what needs to be measured.

3.2.1 Statistical considerations—Because of the variety of situations that may be encountered, it is difficult to define a sampling scheme that would be applicable to all NDT methods and for all investigations. Global techniques, such as infrared thermography, can be used to inspect the entire exposed surface of a structure. Other scanning techniques, such as ground-penetrating radar, can provide complete inspection along each scan line. Point-by-point tests, such as impact-echo, provide information at the test point. Other methods, such as impulse-response, can provide information about an entire structural element.

ASTM Practice C 823 can be adapted to provide some guidance on planning the sampling program. Thus, sampling situations can be assigned to two categories:

- Where preliminary investigation and other information indicate that conditions are similar throughout the structure, and
- Where preliminary investigation and other information indicate that conditions are not similar throughout the structure. The structure may then be divided into portions within which conditions are similar.

For the first category, sampling locations should be distributed randomly or systematically over the region of interest. According to ASTM C 823, “Any method for determining sampling locations may be employed provided the locations are established without bias.” The intent is to select sampling locations in a manner that allows all locations an equal probability of being selected. For the second category, each portion that appears to be of similar condition should be sampled independently and treated as a different category unless and until test results reveal no significant differences.

For point-by-point tests intended to find internal defects, the statistical concepts of quality control testing may be adapted to select the sample size. For example, a grid of points could be laid out on the surface of the structure. The grid spacing would depend on the smallest defect that the evaluation investigator wishes to detect.

The total number of grid points would represent a “lot.” If resources permit, the number of sample points should be

Table 3.1—Nondestructive test methods for determining material properties of hardened concrete in existing construction

Property	Possible Methods		Comment
	Primary	Secondary	
Compressive strength	Cores for compression testing (ASTM C 42 and C 39)	Penetration resistance (ASTM C 803); Pullout testing (drilled-in)	Strength of in-place concrete; comparison of strength in different locations. Drilled-in pullout test not standardized by ASTM
Relative compressive strength	Rebound number (ASTM C 805); Ultrasonic pulse velocity (UPV) (ASTM C 597)		Rebound number influenced by near surface properties; UPV gives "average" result through the thickness
Tensile strength	Splitting tensile strength of core (ASTM C 496)	In-place pulloff test (ACI 503R; BS 1881: Part 207)	Assess tensile strength of concrete
Density	Specific gravity of samples (ASTM C 642)	Nuclear gage	
Moisture content	Moisture meters	Nuclear gage	
Static modulus of elasticity	Compression test of cores (ASTM C 469)		
Dynamic modulus of elasticity	Resonant frequency testing of sawed specimens (ASTM C 215)	Ultrasonic pulse velocity (ASTM C 597); impact-echo; spectral analysis of surface waves(SASW)	Requires knowledge of density and Poisson's ratio (except C 215); dynamic elastic modulus is typically greater than the static elastic modulus
Shrinkage/expansion	Length change of drilled or sawed specimens (ASTM C 341)		Measure of incremental potential length change
Resistance to chloride penetration	90-day ponding test (AASHTO T 259)	Electrical indication of concrete's ability to resist chloride ion penetration (ASTM C 1202)	Establish relative susceptibility of concrete to chloride ion intrusion; assess effectiveness of chemical sealers, membranes, and overlays
Air content; cement content; and aggregate properties (scaling; alkali-silica reactivity; freeze/thaw susceptibility)	Petrographic examination of concrete samples removed from structure (ASTM C 856 and ASTM C 457); cement content (ASTM C 1084)	Petrographic examination of aggregates (ASTM C 294, C 295)	Assist in determination of cause(s) of distress; degree of damage; quality of concrete when originally cast and current
Alkali-silica reactivity (ASR)	Cornell/SHRP rapid test (SHRP-C-315)		Establish in field if observed deterioration is due to ASR
Carbonation, pH	Phenolphthalein (qualitative indication); pH meter	Other pH indicators (e.g., litmus paper)	Assess corrosion protection value of concrete with depth and susceptibility of steel reinforcement to corrosion; depth of carbonation
Fire damage	Petrography; rebound number (ASTM C 805)	SASW; UPV; Impact-echo; Impulse-response	Rebound number permits demarcation of damaged surface
Freezing and thawing damage	Petrography	SASW; Impulse-response	
Chloride ion content	Acid-soluble (ASTM C 1152) and water-soluble (ASTM C 1218)	Specific ion probe (SHRP-S-328)	Chloride ingress increases susceptibility of steel reinforcement to corrosion
Air permeability	SHRP surface airflow method (SHRP-S-329)		Measures in-place permeability index of the near-surface concrete (15 mm)
Electrical resistance of concrete	AC resistance using 4-probe resistance meter	SHRP surface resistance test (SHRP-S-327)	AC resistance useful for evaluating effectiveness of admixtures and cementitious additions; SHRP method useful for evaluating effectiveness of sealers

Table 3.2—Nondestructive test methods to determine structural properties and assess conditions of concrete

Property/Condition	Method		Comment
	Primary	Secondary	
Reinforcement location	Covermeter; Ground penetrating radar (GPR) (ASTM D 4748)	X-ray and γ-ray radiography	Steel location and distribution; concrete cover
Concrete component thickness	Impact-echo(I-E); GPR (ASTM D 4748)	Intrusive probing	Verify thickness of concrete; provide more certainty in structural capacity calculations; I-E requires knowledge of wave speed and GPR of dielectric constant
Steel area reduction	Ultrasonic thickness gage (requires direct contact with steel)	Intrusive probing; radiography	Observe and measure rust and area reduction in steel; observe corrosion of embedded post-tensioning components; verify location and extent of deterioration; provide more certainty in structural capacity calculations.
Local or global strength and behavior	Load test, deflection or strain measurements	Acceleration, strain, and displacement measurements	Ascertain acceptability without repair or strengthening; determine accurate load rating
Corrosion potentials	Half-cell potential (ASTM C 876)		Identification of location of active reinforcement corrosion
Corrosion rate	Linear polarization (SHRP-S-324 and S-330)		Corrosion rate of embedded steel; rate influenced by environmental conditions
Location of delaminations, voids, and other hidden defects	Impact-echo; Infrared thermography (ASTM D 4788); Impulse-response; Radiography; GPR	Sounding (ASTM D 4580); pulse echo; SASW; intrusive drilling and borescope	Assessment of reduced structural properties; extent and location of internal damage and defects; sounding limited to shallow delaminations

Table 3.3—Nondestructive test methods for evaluating repairs

Property/Condition	Method		Comment
	Primary	Secondary	
Bond strength	Pulloff test (ACI 503R), CAN/CSA A23.2-6B; BS 1881: Part 207		
Bond quality (absence of voids at interface)	Pulloff test (as above)	Impact-echo; SASW; Impulse-response	SASW good for layered systems
Injection of cracks or voids	Ultrasonic pulse velocity; Impact-echo	SASW	Proper geometry required for reliability of UPV

chosen to minimize the risk that the structure is declared to have the measured fraction of flawed locations, when in fact the actual fraction exceeds the measured amount. For example, ASTM E 122 gives the following relationship for selecting the sample size to estimate the fraction of a lot that is defective

$$n = \left(\frac{k}{E}\right)^2 p_o(1 - p_o) \quad (3.1)$$

where

n = sample size;

k = statistical factor based on the risk that the estimated fraction defective does not differ from the true fraction by more than $\pm E$, ($k = 1.960$ for a risk of 0.05 and $k = 1.645$ for a risk level of 0.10);

E = maximum acceptable error between true fraction that is defective and the estimated fraction based on the sample; and

p_o = advance estimate of fraction defective.

Note that to use Eq. (3.1) one must have an initial estimate of the fraction defective, because the number of samples depends on this value. Fig. 3.2.1 shows plots of Eq. (3.1) for values of the acceptable error E equal to 0.05, 0.075, 0.10, and 0.15 and for two risk levels. Fig. 3.2.1(a) is for a risk level

of 0.10, and Fig. 3.2.1(b) is for a risk level of 0.05. The figures show that the sample size is affected greatly by the maximum acceptable error E . It is also seen that the largest sample size is needed when the true fraction defective equals 0.5. Thus, one possible approach is to select a maximum sample size based on an assumed value of $p_o = 0.5$, and use a two-stage sampling procedure to perform the testing. In this case, a portion of the required maximum sample size is used to establish an estimate of the fraction defective. With this estimate, a revised sample size is computed using Eq. (3.1), and additional tests are performed so that the cumulative number of tests equals the revised sample size. For two-stage sampling, it is suggested that the first sample size be 50 to 70 percent of the maximum size or at least 30 samples (Natrella, 1963). Random sampling must be used to select the actual test points on the structure.

The choice of sample size based on statistical principles must be tempered with consideration of cost. ASTM E 105 states the following: “No matter how sound a given sampling plan is in a statistical sense, it is not suitable if the cost involved is prohibitive or if the work required is so strenuous that it leads to short cuts or subterfuge by those responsible for sampling.” ASTM E 122 also addresses cost considerations and offers the following recommendations: “After the required size of sample to meet a prescribed precision is computed..., the next step is to compute the cost of testing this size sample. If the cost is too high, it may be possible to relax the required precision (or the equivalent, which is to accept an increase in the probability that the sampling error may exceed the maximum allowable error E) and to reduce the size of the sample to meet the allowable cost.”

3.2.2 Practical considerations—For an evaluation program that includes nondestructive testing to be justifiable, it should satisfy as many of the following requirements as possible:

- It should approximate the cost of an intrusive testing program alone for the same area or volume tested;
- It should give a larger amount of reliable data for the same area or volume examined, thereby yielding more information;
- It should be able to include areas that are difficult to examine thoroughly using more traditional or intrusive methods; and
- The data recovered should be reproducible, so that future surveys of the same structure can rely with confidence on the initial NDT data as a base reference.

Cost criteria—It is desirable that a structural condition survey produce the maximum amount of information for a given investment. With limited available funds, the owner or facility manager is faced with a pressing problem that has to be solved as thoroughly and as quickly as possible with minimum outlay. The evaluation investigator has to come to terms with this conflict; if not, the project will often not be funded.

Some practical problems can be solved only with a combination of intrusive and nondestructive testing. Condition surveys using visual observation and intrusive sampling and

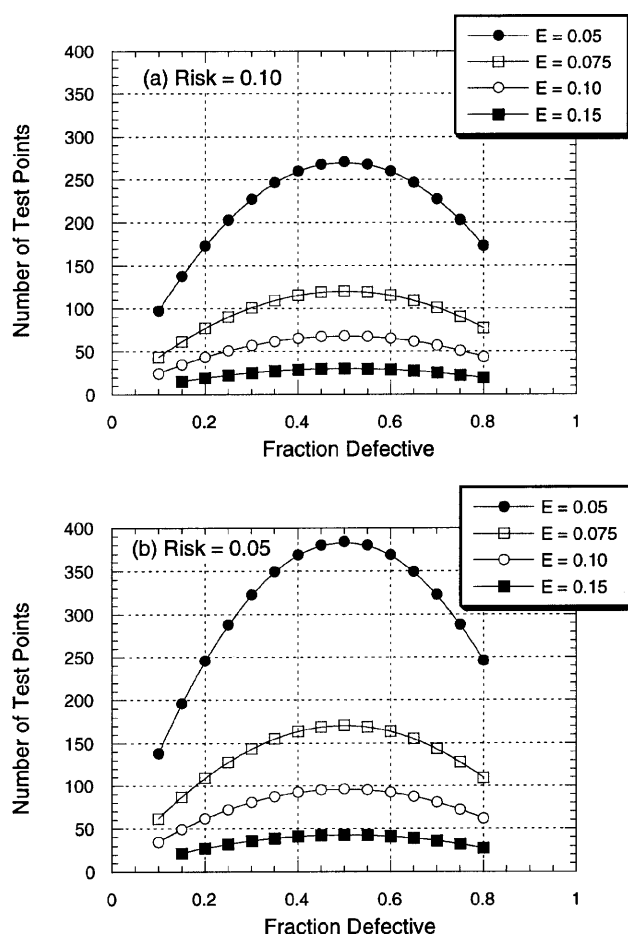


Fig. 3.2.1—Number of test points to estimate fraction defective within an error band of $\pm E$ at risk levels of: (a) 0.10, and (b) 0.05.

testing alone largely rely on the experience of the investigator to interpret the concrete condition by interpolating between intrusive test points. Usually, a number of core samples at a pre-determined sampling density are selected, accompanied by laboratory tests on the cores. This establishes a preliminary cost base for the condition survey.

NDT as an alternative to this approach usually proposes a reduction in the number of core samples taken, and fills in the areas between the core samples with nondestructive tests at a greater test density. This reduces the uncertainty inherent in the visual and intrusive sampling survey. The reduction in intrusive sampling, together with the speed of most NDT programs, maintains the field survey cost at a similar level. Analysis time, however, is usually increased.

Data density—The cost issues discussed above imply that nondestructive surveys provide greater test data density than visual and intrusive surveys. It is usually necessary to interpolate the concrete condition between test points in an NDT survey, because with most NDT procedures it is not feasible to test the entire surface of concrete in the structure due to cost and time considerations. Table 3.4 shows examples of test density (spacing between test points) used in typical NDT investigations with different test methods. The “ideal”

Table 3.4—Frequency of testing for some representative nondestructive testing methods

Test Method	“Ideal” Test Density	“Practical” Test Density	Remarks
Through-transmission pulse velocity	0.3 to 0.6-m grid	1 to 1.5-m grid	Typical spacings to check for concrete density and honeycombing
Rebound hammer (one side of wall or slab)	0.3 to 0.6-m grid	1 to 1.5-m grid	Spacing used to assess fire-damaged walls
Impulse-response	1.5-m grid	1.5-m by 3 to 1-m grid	Typical spacings used in assessment of chimney stacks, cooling towers, and silos

test density represents desirable spacings to achieve a statistically valid assessment of the concrete condition; “practical” density represents spacings used to achieve a balance between statistical rigor and cost.

Also, different testing techniques serve differing purposes, and each test type does not return the same amount of information for the same area or volume of concrete tested. As an example, an impact-echo test on a concrete slab with several layers of steel reinforcement provides information about changes in concrete interface properties immediately below the test point only. The interpretation of the continuity of the detected interfaces between adjacent test points is made subjectively by the evaluation investigator, using available knowledge of the slab details and construction history as well as personal experience. In contrast, a radar survey across the top of the same slab will give a continuous image of the uppermost steel layer, but will yield little information about the conditions at the lower reinforcement layers.

Areas with difficult access—Many concrete structures present access difficulties for programs combining visual inspection and intrusive testing. Examples of such difficult inspection situations include:

- Retaining walls, grade beams, and slabs on grade, where only one side of the element is accessible,
- Deep foundations (piles, drilled shafts, and slurry walls), where nearly all the element is buried, and
- Concrete elements located in hazardous areas, such as hazardous material waste tanks and nuclear sites.

Nondestructive testing in these cases is often the only economically and practically viable way to obtain sufficient concrete condition information. Several publications refer to the successful application of NDT to these problems and give recommendations for the test types to be used (Davis, 1997; Davis, 1995; Davis et al., 1997).

Data reliability and reproducibility—The data collected must be reliable and reproducible. This implies that:

- All points tested on the structure can be easily identified at a later date, so that tests can be repeated if necessary at the exact test location at any time in the future;
- The test results in the preliminary survey should be in such a format (graphs, numerical data) that direct comparisons can be made between the original and later test

results. This is facilitated by storage of raw test data on computer disks; and

- The investigator should have the maximum confidence in the reproducibility of each test result.

3.3—Numerical and experimental simulations

As has been mentioned several times, many NDT methods are based on interactions of certain types of waves (stress or electromagnetic) with the internal structure of the element being tested. For some conditions, the interactions are relatively simple and tests results are easy to interpret. For example, delaminations in slabs or walls can be detected with relative ease using the impact-echo method, or reinforcing bars with shallow cover and wide spacing are located easily with a covermeter or ground-penetrating radar (GPR). However, the evaluation investigator may be faced with complex situations for which the expected responses are not known. In such cases, the investigator should consider performing numerical or experimental simulations prior to planning the field investigation.

Numerical simulation refers to computing the expected response of the test object to a specific type of test. Experimental simulation refers to constructing mock-ups with simulated flaws and testing them with the proposed test method. The simulations can have three objectives:

- To establish whether a given method is capable of detecting the anomaly of interest.
- To establish “unflawed” responses for use as baseline to compare with “flawed” responses.
- To determine the critical size at which detection of a flaw becomes uncertain.

In addition, numerical simulation can be used in conjunction with measured response to infer the internal conditions of the structure. This is usually referred to as solving the inverse problem. Ideally, one would like to be able to use the measured response and use a computer program to compute the internal conditions or material properties of the concrete. Unfortunately, this is usually not possible except for simple conditions. Thus, the inverse problem is often solved by iteration; that is, the theoretical response is calculated for a given assumed set of conditions and compared with the measured response. The assumed conditions are varied until

there is acceptable agreement between the measured and calculated response. Since there is no assurance that a unique set of conditions corresponds to the measured response, the analyst requires an understanding of reasonable values for the assumed conditions.

3.3.1 Numerical simulation of stress-wave propagation—During the 1970s and 1980s, computer programs based on the finite-element method were developed to solve complex dynamic problems involving impact. Those types of programs have been adapted for simulating stress-wave propagation in impact-based NDT methods, such as the impact-echo method (Sansalone and Carino, 1986). A brief description of the basics of this simulation method is provided below (adapted from Sansalone and Streett, 1997).

The finite-element method is a numerical technique for obtaining approximate solutions to problems in continuum mechanics. A continuum (in this case, a concrete structure with or without simulated defects) is divided into a finite number of discrete parts (finite elements) that are interconnected at points called nodes. Equations relating the stresses and strains for the individual elements are combined to construct global equations that describe the behavior of the entire continuum. Solution of these equations gives the displacements or stresses for each element for a particular set of boundary conditions and applied loads. In stress-wave propagation analyses, the calculations are carried forward in small time steps, and time histories of nodal displacements and element stresses are obtained.

The impact is simulated by applying a pressure loading over several elements. The pressure is assumed to vary with time as a half-cycle sine curve, approximating the force-time function associated with the impact of a sphere on the surface of an elastic solid. Impacts of different durations are obtained by changing the period of the half-cycle sine curve. The concrete is modeled as a linear elastic, homogeneous material. This assumption is valid because:

- The strains produced by the stress waves in impact-echo testing are very small.
- The frequency components in the propagating waves are typically less than about 80 kHz and the smallest wavelengths are on the order of 50 mm. At these wavelengths, concrete appears homogeneous to the propagating waves.

Defects can be represented by omitting elements in the finite element mesh used to model the test object, or elements may be assigned much lower values of density and elastic modulus. Absorbing boundaries can be used to allow the analyst to model portions of larger structural members. Greater accuracy or less computational time, or both, are the result. Without such absorbing elements, finite element models have to be sufficiently large so that the responses due to reflections from the boundaries do not interfere with reflections from the simulated defects.

Finite element simulations require an individual experienced in the finite-element method and familiarity with the nature of programs that solve wave propagation problems. Validity of the results hinges on using an acceptable mesh

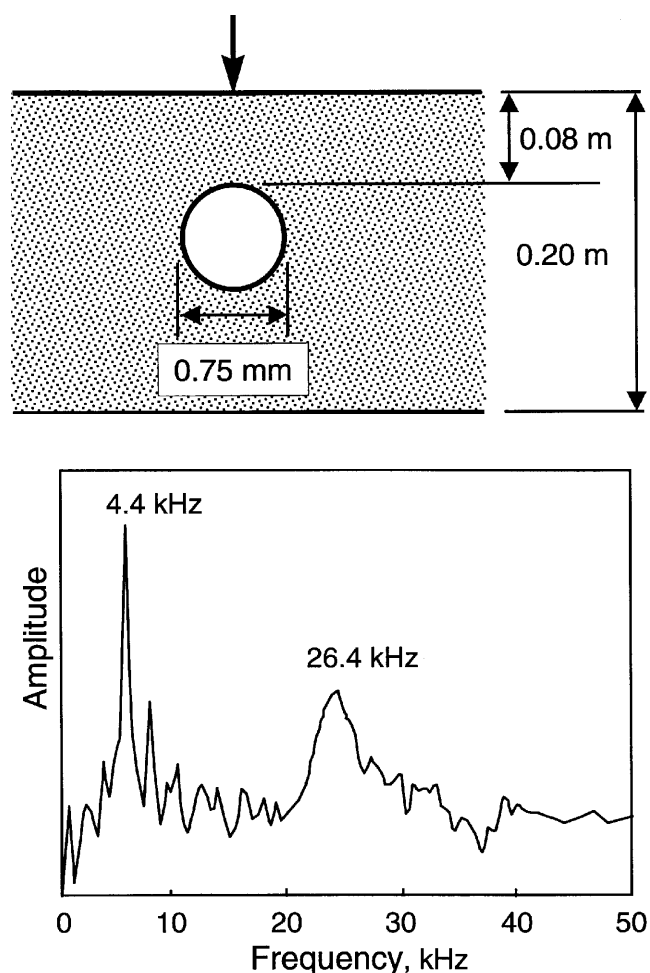


Fig. 3.3.1—Spectrum obtained from finite element simulation of impact-echo test on concrete section containing ungrouted duct.

geometry; choosing the correct time step, and other measures to assure stable calculations (if explicit codes are used) and accurate results; specifying the correct loading and boundary conditions; and correct simulation of the defect to be investigated.

Once the correct model has been developed, the calculated displacement of a node close to the impact point is treated as the transducer signal and used to calculate the amplitude spectrum. Parametric studies can be performed by varying factors such as duration of the impact, location of the impact point and receiver relative to the location of the defect, size and location of defect, or other parameters. Some examples of results obtained by finite simulations include the following: Cheng and Sansalone, 1993; Lin (Y.) and Sansalone, 1992a, 1992b, 1992c; Lin (J. M.) and Sansalone, 1993, 1994a, 1996; Sansalone et al., 1997; Williams et al., 1997.

The following example is taken from the work summarized in Jaeger et al. (1996) and involves detecting a void in the grouted tendon duct of a post-tensioned concrete structure. A three-dimensional numerical model was used to represent the geometry. Fig. 3.3.1 shows the geometry and an amplitude spectrum obtained from the finite element simulation. The

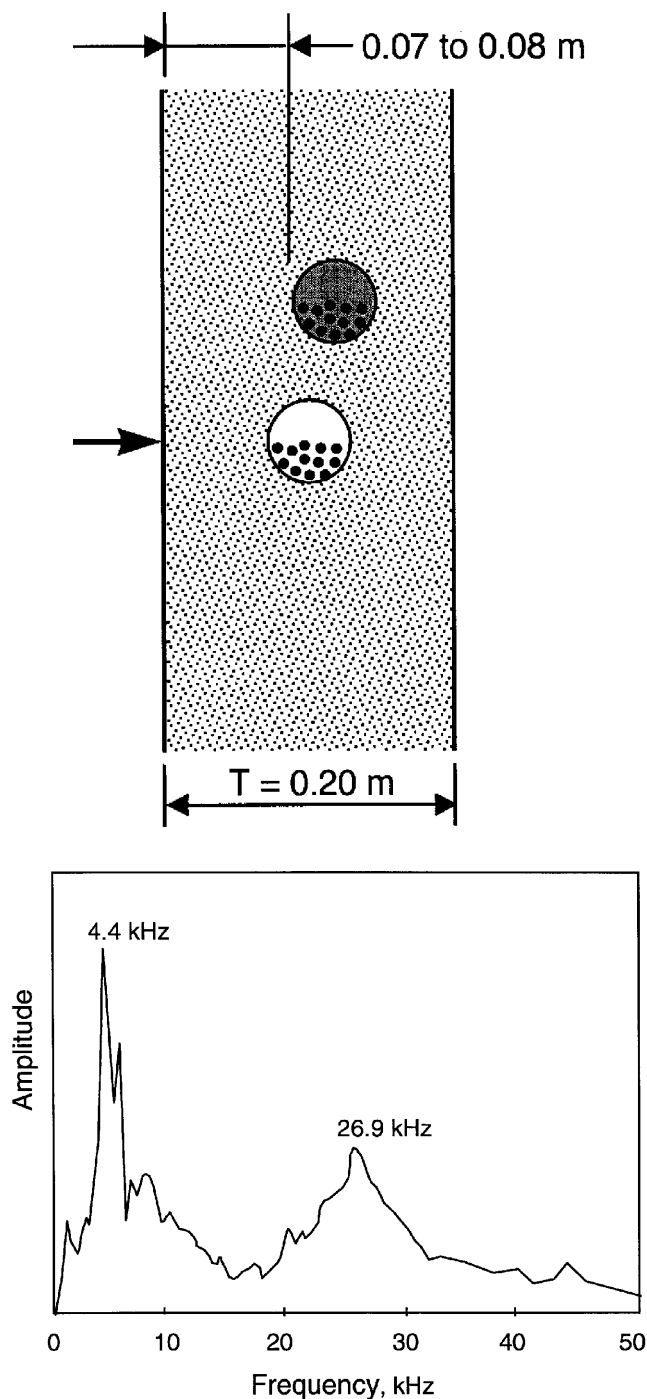


Fig. 3.3.2—Spectrum obtained from impact-echo test carried out over ungrouted duct in post-tensioned beam.

secondary peak at 26.4 kHz corresponds to reflection from the air void in the ungrouted duct. The peak at 4.4 kHz is less than the thickness frequency of the solid plate. The presence of the air void causes the shift to a lower frequency, and this frequency shift is an additional indicator of an anomaly in the plate (Jaeger et al. 1996). Fig. 3.3.2 shows the result from an impact-echo test performed on the web of an I-beam in a post-tensioned bridge. All key features of the responses are similar, and the overall agreement between the numerical

simulation and field test is excellent. (Note that the P-wave speed in the numerical model and actual beam were the same.) Such results are typical, and the finite element method has served as a powerful tool in developing the current understanding of the impact-echo method and its applications.

3.3.2 *Simulation of wave propagation in deep foundations*—Numerical techniques have been used for studying wave propagation in deep foundations in order to:

- Match predicted responses with real test responses for either sonic-echo or impulse-response methods, and
- Model pile behavior for use in the *impedance-logging* analytical method.

Interpretation of low-strain pile testing is based upon the theory of one dimensional stress-wave propagation within the pile shaft. After the shaft head is struck with a hand-held hammer, a low-strain stress wave travels down the shaft at a velocity that depends on the density and elastic modulus of the concrete. Any change in the shaft's shape, continuity, or material properties results in changes in the shaft impedance at the point of the anomaly, and a portion of the incident wave is reflected back to the pile head. Interpretation of the test response depends on the quality of the recorded signals, as well as identification of the parameters controlling the pile response (such as soil conditions, pile size, and shape). Therefore, the result of simulation matching is only as good as the quality of the real test signal.

Impulse-response—The first reference to simulation models using numerical techniques is in Davis and Dunn (1974), where a numerical model was developed for harmonic vibration testing (forerunner of impulse-response) of drilled shafts. Based on the analogy between the equations of motion and those of an electrical circuit, an analog electrical circuit model was used to represent the pile response. The force applied to the pile head was represented by an applied sinusoidal current and the resulting voltage represented the pile head velocity. Other electrical components were used to account for the density of the concrete and of the soil, the wave speed in the concrete and in the soil, and the diameter of the pile. The pile was divided into different segments, with different mechanical characteristics, that were converted to the equivalent analog circuits. The computed response of the circuit was compared with the measured response (velocity/force) and the characteristics of the segments were adjusted until there was good agreement between the two responses. This process is analogous to the inversion procedure used in the SASW test.

The analyst needs to have as much information as can be obtained about the real pile and soil conditions before attempting the simulation. This helps to reduce the number of steps required to obtain a matching fit between the real and simulated mobility-frequency plots. Typical values of material properties that can be used as a first try are:

- Concrete P-wave velocity from 3800 to 4100 m/s,
- Concrete density from 2300 to 2400 kg/m³,
- Soil density from 1700 to 1900 kg/m³,
- Shear wave velocity in soil from 100 to 300 m/s.

The errors in estimated depths of anomalies or pile toe arise principally from error in the estimation of the concrete pile stress-wave velocity. An error of ± 100 m/s will result in a depth error of approximately ± 2.5 percent.

Sonic-echo tests—Simulation of velocity-time waveforms from sonic-echo pile tests became practical with the advent of digital signal processing techniques in the 1980s (Middendorp and Reiding, 1988). The reflections recorded in a sonic-echo signal are caused by impedance changes in the pile shaft (necks, bulges, cracks, pile tip, or changes in concrete quality) and in soil resistance. All the changes in shaft impedance are modeled as variations in shaft cross section. It is necessary to know as much as possible about the site soil profile to simulate the response waveform.

The matching of sonic-echo test signals is performed in three steps:

- A reference pile response for a given pile population at the site is selected, by testing the pile population and selecting an average response.
- The shaft and toe resistances are derived for the reference pile. Because the shaft and toe resistances have a dominant effect on the test response, the derivation of the soil model is a prerequisite. To obtain the soil parameters, it is assumed that the reference pile has a uniform diameter. It is necessary to use as much information as is available about the site soil conditions at the beginning of this step. The shaft and toe resistances are adjusted until there is a good match between the measured and simulated signals.
- The discontinuities in the pile under simulation are derived. Discontinuities cause reflections that are displayed in the sonic-echo waveform. By measuring the travel time for the arrival of the first reflection, the location of the discontinuity can be determined. In the two most frequently used methods (Rausche et al., 1988; Starke and Janes, 1988), the impact force is applied as the input to the pile head in the computer model, and the measured velocity at the pile head is taken as the reference signal for the calculated response. The cross section of the computer model shaft is varied at the signal reflection location until a good match is found between the calculated and the measured signals.

In these simulations, the pile is modeled as a series of springs and dashpots to represent the pile cross section and effect of the surrounding soil. As when modeling the impulse-response test, the analyst needs to have as much information as can be obtained about the real pile and soil conditions before attempting a sonic-echo simulation. The most commonly used simulation methods are proprietary to the equipment manufacturers and are sold with their own testing systems. However, if good-quality sonic-echo test signals can be obtained, it is possible to develop response simulations using the approach outlined above for the impulse-response method. Again, as in the impulse-response simulation, the selected value of the concrete stress-wave velocity is critical in accurately predicting depths of features.

Impedance-logging analysis—The impedance-logging technique (Section 2.3.3) is, in essence, an extension of the matching of measured impulse-response test results, as described above. To obtain an impedance log profile, the following steps are necessary:

- Good-quality test signals must be obtained, including both the force and the velocity responses in the time domain. Minimum sampling rate for most shaft lengths studied should be 10 kHz, with a minimum of 1024 data points for each waveform. A reflected signal from the pile tip must also be present in the velocity waveform.
- The first analytical step is to remove the following from the velocity waveform: 1) the motion of the top of the shaft caused by the hammer impact; and 2) effects of the impedance changes resulting from changes in soil profile. This is achieved by calculating a theoretical mobility plot for an infinitely long, defect-free shaft with the nominal shaft diameter and known lateral soil variations. This computed mobility plot is subtracted from the test response. This gives a “reflected” mobility response containing information about changes in the shaft geometry and in the surrounding soil. Next, the impulse response in the time domain is calculated by taking the inverse fast Fourier transform of the “reflected” mobility plot. This is referred to as a relative reflectogram, which contains the time history of the reflections that return to the top of the shaft.
- By applying a selected amplification function to this calculated time response, the return signal strength can be approximated to a constant value down the entire length of the pile shaft.
- The reflectogram so obtained does not quantify the absolute shaft impedance, nor does it distinguish between changes in impedance caused by shaft conditions or those caused by lateral soil variation. The real impulse-response test result, however, does quantify the shaft impedance at the pile head, that can be used to calculate the impedance down the shaft as a function of time from

$$Z(t) = Z(0) \exp \left(2 \int_0^t R(t) dt \right) \quad (3.2)$$

where $Z(t)$ is the shaft impedance as a function of time, $Z(0)$ is the nominal impedance at the top of the shaft, and $R(t)$ are the reflection coefficients from the scaled relative reflectogram.

- Finally, the impedance as a function of depth is obtained from $Z(t)$ by converting time to depth using the compression wave velocity of the pile material. As in simulation of both the impulse-response and sonic-echo methods, if the density and compression wave velocity of the pile are known, changes in impedance correspond to changes in the cross-sectional area of the pile. The

resulting impedance-depth plot can be drawn as a plot of either diameter or cross-sectional area with depth. This is the final impedance log, and an example is given in Fig. 2.3.4.

As in other simulations of pile response, the analyst must have all available soil data and pile construction records to calculate the relative reflectogram.

3.3.3 Simulation of ground-penetrating radar—Numerical techniques can also be used to model the propagation of electromagnetic waves through concrete and to study the reflection and refraction of these waves at buried interfaces. Two modeling techniques may be used: the finite-element method and the ray tracing method. In the finite-element technique, the same approaches are used as was discussed in regard to stress-wave propagation. The structure is modeled by a mesh of finite elements, with each element having dielectric properties to represent different materials. The electromagnetic field in the test object due to a specified input field is computed as a function of time. This method allows the analyst to visualize (by means of post processing programs) the propagation of the field through the test object and how the field interacts with buried targets.

In the ray tracing technique, the analyst chooses two points: where the electromagnetic pulse is introduced and where the response is to be calculated. A series of possible ray paths that can connect these two points is determined. The response associated with each ray is computed, taking into consideration the reflection coefficients at points of reflection and the attenuation due to travel distance. The responses due to the arrival of each ray at the point of interest are added together to obtain the total response that would represent the theoretical waveform recorded by a perfect receiver.

In addition to ray tracing methods in the time domain, synthesis of the radar waveform may be accomplished by treating the reinforced concrete structures to be tested as a multilayered medium with regular cylindrical subsurface anomalies (reinforcing bars) (Halabe et al., 1995). A frequency-domain synthesis fully accounts for the multiple reflections and the frequency dependence of dielectric properties. Using the fast Fourier transform, a transmitted electromagnetic pulse can be decomposed in the frequency domain into a number of sine waves with different frequencies. A closed-form solution for the complex reflection coefficient for a multilayered medium and a single frequency sine wave can then be used with superposition to synthesize the radar waveform for the multilayer medium in the frequency domain. The presence of the reinforcing bars greatly affects the recorded radar waveform. The reinforcing bars can be treated as regular cylindrical subsurface anomalies with a uniform depth and spacing. Equations for the time-domain response for the reinforcing bar grid combined with the equations for the frequency-domain responses for the multilayered medium are combined to obtain a synthetic waveform for a reinforced concrete structure based on geometric layout and physical properties. This waveform synthesis is sensitive to the exact shape of the pulse emitted by a particular antenna.

Using the radar waveform synthesis model, the effects on the radar waveform of various parameters such as porosity, water and chloride content, cracks and delaminations, and reinforcing bar layout can be assessed.

3.3.4 Simulation of thermal anomalies—Thermography directly senses emitted infrared radiation. Since there is no calibration to an absolute radiation level, what is detected is the relative strength and location of the thermal anomalies. Thermal response of concrete structural members may be numerically simulated using a finite-element program with capabilities for transient heat-flow analysis. The concrete structure is modeled by a mesh of elements, with each element having thermal properties characteristic of the appropriate parts of the concrete structure. For example, a thermal model composed of a damaged zone with altered thermal properties layered between sound concrete zones can be used to model a delaminated concrete deck (Maser and Roddis, 1990). The deck properties that must be specified are:

- Thickness of the cover, delamination, and lower deck layers;
- Thermal conductivity and volumetric-heat capacity of the sound and damaged concrete; and
- Heat-transfer coefficients for the top and bottom of the deck.

The environmental conditions of ambient temperature and incident solar radiation, both varying on a diurnal cycle, drive the thermal response of the model. Since the driving forces are a function of time, the system is not static. The system could be treated as if it were static if the deck response time to variations in the driving forces were short compared with the length of time over which the driving forces fluctuated. This condition for quasi-static behavior is not satisfied for the deck model since the thickness and volumetric heat capacity of the concrete give the deck significant thermal inertia, slowing the system's response time. The thermal model must therefore account for transient heat-flow behavior.

3.3.5 Laboratory and field mock-ups—A possible alternative to numerical modeling when the evaluation investigator is faced with a new or unusual testing condition is to fabricate and test specimens (mock-ups) that simulate the expected field conditions. It may be possible to use portions of the actual structure as a mock-up if it known for certain that the tested area is sound or contains a flaw. Such experimental mock-ups can also be used to verify new numerical models. As in the case of numerical simulation, the mock-ups can be used to establish:

- Whether a certain anomaly can be detected,
- The best testing configuration to detect a specific defect, and
- The baseline response of an unflawed object.

When NDT methods based on wave propagation are used, the specimens need to be designed carefully to ensure that the boundary reflections do not interfere with reflections from the anomaly of interest. The material for the mock-ups should be selected so that it has properties similar to that expected in the field. Depending on the test method, similar

properties may mean similar density, elastic constants, conductivity, or dielectric properties. For example, if the evaluation investigator is interested in evaluating the ability of different covermeters to detect individual reinforcing bars when there is a complex or congested layout, it is not necessary to make concrete specimens. Since the response of covermeters is not influenced by the concrete (except when field concrete contains a significant amount of iron bearing aggregate), the mock-up can be made using a wooden frame to support the bars or the bars can be embedded in sand. This allows the investigator to consider different situations with little additional effort. Likewise, for a mock-up to be tested with GPR, it is not necessary to use concrete. Depending on the specific objective of the tests, it may be possible to make mock-ups using moist sand to represent the concrete. The moisture content of the sand will affect the attenuation of the electromagnetic pulses. Investigators have also used water/oil emulsions for accurate modeling of the dielectric and conductivity properties of concrete (Bungey et al., 1994). The use of the emulsion instead of concrete permits changing the testing configuration without having to cast new concrete specimens.

For test methods based on stress-wave propagation, concrete specimens have to be used because of the need to model the correct mismatch in acoustic impedance (wave speed times density) between concrete and the anomaly. A variety of approaches may be used to simulate defects. For example, rigid foam insulation board can be used to simulate air voids (Sansalone and Carino, 1986), thin sheets of flexible plastic foam have been used to simulate cracks (Cheng and Sansalone, 1993), and thin metal sheets that are withdrawn after final setting have been used to simulate surface opening cracks (Sansalone et al., 1997). Honeycombing has been simulated by casting a mass composed of cement paste and coarse aggregate (Sansalone and Carino, 1986). The absence of fine aggregate leads to voids between the coarse aggregate, simulating the structure of honeycombed concrete. After the mass has hardened, it is cast into the mock-up specimen.

Field mock-ups of deep foundations—Stress-wave methods evaluate the integrity and continuity of concrete piles and drilled shafts, either by direct transmission testing (sonic logging, see Section 2.3.4) or by reflection of stress waves propagated down the shaft by impacting the head of the pile (sonic-echo or impulse-response testing, see Sections 2.3.1 and 2.3.2).

Sonic logging of piles can be modeled in the laboratory, as described in the previous section. However, pile head impact tests rely upon the channeling of dispersive stress waves down cylindrical or prismatic structural members with length/diameter ratios typically between 10:1 and 40:1. Paquet (1968) points out that the frequencies used for both harmonic (vibration and impulse-response) and echo tests are relatively low, and the corresponding wave lengths are great compared with typical pile diameters.

Both the impulse-response and sonic-echo tests are affected by soil damping. If it is required to study the effect of soil damping on the pile response, then the wavelengths in the soil

are much greater than the pile diameter. Take, for example, a soil with a shear wave velocity of 800 m/s; at a frequency of 500 Hz, the wave length is 1.6 m, close to the pile diameter. At higher frequencies, the calculated damping would be a poor approximation of the true value.

For these reasons, tests on scaled-down laboratory pile models do not produce satisfactory results. This was realized early in the development of the methods, and several full-scale test sites have been constructed worldwide to test the validity and accuracy of various NDT methods. Usually, various defects or shape changes have been included in the test shafts. These full-scale experimental sites include:

- London, England, 1969 (Levy, 1970)
- Ghent, Belgium, 1987 (Holeyman et al., 1988)
- Northumberland, England, 1987 (Kilkenny et al., 1988)
- Federal Highway Administration (FHWA) trials, USA (Baker et al., 1993)
 - California, 1989
 - Texas, 1990
- Delft, Netherlands, 1992 (Anon., 1992)
- University of Houston, 1996 (Samman and O'Neill, 1997)

In several of these cases, initial tests were performed blind, that is, without prior knowledge of the lengths of the shafts or the location and type of built-in defects or shape changes. The accuracy and reliability of the test methods were then assessed by the sponsors of the test sites. At least two of the sites have been preserved for future testing as methods are refined and developed (Northumberland and FHWA Texas).

Descriptions of the test shafts, the installed defects, and the results of initial test programs are described in the references listed above. In particular, reference should be made to the FHWA report (Baker et al., 1993) for the evaluation of the most recent state of development of stress-wave methods as well as the nuclear-based, gamma-gamma logging method.

3.4—Correlation with intrusive testing

Because NDT methods provide indirect information about the conditions of the test object, it is not good practice to rely only on nondestructive testing for most condition surveys. A minimum amount of supplemental intrusive sampling or probing is often necessary to make a sound evaluation. Such intrusive techniques can serve several functions:

- Provide verification of the NDT results;
- Assess the conditions at selected points when the NDT results are inconclusive;
- Provide samples for additional testing to supplement the NDT investigation; and
- Refine the correlation between NDT results and actual conditions.

Because the NDT methods that have been discussed are not generally well understood by those requesting the investigation, providing the results of intrusive sampling or probing to compare with the NDT results is an effective means to instill confidence in the NDT results. If intrusive probing does not confirm the NDT results, such information must

also be provided to help explain the inherent limitations of a given method. Probing will increase the cost of the investigation, but it is a necessity when difficult investigations are undertaken.

Confirmation of NDT test results on a routine basis is necessary to ensure consistency and veracity of the testing. Ideally, the selection of the confirmation probing should be based on a sample size that is sufficient to provide some predetermined measure of statistical confidence. As a minimum, it is recommended that confirmation be conducted on a routine basis such as daily on small-scale testing projects, or weekly on large-scale projects.

When samples are needed for other tests, these can be obtained by coring or sawing. The NDT tests should be performed first and the sampling locations selected after preliminary analysis of the results. If possible, samples should be recovered at those test points where an anomaly has been clearly detected, where there is no indication of an anomaly, and where the NDT results are inconclusive.

When samples are not required for additional tests, different intrusive probing methods may be used. These may include chipping away the concrete with a hammer and chisel, using power-driven jackhammers, or drilling holes. A very effective approach is to drill a hole and inspect the inside of the hole using a rigid borescope or flexible fiberscope. Another example is to pour water into a drilled hole to provide information about the relative size of interconnected void space.

3.5—Reporting results

Vast amounts of data can be acquired during the NDT investigation. A challenge for the evaluation investigator is to select a data-presentation format that will be understood by those that have to make decisions based on the results of the investigation. On the other hand, all of the data should be preserved and arranged so that it can be easily understood by others. This is especially important when it is desired to investigate how conditions change with time. In such cases, it is critical that the test locations be documented accurately. The use of photographs to supplement written records is recommended. Before beginning the investigation, the evaluation investigator should reach an agreement with the client on the method of presenting the results. The format of the final report may have to be adjusted due to changes in the nature of the investigation due to unexpected conditions.

The use of drawings to summarize the reduced data is an effective supplement to tabular data. For example, contour plots can be used to summarize the results of ultrasonic pulse velocity or half-cell potential surveys. Background data can be documented in an appendix. On large-scale testing programs, electronic storage can be a beneficial way to manage the data. Moreover, the permanent record of all test results is convenient for follow-up testing at a later date to assess changes in conditions of the structure.

CHAPTER 4—REFERENCES

4.1—Specified references

The documents of the various standards producing organizations referred to in this document are listed below with their serial designations.

ACI Reports

- 201.1R Guide for Making a Condition Survey of Concrete in Service
- 207.3R Practices for Evaluation of Concrete in Existing Massive Structures for Service Conditions
- 222R Corrosion of Metals in Concrete
- 224.1R Causes, Evaluation and Repair of Cracks in Concrete Structures
- 228.1R In-Place Methods to Estimate Concrete Strength
- 362R State-of-the-Art Report on Parking Structures
- 437R Strength Evaluation of Existing Concrete Buildings
- 503R Standard Specification for Bonding Hardened Concrete, Steel, Wood, Brick, and Other Materials to Hardened Concrete with a Multi-Component Epoxy Adhesive

ASTM Standards

- ASTM C 39 Test Method for Compressive Strength of Cylindrical Concrete Specimens
- ASTM C 42 Test Method for Obtaining and Testing Drilled Cores and Sawed Beams of Concrete
- ASTM C 215 Test Method for Fundamental Transverse, Longitudinal, and Torsional Frequencies of Concrete Specimens
- ASTM C 294 Descriptive Nomenclature for Constituents of Natural Mineral Aggregates
- ASTM C 295 Guide for Petrographic Examination of Aggregates for Concrete
- ASTM C 341 Test Method for Length Change of Drilled or Sawed Specimens of Hydraulic-Cement Mortar and Concrete
- ASTM C 457 Test Method for Microscopical Determination of the Air-Void System in Hardened Concrete
- ASTM C 469 Test Method for Static Modulus of Elasticity and Poisson's Ratio of Concrete in Compression
- ASTM C 496 Test Method for Splitting Tensile Strength of Cylindrical Concrete Specimens
- ASTM C 597 Test Method for Pulse Velocity Through Concrete
- ASTM C 642 Test Method for Specific Gravity, Absorption, and Voids in Hardened Concrete
- ASTM C 805 Test Method for Rebound Number in Concrete
- ASTM C 803 Test Method for Penetration Resistance of Hardened Concrete
- ASTM C 823 Practice for Examination and Sampling of Hardened Concrete in Constructions
- ASTM C 856 Practice for Petrographic Examination of Hardened Concrete

- ASTM C 876 Test Method for Half-Cell Potentials of Uncoated Reinforcing Steel in Concrete
- ASTM C 1040 Test Methods for Density of Unhardened and Hardened Concrete in Place by Nuclear Methods
- ASTM C 1084 Test Method for Portland-Cement Content of Hardened Hydraulic-Cement Concrete
- ASTM C 1152 Test Method for Acid-Soluble Chloride in Mortar and Concrete
- ASTM C 1202 Test Method for Electrical Indication of Concrete's Ability to Resist Chloride Ion Penetration
- ASTM C 1218 Test Method for Water-Soluble Chloride in Mortar and Concrete
- ASTM C 1383 Test Method for Measuring P-Wave Speed and the Thickness of Concrete Plates Using the Impact-Echo Method
- ASTM D 4748 Test Method for Determining the Thickness of Bound Pavement Layers Using Short-Pulse Radar
- ASTM D 4580 Practice for Measuring Delaminations in Concrete Bridge Decks by Sounding
- ASTM D 4748 Test Method for Determining the Thickness of Bound Pavement Layers Using Short-Pulse Radar
- ASTM D 4788 Test Method for Deflecting Delaminations in bridge Decks Using Infrared Thermography
- ASTM E 105 Practice for Probability Sampling of Materials
- ASTM E 122 Practice for Choice of Sample Size to Estimate a Measure of Quality for a Lot or Process
- ASTM G 15 Terminology Relating to Corrosion and Corrosion Testing

AASHTO Standard

- AASHTO T 259 Method of Test for Resistance of Concrete to Chloride Ion Penetration

British Standard

- BS 1881 Part 204: Recommendations on the Use of Electromagnetic Covermeters
- BS 1881 Part 205: Recommendations for Radiography of Concrete
- BS 1881 Part 207: Recommendations for the Assessment of Concrete Strength by Near-to-surface Tests
- BS 1881 Part 5: Methods of Testing Concrete for Other Than Strength

CSA Standards

- CSA-A23.2-M94 Methods of Test for Concrete

The above publications may be obtained from the following organizations:

American Concrete Institute (ACI)
P.O. Box 9094
Farmington Hills, Mich. 48333-9094

American Society for Testing and Materials (ASTM)
100 Barr Harbor Drive
West Conshohocken, Pa. 19428-2959

American Association of State Highway and Transportation Officials (AASHTO)
444 N. Capitol St., NW
Washington, D.C. 20001

Canadian Standards Association (CSA)
178 Rexdale Boulevard
Rexdale, Ontario M9W 1R3
Canada

British Standards Institution (BS)
2 Park Street
London W1A 2BS
England

4.2—Cited references

- Alexander, A. M., and Thornton, H. T., Jr. (1989). "Ultrasonic Pitch-Catch and Pulse-Echo Measurements in Concrete," *Nondestructive Testing of Concrete*, H. S. Lew, ed., ACI SP-112, American Concrete Institute, Farmington Hills, Mich., Mar., pp. 21-40.
- Anonymous (1992). "Results of Delft University Pile Integrity Testing Competition," *Ground Engineering*, V. 25, Oct.-Nov. (See also subsequent discussions in *Ground Engineering*, Apr. 1993 and Jul.-Aug. 1993).
- Baker, C. N., Jr.; Drumwright, E. E.; Briaud, J.-L.; Mensah-Dumwah, F.; and Parikh, G. (1993). *Drilled Shafts for Bridge Foundations*, Pub. No. FHWA-RD-92-004, Federal Highway Administration, Washington, D.C.
- Baker, C. N., and Khan, F. (1971). "Caisson Construction Problems and Correction in Chicago," *Journal of Soil Mechanics and Foundation Engineering Division*, ASCE, V. 97, No. 2, pp. 417-440.
- Basheer, P. A. M.; Montgomery, F. R.; and Long, A. E. (1992). "In Situ Assessment of Durability of Concrete Motorway Bridges," *Durability of Concrete: G.M. Idorn International Symposium*, J. Holm and M. Geiker, eds., ACI SP-131, American Concrete Institute, Farmington Hills, Mich., pp. 305-319.
- Bay, J. A., and Stokoe, K. H. (1990). "Field Determination of Stiffness and Integrity of PCC Members Using SASW Method," *Proceedings Conference on Nondestructive Evaluation of Civil Structures and Materials*, Oct. 15-17, Boulder, Colo., National Science Foundation (sponsor), pp. 71-85.
- Bradfield, G., and Gatfield, E. (1964). "Determining the Thickness of Concrete Pavements by Mechanical Waves: Directed Beam Method," *Magazine of Concrete Research*, V. 16, No. 46, Mar., pp. 49-53.
- Briard, M. (1970). "Controle de Pieux par la Methode de Vibrations, (Pile Construction Control Using the Vibration Method)," *Annl. Inst. Tech. Batim.*, V. 23, No. 270, Jun., pp. 105-107.
- Bungey, J. H. (1989). *Testing of Concrete in Structures*, 2nd ed., Chapman and Hall, New York.
- Bungey, J. H.; Millard, S. G.; Shaw, M. R.; and Thomas, C. (1991). "Operational Aspects of Radar Investigations," *British Journal of NDT*, V. 33, No. 12, Dec., pp. 599-605.
- Bungey, J. H., and Millard, S. G. (1993). "Radar Inspection of Structures," *Proceedings, Institute of Civil Engineers, Structures and Buildings Journal* (London), V. 99, May, pp. 173-186.
- Bungey, J. H.; Millard, S. G.; and Shaw, M. R. (1994). "The Influence of Reinforcing Steel on Radar Surveys of Structural Concrete," *Construction and Building Materials*, V. 8, No. 2, pp. 119-126.
- Bungey, J. H., and Millard, S. G. (1995). "Detecting Sub-Surface Features in Concrete by Impulse Radar," *Nondestructive Testing and Evaluation*, V. 12, pp. 33-51.
- Cady, P. D., and Gannon, E. J. (1992). "Condition Evaluation of Concrete Bridges Relative to Reinforcement Corrosion," *Volume 8: Procedure Manual*, SHRP-S/FR-92-110, Strategic Highway Research Program, National Research Council, Washington, D.C., 124 pp.
- Cantor, T. R. (1984). "Review of Penetrating Radar as Applied to Non-destructive Evaluation of Concrete," *In Situ/Nondestructive Testing of*

- Concrete, V. M. Malhotra, ed., ACI SP-82, American Concrete Institute, Farmington Hills, Mich., pp. 581-601.
- Carino, N. J.; Sansalone, M.; and Hsu, N. N. (1986). "Flaw Detection in Concrete by Frequency Spectrum Analysis of Impact-Echo Waveforms," *International Advances in Nondestructive Testing*, V. 12, W. J. McGonagle, ed., Gordon & Breach Science Publishers, New York, pp. 117-146.
- Carino, N. J. (1992). "Performance of Electromagnetic Covermeters for Nondestructive Assessment of Steel Reinforcement," NISTIR 4988, National Institute of Standards and Technology, Sept., 130 pp.
- Carino, N. J. (1994). "Recent Developments in Nondestructive Testing of Concrete," *Advances in Concrete Technology*, 2nd ed., V. M. Malhotra, ed., MSL 94-1(R), CANMET, Natural Resources Canada, Ottawa, pp. 281-337.
- Carter, C. R.; Chung T.; Holt, F. B.; and Manning, D. (1986). "An Automated Signal Processing System for the Signature Analysis of Radar Waveforms from Bridge Decks," *Canadian Electrical Engineering Journal*, V. 11, No. 3, pp. 128-137.
- Cather, R.; Figg, J. W.; Marsden, A. F.; and O'Brien, T. P. (1984). "Improvements to the Figg Method of Determining the Air Permeability of Concrete," *Magazine of Concrete Research*, V. 36, No. 129, Dec., pp. 241-245.
- Chen, H. L. R.; Halabe, U. B.; Sami, Z.; and Bhandarkar, V. (1994). "Impulse Radar Reflection Waveforms of Simulated Reinforced Concrete Bridge Decks," *Materials Evaluation*, V. 52, No. 12, pp. 1382-1388.
- Cheng, C., and Sansalone, M. (1993). "The Impact-Echo Response of Concrete Plates Containing Delaminations: Numerical, Experimental, and Field Studies," *Materials and Structures*, V. 26, No. 159, Jun., pp. 274-285.
- Chung, H. W., and Law, K. S. (1985). "Assessing Fire Damage of Concrete by the Ultrasonic Pulse Technique," *Cement, Concrete, and Aggregates*, V. 7, No. 2, Winter, pp. 84-88.
- Clear, K. C. (1989). "Measuring Rate of Corrosion of Steel in Field Concrete Structures," *Transportation Research Record* No. 1211, Transportation Research Board, Washington, D.C., pp. 28-37.
- Clemeña, G. (1983). "Nondestructive Inspection of Overlaid Bridge Decks with Ground Probing Radar," *Transportation Research Record* No. 899, Transportation Research Board, Washington, D.C., pp. 21-32.
- Clemeña, G. G. (1991). "Short-Pulse Radar Methods," *Handbook on Nondestructive Testing of Concrete*, Chapter 3, V. M. Malhotra and N. J. Carino, eds., CRC Press, Boca Raton, Fla., pp. 253-274.
- Clemeña, G. G.; Jackson, D. R.; and Crawford, G. C. (1992a). "Benefits of Using Half-Cell Potential Measurements in Condition Surveys of Concrete Bridge Decks," *Transportation Research Record* No. 1347, Transportation Research Board, Washington, D.C., pp. 46-55.
- Clemeña, G. G.; Jackson, D. R.; and Crawford, G. C. (1992b). "Inclusion of Rebar Corrosion Rate Measurements in Condition Surveys of Concrete Bridge Decks," *Transportation Research Record* No. 1347, Transportation Research Board, Washington, D.C., pp. 37-45.
- "Condition Evaluation of Concrete Bridges Relative to Reinforcement Corrosion, Volume 2: Method for Measuring the Corrosion Rate of Reinforcing Steel," *Strategic Highway Research Program (SHRP) Reports*, SHRP-S-324, Transportation Research Board, National Research Council, Washington, D.C.
- "Condition Evaluation of Concrete Bridges Relative to Reinforcement Corrosion, Volume 5: Method for Evaluating the Effectiveness of Penetrating Sealers," *Strategic Highway Research Program (SHRP) Reports*, SHRP-S-327, Transportation Research Board, National Research Council, Washington, D.C.
- "Condition Evaluation of Concrete Bridges Relative to Reinforcement Corrosion, Volume 6: Method for Field Determination of Total Chloride Content," *Strategic Highway Research Program (SHRP) Reports*, SHRP-S-328, Transportation Research Board, National Research Council, Washington, D.C.
- "Condition Evaluation of Concrete Bridges Relative to Reinforcement Corrosion, Volume 7: Method for Field Measurement of Concrete Permeability," *Strategic Highway Research Program (SHRP) Reports*, SHRP-S-329, Transportation Research Board, National Research Council, Washington, D.C.
- "Condition Evaluation of Concrete Bridges Relative to Reinforcement Corrosion, Volume 8: Procedure Manual," *Strategic Highway Research Program (SHRP) Reports*, SHRP-S-330, Transportation Research Board, National Research Council, Washington, D.C.
- Daniels, D. J.; Gunton, D. J.; and Scott, H. F. (1988). "Introduction to Subsurface Radar," *Proceedings Institution of Electrical Engineers*, V. 135, Part F, No. 4, Aug., pp. 278-320.
- Das Gupta, N. C., and Tam, C. T. (1983). "Non-Destructive Technique for Simultaneous Detection of Size and Cover of Embedded Reinforcement," *British Journal of Non-Destructive Testing*, V. 25, No. 6, Nov., pp. 301-304.
- Davis, A. G. (1995). "Nondestructive Evaluation of Existing Deep Foundations," *Journal of Performance of Constructed Facilities*, ASCE, V. 9, No. 1, Feb., pp. 57-74.
- Davis, A. G., and Dunn, C. S. (1974). "From Theory to Field Experience with the Nondestructive Vibration Testing of Piles," *Proceedings Institute of Civil Engineers*, Part 2, 57, Dec., pp. 571-593.
- Davis, A. G., and Robertson, S. A. (1975). "Economic Pile Testing," *Ground Engineering*, V. 8, No. 3, pp. 40-43.
- Davis, A. G., and Hertlein, B. H. (1990). Assessment of Bridge Deck Repairs by a Nondestructive Technique, *Proceeding of the NATO Advanced Research Workshop on Bridge Evaluation, Repair, and Rehabilitation*, Apr. 30-May 2, 1990, Baltimore, Md., A. J. Nowak, ed., Kluwer Academic Publishers, Boston, Mass., April, pp. 229-233.
- Davis, A. G., and Hertlein, B. H. (1994). "A Comparison of the Efficiency of Drilled Shaft Down-Hole Integrity Tests," *Proceedings International Conference on Design and Construction of Deep Foundations*, FHWA, Orlando, Fla., Dec., V. 3, pp. 1272-1286.
- Davis, A. G., and Hertlein, B. H. (1997). "Evaluation of the Integrity of Some Large Concrete Foundations Using NDT," ACI SP-168, *Innovations in Nondestructive Testing of Concrete*, S. Pessiki and L. Olson, eds., pp. 333-356.
- Davis, A. G., Evans, J. G., and Hertlein, B. H. (1997). "Nondestructive Evaluation of Concrete Radioactive Waste Tanks," *Journal of Performance of Constructed Facilities*, ASCE, V. 11, No. 4, pp. 161-167.
- Dhir, R. K.; Hewlett, P. C.; and Chan, Y. N. (1987). "Near Surface Characteristics of Concrete: Assessment and Development of In Situ Test Methods," *Magazine of Concrete Research*, V. 39, No. 141, Dec., pp. 183-195.
- Escalante, E. (1989). "Elimination of IR Error in Measurements of Corrosion in Concrete," *The Measurement and Correction of Electrolyte Resistance in Electrochemical Tests*, ASTM STP 1056, L. L. Scribner and S. R. Taylor, eds., American Society for Testing and Materials, Philadelphia, Pa., pp. 180-190.
- Feliu, S.; González, J. A.; Andrade, C.; and Feliu, V. (1989). "Polarization Resistance Measurements in Large Concrete Specimens: Mathematical Solution for Unidirectional Current Distribution," *Materials and Structures: Research and Testing (RILEM)*, V. 22, No. 129, May, pp. 199-205.
- Feliu, S.; González, J. A.; Feliu, S., Jr.; and Andrade, M. C. (1990). "Confinement of the Electrical Signal for In Situ Measurement of Polarization Resistance in Reinforced Concrete," *ACI Materials Journal*, V. 87, No. 5, Sept.-Oct., pp. 457-460.
- Feliu, S.; González, J. A.; Escudero, M. L.; Feliu, S., Jr.; and Andrade, M. C. (1990). "Possibilities of the Guard Ring for Electrical Signal Confinement in the Polarization Measurements of Reinforcements," *Journal of Science and Engineering Corrosion*, V. 46, No. 12, pp. 1015-1020.
- Figg, J. W. (1973). "Methods of Measuring the Air and Water Permeability of Concrete," *Magazine of Concrete Research*, V. 25, No. 85, Dec., pp. 213-219.
- Figg, J. W. (1989). "Concrete Surface Permeability: Measurement and Meaning," *Chemistry and Industry*, Nov. 6, pp. 714-719.
- Fitzgerald, A. E.; Higginbotham, D. E.; and Grabel, A. (1967). *Basic Electrical Engineering*, McGraw-Hill Book Co., New York.
- Flis, J.; Sehgal, A.; Li, D.; Kho, Y. T.; Sabol, S.; Pickering, H.; Osseao-Asare, K.; and Cady, P. D. (1992). "Condition Evaluation of Concrete Bridges Relative to Reinforcement Corrosion," *Volume 2: Method for Measuring the Corrosion Rate of Reinforcing Steel*, SHRP-S/FR-92-104, Strategic Highway Research Program, National Research Council, Washington, D.C., 105 pp.
- Hagemeyer, D. J. (1990). *Fundamentals of Eddy Current Testing*, American Society for Nondestructive Testing, Inc., Columbus, Ohio.
- Halabe, U. B.; Sotoodehnia, A.; Maser, K. R.; and Kausel, E. A. (1993). "Modeling the Electromagnetic Properties of Concrete," *ACI Materials Journal*, V. 90, No. 6, Nov.-Dec., pp. 552-563.
- Halabe, U. B.; Maser, K. R.; and Kausel, E. A. (1995). "Condition Assessment of Reinforced Concrete Structures Using Electromagnetic Waves," *ACI Materials Journal*, V. 92, No. 5, Sept.-Oct., pp. 511-523.

- Hall, C. (1989). "Water Sorptivity of Mortars and Concretes: A Review," *Magazine of Concrete Research*, V. 41, No. 147, Jun., pp. 51-61.
- Halliday, D., and Resnick, R. (1978). *Physics*, 3rd ed., John Wiley & Sons, New York.
- "Handbook for the Identification of Alkali-Silica Reactivity in Highway Structures," *Strategic Highway Research Program (SHRP) Reports*, SHRP-C-315, Transportation Research Board, National Research Council, Washington, D.C.
- Heisey, J. S.; Stokoe, K. H., II; and Meyer, A. H. (1982). "Moduli of Pavement Systems From Spectral Analysis of Surface Waves," *Transportation Research Record*, No. 853, Transportation Research Board, Washington, D.C., pp. 22-31.
- Hillger, W. (1993). "Imaging of Defects in Concrete by Ultrasonic Pulse-Echo Technique," *Proceedings Fifth International Conference on Structural Faults and Repair*, July 1, University of Edinburgh, Engineering Technics Press, pp. 59-65.
- Holeyman, A.; Legrand, C.; Lousberg, E.; and D'Haenens, A. (1988). "Comparative Dynamic Pile Testing in Belgium," *Proceedings Third International Conference on the Application of Stress-Wave Theory to Piles*, B. H. Fellenius, ed., Ottawa, Canada, May 25-27, pp. 542-554.
- Holt, F. B., and Manning, D. G. (1978). "Infrared Thermography for the Detection of Delaminations in Concrete Bridge Decks," *Proceedings Fourth Biennial Infrared Information Exchange*, pp. A61-A71.
- Höing, A. (1984). "Radiometric Determination of the Density of Fresh Shielding Concrete In Situ," *In Situ/Nondestructive Testing of Concrete*, V. M. Malhotra, ed., ACI SP-82, American Concrete Institute, Farmington Hills, Mich., pp. 603-618.
- Howkins, S. D. (1968). "Measurement of Pavement Thickness by Rapid and Nondestructive Methods," *NCHRP Report 52*, Highway Research Board, National Research Council, Washington, D.C., 82 pp.
- Iddings, F. A., and Melancon, J. L. (1986). "Detection of Voids in Plastic Concrete Roadways," *Review of Progress in Quantitative Nondestructive Evaluation*, D. O. Thompson and D. E. Chimenti, eds., V. 5B, Plenum Press, New York, pp. 1655-1663.
- Jaeger, B. J.; Sansalone, M. J.; and Poston, R. W. (1996). "Detecting Voids in Grouted Tendon Ducts of Post-Tensioned Concrete Structures Using the Impact-Echo Method," *ACI Structural Journal*, V. 93, No. 4, July-Aug., pp. 462-472.
- Jones, R. (1949). "The Non-Destructive Testing of Concrete," *Magazine of Concrete Research*, No. 2, June, pp. 67-78.
- Jones, R. (1955). "A Vibration Method for Measuring the Thickness of Concrete Road Slabs In Situ," *Magazine of Concrete Research*, V. 7, No. 20, July, pp. 97-102.
- Jones, R. (1962). "Surface Wave Technique for Measuring the Elastic Properties and Thickness of Roads: Theoretical Development," *British Journal of Applied Physics*, V. 13, pp. 21-29.
- Kalinski, M. E.; Stokoe, K. H., II; Jirsa, J. O.; and Roesset, J. M. (1994). "Nondestructive Evaluation of Internally Damaged Areas of a Concrete Beam Using the SASW Method," Preprint 9407114, Transportation Research Board 73rd Annual Meeting, Washington, D.C., Jan.
- Kaplan, H. (1994). "Commercial Applications for Thermal Imaging Instruments: An Update," *Proceedings Infrared Technology XX*, SPIE The International Society for Optical Engineering, V. 2269, pp. 8-17.
- Kilkenny, W. M.; Lilley, D. M.; and Akroyd, R. F. (1988). "Steady State Vibration Testing of Piles with Known Defects," *Proceedings Third International Conference on the Application of Stress-Wave Theory to Piles*, B. H. Fellenius, ed., Ottawa, Canada, May 25-27, pp. 91-98.
- Krautkrämer, J., and Krautkrämer, H. (1990). *Ultrasonic Testing of Materials*, 4th Edition, Springer-Verlag, New York.
- Kropp, J., and Hilsdorf, H. K. (eds.) (1995). *Performance Criteria for Concrete Durability*, E & FN Spon, London, 327 pp.
- Kunz, J. T., and Eales, J. W. (1985). "Remote Sensing Techniques Applied to Bridge Deck Evaluation," *Strength Evaluation of Existing Concrete Bridges*, T. C. Liu, ed., ACI SP-88, American Concrete Institute, Farmington Hills, Mich., pp. 237-258.
- Lauer, K. R. (1991). Magnetic/Electrical Methods, *Handbook on Nondestructive Testing of Concrete*, Chapter 9, V. M. Malhotra and N. J. Carino, eds., CRC Press, Boca Raton, Fla., pp. 203-225.
- Leslie, J. R., and Cheesman, W. J. (1949). "An Ultrasonic Method of Studying Deterioration and Cracking in Concrete Structures," *Journal of the American Concrete Institute*, V. 21, No. 1, Sept., *Proceedings* V. 46, pp. 17-36.
- Levitt, M. (1971). "The ISAT—A Non-Destructive Test for the Durability of Concrete," *British Journal of Non-Destructive Testing*, V. 13, No. 4, July, pp. 106-112.
- Levy, J. F. (1970). "Sonic Pulse Method of Testing Cast In Situ Piles," *Ground Engineering*, V. 3, No. 3, pp. 17-19.
- Lin, J. M., and Sansalone, M. (1993). "The Transverse Elastic Impact Response of Thick Hollow Cylinders," *Journal of Nondestructive Evaluation*, V. 12, No. 2, pp. 139-149.
- Lin, J. M., and Sansalone, M. (1994a). "The Impact-Echo Response of Hollow Cylindrical Concrete Structures Surrounded by Soil or Rock, Part 1—Numerical Studies," *ASTM Geotechnical Testing Journal*, V. 17, No. 2, June, pp. 207-219.
- Lin, J. M., and Sansalone, M. (1994b). "The Impact-Echo Response of Hollow Cylindrical Concrete Structures Surrounded by Soil or Rock, Part 2—Field Studies," *ASTM Journal of Geotechnical Testing*, V. 17, No. 2, June, pp. 220-226.
- Lin, J. M., and Sansalone, M. (1996). "Impact-Echo Studies of Interfacial Bond Quality in Concrete: Part I—Effects of Unbonded Fraction of Area," *ACI Materials Journal*, V. 93, No. 3, May-June, pp. 223-232.
- Lin, Y., and Sansalone, M. (1992a). "Transient Response of Thick Circular and Square Bars Subjected to Transverse Elastic Impact," *Journal of the Acoustical Society of America*, V. 91, No. 2, Feb., pp. 885-893.
- Lin, Y., and Sansalone, M. (1992b). "Transient Response of Thick Rectangular Bars Subjected to Transverse Elastic Impact," *Journal of the Acoustical Society of America*, V. 91, No. 5, May, pp. 2674-2685.
- Lin, Y., and Sansalone, M. (1992c). "Detecting Flaws in Concrete Beams and Columns Using the Impact-Echo Method," *ACI Materials Journal*, V. 89, No. 4, July-Aug., pp. 394-405.
- Lin, Y., and Su, W. C. (1996). "Use of Stress Waves for Determining the Depth of Surface-Opening Cracks in Concrete Structures," *ACI Materials Journal*, V. 93, No. 5, Sept.-Oct., pp. 494-505.
- Mailier, H. (1972). "Pavement Thickness Measurement Using Ultrasonic Techniques," *Highway Research Record*, No. 378, pp. 20-28.
- Malhotra, V. M. (1976). *Testing Hardened Concrete: Nondestructive Methods*, American Concrete Institute Monograph No. 9, ACI/Iowa State University Press, 204 pp.
- Manning, D. G. and Holt, F. B. (1980). "Detecting Deterioration in Concrete Bridge Decks," *Concrete International*, V. 2, No. 11, Nov., pp. 34-41.
- Maser, K. R. (1986). "Detection of Progressive Deterioration in Bridge Decks Using Ground Penetrating Radar, Experimental Assessment of the Performance of Bridges," *Proceedings ASCE/EM Division Specialty Conference*, Boston, Mass., Oct., pp. 42-57.
- Maser, K. R. (1989-90). "New Technology for Bridge Deck Assessment, New England Transportation Consortium Final Reports" (Phase I Report FHWA-NETC-89-01, Phase II Report FHWA-NETC-90-1), Center for Transportation Studies, MIT, Oct. and Apr.
- Maser, K. R., and Roddis, W. M. K. (1990). "Principles of Thermography and Radar for Bridge Deck Assessment," *Journal of Transportation Engineering*, ASCE, V. 116, No. 5, Sept.-Oct., pp. 583-601.
- Mast, J. E.; Lee, H.; Chew, C.; and Murtha, J. (1990). "Pulse-Echo Holographic Techniques for Microwave Subsurface NDE," *Proceedings Conference on Nondestructive Evaluation of Civil Structures and Materials*, Oct. 15-17, Boulder, Colo., National Science Foundation (sponsor), pp. 177-191.
- Mast, J. E. and Johansson, E. M. (1994). "Three-Dimensional Ground Penetrating Radar Imaging Using Multi-Frequency Diffraction Tomography," *Proceedings SPIE The International Society for Optical Engineering*, Advanced Microwave and Millimeter-Wave Detectors, V. 2275, pp. 196-204.
- Mathews, J. H.; Porter, S. G.; Dennis, P. N. J.; and Watton, R. (1994). "Infrared Detectors in the UK—A 10 Year Update Benefits of Uncooled IR Sensors," *Proceedings Infrared Technology XX*, SPIE The International Society for Optical Engineering, V. 2269, pp. 678-686.
- Middendorp, P., and Reiding, F. J. (1988). "Determination of Discontinuities in Piles by TNO Integrity Testing and Signal Matching Techniques," *Proceedings Third International Conference on the Application of Stress-Wave Theory to Piles*, International Society of Soil Mechanics and Foundation Engineering, B. H. Fellenius, ed., Ottawa, Canada, May 25-27, pp. 33-43.
- Millard, S. G.; Bungey, J. H.; and Shaw, M. (1993). "The Assessment of Concrete Quality Using Pulsed Radar Reflection and Transmission Techniques," *Proceedings International Conference NDT in Civil Engineering*,

- Apr. 14-16, Liverpool, The British Institute of NDT, Southampton, pp. 161-185.
- Mitchell, T. M.; Lee, P. L.; and Eggert, G. J. (1979). "The CMD: A Device for the Continuous Monitoring of the Consolidation of Plastic Concrete," *Public Roads*, V. 42, No. 148.
- Mitchell, T. W. (1991). "Radioactive/Nuclear Methods," *Handbook on Nondestructive Testing of Concrete*, Chapter 10, V. M. Malhotra and N. J. Carino, eds., CRC Press, Boca Raton, Fla., pp. 227-252.
- Montgomery, F. R., and Adams, A. (1985). "Early Experience with a New Concrete Permeability Apparatus," *Proceedings Second International Conference on Structural Faults and Repair*, Apr. 30-May 2, London, Engineering Technics Press, Edinburgh, pp. 359-363.
- Naik, T. R., and Malhotra, V. M. (1991). "The Ultrasonic Pulse Velocity Method," *Handbook on Nondestructive Testing of Concrete*, Chapter 7, V. M. Malhotra and N. J. Carino, eds., CRC Press, Boca Raton, Fla., pp. 169-188.
- Natrella, M. (1963). *Experimental Statistics*, NBS Handbook 91, U.S. Government Printing Office.
- Nazarian, S.; Stokoe, K. H., II; and Hudson W. R. (1983). "Use of Spectral Analysis of Surface Waves Method for Determination of Moduli and Thickness of Pavement Systems," *Transportation Research Record*, No. 930, Transportation Research Board, Washington, D.C., pp. 38-45.
- Nazarian, S., and Stokoe, K. H., II (1986). "In-Situ Determination of Elastic Moduli of Pavement Systems by Spectral-Analysis-of-Surface-Waves Method (Practical Aspects)," *Research Report 368-1F*, Center for Transportation Research, University of Texas at Austin, May.
- Nazarian, S., and Stokoe, K. H., II (1986). "In-Situ Determination of Elastic Moduli of Pavement Systems by Spectral-Analysis-of-Surface-Waves Method (Theoretical Aspects)," *Research Report 437-2*, Center for Transportation Research, University of Texas at Austin, Aug.
- Nazarian, S., and Desai, M. R. (1993). "Automated Surface Wave Method: Field Testing," *Journal of Geotechnical Engineering*, ASCE, V. 119, No. 7, July, pp. 1094-1111.
- Olson, L. D., and Wright, C. C. (1990). "Nondestructive Testing for Repair and Rehabilitation," *Concrete International*, V. 12, No. 3, Mar., pp. 58-64.
- Olson, L. D.; Wright, C. C.; and Stokoe, K. H. (1990). "Strides in Nondestructive Testing," *Civil Engineering*, ASCE, V. 60, No. 5, May, pp. 52-55.
- Paquet, J. (1968). "Etude Vibratoire des Pieux en Beton: Reponse Harmonique (Vibration Study of Concrete Piles: Harmonic Response)," *Annls. Inst. Tech. Batim.*, France, V. 21, No. 245, pp 789-803. (English translation by Xiang Yee in Master of Eng. Report, University of Utah, pp. 33-77, 1991).
- Paquet, J. (1991). "The Impedance Log, Conference on Pile Behavior," Ecole des Ponts et Chaussees, Paris, France, Mar.
- Perenchio, W. F. (1989). "The Condition Survey," *Concrete International*, V. 11, No. 1, Jan., pp. 59-62.
- Pichot, C., and Trouillet, P. (1990). "Diagnosis of Reinforced Structures: An Active Microwave Imaging System," *Proceedings NATO Advanced Research Workshop on Bridge Evaluation, Repair and Rehabilitation*, A. S. Nowak, ed., Kluwer Academic Publishers, pp. 201-215.
- Pratt, D., and Sansalone, M. (1992). "Impact-Echo Signal Interpretation Using Artificial Intelligence," *ACI Materials Journal*, V. 89, No. 2, Mar.-Apr., pp. 178-187.
- Preiss, K. (1971). "Checking of Cast-in-Place Concrete Piles by Nuclear Radiation Methods," *British Journal of Non-Destructive Testing*, V. 13, No. 3, pp.70-76.
- Preiss, K., and Caiserman, A. (1975). "Nondestructive Integrity Testing of Bored Piles by Gamma Ray Scattering," *Ground Engineering*, V. 8, No. 3, pp. 44-46.
- Proctor, T. M., Jr. (1982). "Some Details on the NBS Conical Transducer," *Journal of Acoustic Emission*, V. 1, No. 3, pp. 173-178.
- Rausche, F., and Seitz, J. (1983). *Integrity Testing of Shafts and Caisson*, Specialty Session on Shafts and Caissons, ASCE Annual Convention, Philadelphia, Pa., 17 pp.
- Rausche, F.; Likins, G. E.; and Hussein, M. (1988). "Pile Integrity by Low and High Strain Impacts," *Proceedings Third International Conference on the Application of Stress-Wave Theory to Piles*, International Society of Soil Mechanics and Foundation Engineering, B. H. Fellenius, ed., Ottawa, Canada, May 25-27, pp. 44-55.
- Richart, F. E., Jr.; Woods, R. D.; and Hall, J.R. (1970). *Vibrations of Soils and Foundations*, Prentice-Hall, Inc., Englewood Cliffs, N.J.
- Rix, G. J., and Stokoe, K. H. (1989). "Stiffness Profiling of Pavement Subgrades," *Transportation Research Record* No. 1235, Transportation Research Board, Washington, D.C., pp. 1-9.
- Rodríguez, P.; Ramírez, E.; and González, J. A. (1994). "Methods for Studying Corrosion in Reinforced Concrete," *Magazine of Concrete Research*, V. 46, No. 167, June, pp. 81-90.
- Samman, M. M., and O'Neill, M. W. (1997). "The Reliability of Sonic Testing of Drilled Shafts," *Concrete International*, V. 19, No. 1, Jan., pp. 49-54.
- Sansalone, M., and Carino, N. J. (1986). "Impact-Echo: A Method for Flaw Detection in Concrete Using Transient Stress Waves," NBSIR 86-3452, National Bureau of Standards, Sept., 222 pp.
- Sansalone, M., and Carino, N. J. (1988). "Impact-Echo Method: Detecting Honeycombing, the Depth of Surface-Opening Cracks, and UngROUTED Ducts," *Concrete International*, V. 10, No. 4, Apr., pp. 38-46.
- Sansalone, M., and Carino, N. J. (1989a). "Detecting Delaminations in Concrete Slabs With and Without Overlays Using the Impact-Echo Method," *Journal of the American Concrete Institute*, V. 86, No. 2, Mar., pp. 175-184.
- Sansalone, M., and Carino, N. J. (1989b). "Laboratory and Field Study of the Impact-Echo Method for Flaw Detection in Concrete," *Nondestructive Testing of Concrete*, H. S. Lew, ed., SP-112, American Concrete Institute, Farmington Hills, Mich., pp. 1-20.
- Sansalone, M., and Carino, N. J. (1991). "Stress Wave Propagation Methods," *Handbook on Nondestructive Testing of Concrete*, Chapter 12, V. M. Malhotra and N. J. Carino, eds., CRC Press, Boca Raton, Fla., pp. 275-304.
- Sansalone, M. J., and Streett, W. B. (1997). *Impact-Echo: Nondestructive Evaluation of Concrete and Masonry*, Bullbrier Press, Ithaca, N.Y., 339 pp.
- Sansalone, M. (1997). "Impact Echo: The Complete Story," *ACI Structural Journal*, V. 94, No. 6, Nov.-Dec., pp. 777-786.
- Schlessinger, M. (1995). *Infrared Technology Fundamentals*, Marcel Dekker, Inc., New York, 462 pp.
- Schönlín, K., and Hilsdorf, H. (1987). "Evaluation of the Effectiveness of Curing of Concrete Structures," *Concrete Durability: Katharine and Bryant Mather International Conference*, J. M. Scanlon, ed., ACI SP-100, American Concrete Institute, Farmington Hills, Mich., pp. 207-226.
- Serway, R. A. (1983). *Physics for Scientists and Engineers/with Modern Physics*, Saunders College Publishing, Philadelphia, Pa.
- Shaw, M. R.; Millard, S. G.; Houlden, M. A.; Austin, B. A.; and Bungey, J. H. (1993). "A Large Diameter Transmission Line for the Measurement of Relative Permittivity of Construction Materials," *British Journal of Non-Destructive Testing*, V. 35, No. 12, pp. 696-704.
- Stain, R. T. (1982). "Integrity Testing," *Civil Engineering* (United Kingdom), Apr., pp. 55-59, and May, pp. 77-87.
- Starke, W. F., and Janes, M. C. (1988). "Accuracy and Reliability of Low Strain Integrity Testing," *Proceedings Third International Conference on the Application of Stress-Wave Theory to Piles*, International Society of Soil Mechanics and Foundation Engineering, B. H. Fellenius, ed., Ottawa, Canada, May 25-27, pp. 19-32.
- Steinbach, J., and Vey, E. (1975). "Caisson Evaluation by Stress Wave Propagation Method," *Journal of Geotechnical Engineering*, ASCE, V. 101, No. GT4, Apr., pp. 361-378.
- Steinert, J. (1979). "Nondestructive Determination of the Depth of Penetration of Water in Gravel Concrete at the Structure," Translation of article in *Forschungsbeiträge für die Baupraxis*, pp. 151-162.
- Steinway, W. J.; Echard, J. D.; and Luke, C. M. (1981). "Locating Voids beneath Pavements Using Pulsed Electromagnetic Waves," *NCHRP Report 237*, Transportation Research Board, National Research Council, Washington, D.C., Nov.
- Stern, M., and Roth, R. M. (1957). "Anodic Behavior of Iron in Acid Solutions," *Journal of the Electrochemical Society*, V. 104, No. 6, Jun., pp. 390-392.
- Stern, M., and Geary, A. L. (1957). "Electrochemical Polarization: I—A Theoretical Analysis of the Shape of Polarization Curves," *Journal of the Electrochemical Society*, V. 104, No. 1, Jan., pp. 56-63.
- Tam, C. T.; Lai, L. H.; and Lam, P. W. (1977). "Orthogonal Detection Technique for Determination of Size and Cover of Embedded Reinforcement," *Journal of Institution of Engineers*, Malaysia, V. 22, Jun., pp. 6-16.
- Teodoru, G. V. M. (1994). "Nondestructive Testing of Concrete from Research to the Use in the Practice," *International Advances in Nondestructive*

Testing, V. 17, W. J. McGonagle, ed., Gordon & Breach Science Publishers, New York, pp. 117-137.

Teodoru, G. V. M. (1996). "NDT-Methods for Concrete on the Move into the 21st Century," *Proceedings Fourteenth World Conference on NDT*, Dec. 8-13, New Delhi, India, C. G. Krishnadas et al., eds., Oxford & IBH Publishing Co., V. 1, pp. 123-129.

Teodoru, G. V. M., and Herf, J. (1996). "Engineering Society Cologne Presents Itself (NDT Methods)," *Proceedings Fourteenth World Conference on NDT*, Dec. 8-13, New Delhi, India, C. G. Krishnadas et al., eds., Oxford & IBH Publishing Co., V. 2, pp. 939-943.

Tomsett, H. N. (1980). "The Practical Use of Ultrasonic Pulse Velocity Measurements in the Assessment of Concrete Quality," *Magazine of Concrete Research*, V. 32, No. 110, Mar., pp. 7-16.

Ulriksen, C. P. F. (1983). *Application of Impulse Radar to Civil Engineering*, PhD thesis, Lund University, Dept. of Engineering Geology, Sweden. Published by Geophysical Survey Systems, Inc., Salem, N.H.

Van Koten, H., and Middendorp, P. (1981). "Interpretation of Results From Integrity Tests and Dynamic Load Tests," *Application of Stress Wave Theory in Piles*, Balkema, Rotterdam.

Weil, G. J. (1989). "Nondestructive Remote Sensing of Subsurface Utility Distribution Pipe Problems Using Infrared Thermography," *Proceedings Second International Conference on Pipeline Construction Congress*, Centrum Hamburg, Germany, Oct.

Weil, G. J. (1991). "Infrared Thermographic Techniques," *Handbook on Nondestructive Testing of Concrete*, Chapter 13, V. M. Malhotra and N. J. Carino, eds., CRC Press, Boca Raton, Fla., pp. 305-316.

Whitehurst, E. A. (1967). *Evaluation of Concrete Properties from Sonic Tests*, American Concrete Institute Monograph No. 2, ACI/Iowa State University Press, 94 pp.

Whiting, D. (1987). "Permeability of Selected Concrete," *Permeability of Concrete*, D. Whiting and A. Walit, eds., ACI SP-108, American Concrete Institute, Farmington Hills, Mich., pp. 195-222.

Whiting, D., and Cady, P. D. (1992). "Condition Evaluation of Concrete Bridges Relative to Reinforcement Corrosion," *Volume 7: Method for Field Measurement of Concrete Permeability*, SHRP-S/FR-92-109, National Research Council, Washington, D.C., 87 pp.

Williams, T. J.; Sansalone, M.; Streett, W. B.; Poston, R.; and Whitlock, R. (1997). "Nondestructive Evaluation of Masonry Structures Using the Impact-Echo Method," *The Masonry Society Journal*, V. 15, No. 1, Jun., pp. 47-57.

Yuan, D., and Nazarian, S. (1993). "Automated Surface Wave Method: Inversion Technique," *Journal of Geotechnical Engineering*, ASCE, V. 119, No. 7, Jul., pp. 1112-1126.

APPENDIX A—THEORETICAL ASPECTS OF MOBILITY PLOT OF PILE

Dynamic pile mobility is defined as the pile mechanical admittance (which is the inverse of the pile impedance) when the pile is subjected to a vertical dynamic force. Mobility is measured as velocity/force (V/F) and is expressed in metric units as m/s/N.

The theory of the mobility response of a pile in soil has been fully developed in Davis and Dunn (1974). The principles of mobility-frequency response curve interpretation are based on the following premises:

When a perfect, laterally unrestrained (free) pile of length L resting on the surface of an elastic foundation is excited by a continuous sinusoidal axial force with peak value F_0 , the pile head achieves a maximum velocity V_0 . As the frequency of the applied force is varied, the amplitude of the pile head velocity has peak values at equally spaced frequencies (resonant frequencies). The frequency interval, Δf , between the peaks is given by

$$\Delta f = \frac{C_b}{2L} \quad (A.1)$$

where C_b is the speed of stress-wave propagation along the pile axis.

In the case of an infinitely rigid elastic base, the lowest resonant frequency = $C_b/4L$. In contrast, when the pile rests on an infinitely compressible base, the lowest resonant frequency approaches zero. In real conditions, the lowest resonant frequency lies between zero and $C_b/4L$.

When the pile is embedded in soil, the pile movement is damped by that lateral soil. The mobility curve is attenuated to give the typical response shown in Fig. 2.3.2. The denser the soil and the longer the pile, the greater is the attenuation, with increasing reduction in the difference between the maximum and minimum amplitudes. Fig. A.1 summarizes the mobility response from a perfect pile. A soil damping factor σ (Briard, 1970) can be given by

$$\sigma = \frac{\rho_s \beta_s}{\rho_c C_b r} \quad (A.2)$$

where

- ρ_s = soil density,
- ρ_c = concrete density,
- β_s = lateral soil shear wave velocity at the pile/soil interface, and
- r = pile radius.

The geometric mean value of mobility in the resonant portion of the plot is known as the average mobility N and is given by

$$N = \frac{1}{\rho_c C_b A_c} \quad (A.3)$$

where A_c is the pile cross-sectional area. This is the inverse of the pile impedance.

The maximum and the minimum amplitudes P and Q provide a measure of the soil damping effect from the relationships

$$\begin{aligned} P &= N \coth(\sigma L) \\ Q &= N \tanh(\sigma L) \end{aligned} \quad (A.4)$$

This can also be expressed as

$$N = \sqrt{PQ} \quad (A.5)$$

and σL can be calculated from

$$\coth(\sigma L) = \sqrt{\frac{P}{Q}} \quad (A.6)$$

The mass of the pile M_p is calculated as follows

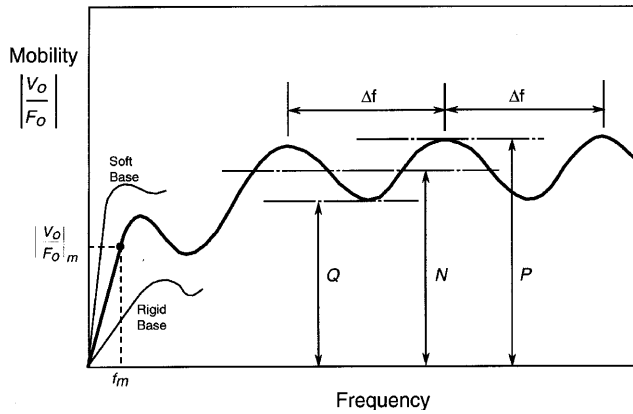


Fig. A.1—Theoretical mobility plot for impulse-response test of perfect pile in homogeneous soil.

$$M_p = L\rho_c A_c = \frac{1}{2 \Delta f N} \quad (\text{A.7})$$

The pile dynamic stiffness k_d is calculated from the mobility response curve at very low frequencies (usually in the range 0 - 60 Hz). At these low frequencies, inertial effects are insignificant and the pile-soil unit behaves as a spring, giving a linear response at the start of the mobility curve. The slope of this line is the pile compliance, and the inverse of the compliance is the pile dynamic stiffness k_d

$$k_d = \frac{2\pi f_m}{\left(\frac{V_o}{F_o}\right)_m} \text{ in units of N/m} \quad (\text{A.8})$$

where f_m is the frequency corresponding to the end of the initial linear portion of the mobility plot.

The mobility response curves obtained from real piles are seldom as simple as the theoretical curve for a perfect pile in homogeneous soil shown in Fig. A.1. Several factors affect the shape of the mobility curve, of which the most common are:

- Variations in pile diameter,
- Variations in the pile concrete quality with pile depth,
- Variations in the lateral soil stiffness, and
- The top section of pile being exposed above ground level.

The general effect of these factors is to produce superimposed variations in the geometric mean mobility on the general mobility plot. Fig. 2.3.2 shows such a variation in the mean between 460 Hz and 1360 Hz, which is a result of a free pile head 2.1 m in length ($2\Delta f = 1800$ Hz). The interpretation of mobility plots with superimposed features requires experience. Help can be provided by computer simulation models, as described in Davis and Dunn (1974).